Quantifying Flow and Sediment Yield of an Ungauged Catchment using a Combination of Continuous Soil Moisture Accounting and Event-based Curve Number Method

by

Sagar Kumar Tamang

A thesis submitted to the Graduate Faculty of

Auburn University

in partial fulfillment of the

requirements for the Degree of

Masters of Science

Auburn, Alabama

December 16, 2017

Keywords:

Surface Hydrology, Ungauged catchment, Soil moisture accounting, Sediment yield

Approved by

Xing Fang, Chair, Arthur H. Feagin Chair Professor of Civil Engineering

Jose Vasconcelos, Associate Professor of Civil Engineering

J. Brian Anderson, Associate Professor of Civil Engineering

ABSTRACT

A serious aggradation problem has been identified in the Soapstone branch, a tributary to Little Choctawhatchee River. A study of historical aerial imageries shows deforestation of the catchment by a significant amount in the period consistent with the first identification of the problem. The calculation of sediment yield from the catchment and its change during recent years require discharge data. However, due to the lack of any gauging stations and the difficulty of installing an area-velocity sensor to monitor discharge, parameter transfer for a hydrological model from a nearby donor catchment to the Soapstone branch was therefore investigated. However, due to the vast difference in the land cover composition of donor and soapstone branch catchment, event based curve number method was unfit for parameter transfer. Therefore, the soil moisture accounting, a continuous model available within HEC-HMS was used for the parameter transfer from a donor catchment after performing transfer validation process on an assumed ungauged receiver catchment. A continuous model of the Soapstone branch catchment was then built utilizing both transferred and locally developed parameters. This calibrated SMA model was used for calibrating locally developed curve number (CN) model of the catchment for a range of antecedent runoff conditions and for different years, i.e., 2011 and 2015. Calculations performed using calibrated CN model showed a significant amount of increase in sediment yield from 2011 to 2015.

This study concluded that HEC-HMS SMA model can be effectively used for prediction in ungauged catchment using the spatial proximity approach. Also, a combination of the soil moisture accounting together with the event-based curve number method can be used for quantifying discharge and change in sediment yield of an ungauged catchment.

ACKNOWLEDGEMENT

The author would like to extend a special thanks to Dr. Xing Fang for his devotion, guidance, and mentorship throughout the course of this research, as well as for enlisting an inspiration to further pursue graduate studies. The author would also like to thank committee members Dr. Jose Vasconcelos and Dr. J. Brian Anderson for their time and guidance throughout this research effort. The author would also like to thank the Alabama Department of Transportation (ALDOT) who funded the project and fellow research group members who put in their precious time for suggestions and feedback. Finally, the author would like to especially thank his parents D.B. Tamang and Usha Tamang, and his sister Sushma Tamang who through love, hard work, and sacrifice, provided the author support throughout his educational endeavor.

TABLE OF CONTENTS

ABSTRACT ii

ACKNOWLEDGEMENT iv

LIST OF FIGURES x

LIST OF TABLES xv

CHAPTER 1: INTRODUCTION 1

1.1 BACKGROUND 1

1.2 HYDROLOGIC CYCLE AND HYDROLOGIC MODEL 5

1.3 SCOPE AND OBJECTIVES 7

1.4 THESIS ORGANIZATION 8

CHAPTER 2: LITERATURE REVIEW 9

2.1 PREDICTION IN UNGAUGED CATCHMENT 9

2.2 HEC-HMS MODEL 11

2.2.1 SOIL MOISTURE ACCOUNTING ALGORITHM 13

2.2.2 CALIBRATION IN HEC-HMS AND PERFORMANCE CRITERIA 17

2.3 MODIFIED UNIVERSAL SOIL LOSS EQUATION 20

CHAPTER 3: STUDY AREA AND INPUT DATA 23
3.1 STUDY AREA 23
3.1.1 DONOR CATCHMENT 23
3.1.2 RECEIVER CATCHMENT 24
3.2 INPUT DATA 27
3.2.1 DIGITAL ELEVATION MODEL 27
3.2.2 LAND COVER DATA 27
3.2.3 SOIL DATA 31
3.2.4 PRECIPITATION DATA 34
3.2.5 EVAPOTRANSPIRATION DATA 35
3.2.6 STREAMFLOW DATA 37
CHAPTER 4: METHODOLOGY 39
4.1 CATCHMENT DELINEATION AND STREAM DEFINITION 39
4.2 PARAMETER ESTIMATION FOR SMA MODEL 39
4.2.1 PARAMETER ESTIMATION FROM LAND COVER 40
4.2.2 PARAMETER ESTIMATION FROM SOIL DATA 41
4.2.3 PARAMETERS ESTIMATION FROM STREAMFLOW DATA 45
4.3 CURVE NUMBER DEVELOPMENT AND BASIN LAG 48

4.4 HEC-HMS MODEL SETUP 55
4.4.1 THIESSEN POLYGON METHOD 55
4.4.2 INITIAL WARMUP PERIOD 58
4.5 SENSITIVITY ANALYSIS 59
4.6 CALIBRATION AND VALIDATION FOR DONOR CATCHMENT 62
4.6.1 SEMI-ANNUAL PARAMETERIZATION 65
4.7 PARAMETER TRANSFER TO RECEIVER CATCHMENT 65
CHAPTER 5: RESULTS AND DISCUSSIONS 67
5.1 CALIBRATION OF DONOR CATCHMENT 67
5.1.1 ANNUAL PARAMETERIZATION APPROACH 67
5.1.2 SEMI-ANNUAL PARAMETERIZATION APPROACH 72
5.2 VALIDATION OF DONOR CATCHMENT 76
5.3 TRANSFER OF PARAMETER AND VALIDATION 78
CHAPTER 6: APPLICATION TO SOAPSTONE BRANCH 84
6.1 STUDY AREA 84
6.2 INPUT DATA 86
6.2.1 DIGITAL ELEVATION MODEL 86
6.2.2 MULTISPECTRAL AERIAL IMAGERY 87

6.2.3 PRECIPITATION DATA 89
6.2.4 EVAPOTRANSPIRATION DATA 91
6.3 METHODOLOGY FOR STREAMFLOW SIMULATION 91
6.3.1 CATCHMENT DELINEATION AND STREAM DEFINITION 91
6.3.2 LAND COVER MAP GENERATION 92
6.3.3 CURVE NUMBER AND BASIN LAG 97
6.3.4 PARAMETER TRANSFER 99
6.4 PARAMETER ESTIMATION FOR MUSLE 100
6.4.1 SOIL ERODIBILITY FACTOR 100
6.4.2 TOPOGRAPHIC FACTOR 101
6.4.3 COVER MANAGEMENT FACTOR 103
6.4.4 SUPPORT PRACTICE FACTOR 110
6.5 HEC-HMS MODEL SETUP 111
6.6 CONTINUOUS STREAMFLOW SIMULATION 112
6.7 EVENT BASED CURVE NUMBER METHOD 113
6.7.1 MODEL DEVELOPMENT 113
6.7.2 COMPARISON WITH SMA MODEL 117
6.7.3 CALIBRATION OF EVENT BASED MODEL USING SMA MODEL 122

6.8 SEDIMENT YIELD AT DEAN ROAD BRIDGE 127

CHAPTER 7: SUMMARY AND CONCLUSIONS 131

7.1 SUMMARY 131

7.2 CONCLUSIONS 133

7.3 FUTURE STUDIES 134

REFERENCES 135

LIST OF FIGURES

FIGURE 1.1 LOCATION OF DEAN ROAD BRIDGE AND AGGRADATION PROBLEM 2

FIGURE 1.2 OVERTOPPING AT DEAN ROAD BRIDGE DURING A STORM EVENT OF 3RD FEBRUARY 2016 3

FIGURE 1.3 ANNUAL PRECIPITATION FOR DOTHAN RAINFALL STATION (2006–2016) 4

FIGURE 1.4 AERIAL IMAGERY OF A PORTION OF SOAPSTONE BRANCH CATCHMENT IN 2011 (LEFT) AND 2015 (RIGHT) 5

FIGURE 1.5 EARTH'S HYDROLOGIC CYCLE (SOURCE: US GEOLOGICAL SURVEY) 6

FIGURE 2.1 SYSTEMS PROCESSES IN HEC-HMS FOR SIMULATING WATERSHED RUNOFF (FELDMAN 2000) 12

FIGURE 2.2 SCHEMATIC OF HEC-HMS SMA MODEL (FELDMAN 2000) 14

FIGURE 3.1 LOCATION OF DONOR CHOCTAWHATCHEE RIVER CATCHMENT 25

FIGURE 3.2 LOCATION OF DOUBLE BRIDGES CREEK RECEIVER CATCHMENT 26

FIGURE 3.3DIGITAL ELEVATION MODEL OF DONOR CATCHMENT (LEFT) AND RECEIVER CATCHMENT (RIGHT) 29

FIGURE 3.4 NLCD 2011 LAND COVER MAP OF DONOR CATCHMENT (LEFT) AND RECEIVER CATCHMENT (RIGHT) 30

FIGURE 3.5 STATUS OF SOIL SURVEY IN ALABAMA 32

FIGURE 3.6 SOIL SURFACE TEXTURE OF DONOR CATCHMENT 33

FIGURE 3.7 HOURLY PRECIPITATION VALUES FOR TROY (2009–2015) 34

FIGURE 3.8 ANNUAL PRECIPITATION FOR RAINFALL STATIONS (2009–2015) 35

FIGURE 3.9 PAN EVAPOTRANSPIRATION DATA FOR MARTIN DAM (2009–2013) 36

FIGURE 3.10 STREAMFLOW HYDROGRAPH FOR DONOR CATCHMENT 37

FIGURE 3.11 STREAMFLOW HYDROGRAPH FOR RECEIVER CATCHMENT 38

FIGURE 4.1 ORGANIZATION OF SSURGO MAP DATA (HOLBERG 2015) 42

FIGURE 4.2 BASEFLOW SEPARATION FOR STORM OF 15TH MARCH 2009 48

FIGURE 4.3 HYDROLOGIC SOIL GROUP OF DONOR CATCHMENT (LEFT) AND RECEIVER CATCHMENT (RIGHT) 50

FIGURE 4.4 SIMPLIFIED LAND COVER MAP OF DONOR CATCHMENT (LEFT) AND RECEIVER CATCHMENT (RIGHT) 52

FIGURE 4.5 CURVE NUMBER GRID FOR DONOR CATCHMENT (LEFT) AND RECEIVER CATCHMENT (RIGHT) 54

FIGURE 4.6 HEC-HMS MODEL SETUP FOR DONOR CATCHMENT 56

FIGURE 4.7 LOCATION OF RAIN GAUGES NEAR THE DONOR CATCHMENT (LEFT) AND THIESSEN POLYGON FOR DONOR CATCHMENT (RIGHT) 57

FIGURE 4.8 EFFECT OF VARIATION OF INITIAL MOISTURE IN DIFFERENT STORAGE ZONES ON MODEL OUTPUT 58

FIGURE 4.9 NASH-SUTCLIFFE EFFICIENCY OF THE MODEL OUTPUT DUE TO PERCENT CHANGE IN PARAMETER VALUES 60

FIGURE 4.10 PERCENT ERROR IN VOLUME OF THE MODEL OUTPUT DUE TO PERCENT CHANGE IN PARAMETER VALUES 60

FIGURE 4.11 FLOWCHART OF THE MANUAL CALIBRATION 64

FIGURE 5.1 HOURLY SIMULATED VERSUS OBSERVED DISCHARGE FOR DONOR CATCHMENT (OCT 2009–SEP2012) 69

FIGURE 5.2 SCATTERPLOT OF SIMULATED VERSUS OBSERVED DISCHARGE DURING CALIBRATION PERIOD (OCT 2009–SEP 2012) 70

FIGURE 5.3 CUMULATIVE SIMULATED VERSUS OBSERVED DISCHARGE VOLUME DURING CALIBRATION PERIOD FOR DONOR CATCHMENT (OCT 2009–SEP 2012) 71

FIGURE 5.4 HOURLY SIMULATED VERSUS OBSERVED DISCHARGE FOR DONOR CATCHMENT DURING CALIBRATION PERIOD (OCT 2012–SEP2015) USING SEMI-ANNUAL APPROACH 74

FIGURE 5.5 SEMI-ANNUAL MODEL COMPARISON WITH ANNUAL PARAMETER MODEL FOR DONOR CATCHMENT (MAY 2010–OCTOBER 2010)..... 75

FIGURE 5.6 HOURLY SIMULATED VERSUS OBSERVED DISCHARGE FOR DONOR CATCHMENT DURING VALIDATION PERIOD (OCT 2012–SEP2015) 76

FIGURE 5.7 SCATTERPLOT OF SIMULATED VERSUS OBSERVED DISCHARGE DURING VALIDATION PERIOD (OCT 2012–SEP 2015) 77

FIGURE 5.8 CUMULATIVE SIMULATED VERSUS OBSERVED DISCHARGE VOLUME DURING VALIDATION PERIOD FOR DONOR CATCHMENT (OCT 2012–SEP 2015) 78

FIGURE 5.9 HOURLY SIMULATED VERSUS OBSERVED DISCHARGE FOR RECEIVER CATCHMENT DURING THE TRANSFER VALIDATION PERIOD (OCT 2009–SEP2012) 80

FIGURE 5.10 SCATTERPLOT OF SIMULATED VERSUS OBSERVED DISCHARGE DURING THE TRANSFER VALIDATION PERIOD (OCT 2009–SEP 2012) FOR RECEIVER CATCHMENT..... 81

FIGURE 5.11 CUMULATIVE SIMULATED VERSUS OBSERVED DISCHARGE VOLUME DURING TRANSFER VALIDATION PERIOD FOR RECEIVER CATCHMENT (OCT 2009–SEP 2012)..... 82

FIGURE 5.12 ANNUAL PRECIPITATION FOR ALABAMA IN 2010 (SOURCE: NATIONAL WEATHER SERVICE)..... 83

FIGURE 6.1 LOCATION OF SOAPSTONE BRANCH CATCHMENT RELATIVE TO DONOR AND RECEIVER CATCHMENT 85

FIGURE 6.2 DIGITAL ELEVATION MODEL OF SOAPSTONE BRANCH CATCHMENT..... 87

FIGURE 6.3 FALSE COLOR COMPOSITE (4-1-2 SCHEME) IMAGE OF SOAPSTONE BRANCH CATCHMENT IN 2011(LEFT) AND 2015 (RIGHT)..... 89

FIGURE 6.4 RAIN GAUGE LOCATIONS IN THE CATCHMENT (LEFT) AND INSTALLED RAIN GAUGE (RIGHT)..... 90

FIGURE 6.5 DELINEATED SOAPSTONE BRANCH CATCHMENT AND PARTITION INTO SUBCATCHMENTS 92

FIGURE 6.6 CLUSTER BUSTING TECHNIQUE APPLIED TO AREA SURROUNDING FOREST: BEFORE (LEFT), CLUSTER BUSTING (MIDDLE) AND AFTER (RIGHT)..... 95

FIGURE 6.7 LAND COVER MAP OF SOAPSTONE BRANCH CATCHMENT DEVELOPED FROM NAIP IMAGERY FOR 2011 (LEFT) AND 2015 (RIGHT) 96

FIGURE 6.8 HYDROLOGIC SOIL GROUP MAP OF SOAPSTONE BRANCH CATCHMENT 97

FIGURE 6.9 CURVE NUMBER GRID OF SOAPSTONE BRANCH CATCHMENT FOR 2011 (LEFT) AND 2015 (RIGHT) 98

FIGURE 6.10 SPATIAL DISTRIBUTION OF K FACTOR IN THE SOAPSTONE BRANCH CATCHMENT ... 101

FIGURE 6.11 SPATIAL DISTRIBUTION OF LS FACTOR IN THE SOAPSTONE BRANCH CATCHMENT . 103

FIGURE 6.12 SPATIAL VARIATION OF NDVI VALUES OF THE SOAPSTONE BRANCH CATCHMENT IN 2011 (LEFT) AND 2015 (RIGHT) 105

FIGURE 6.13 SPATIAL DISTRIBUTION OF C FACTOR RASTER GRID OF SOAPSTONE BRANCH CATCHMENT IN 2011 (LEFT) AND 2015 (RIGHT) 107

FIGURE 6.14 MODIFIED C FACTOR RASTER GRID OF THE SOAPSTONE BRANCH CATCHMENT IN 2015 108

FIGURE 6.15 C FACTOR GRID OF SOAPSTONE BRANCH IN 2015 OBTAINED BY NEGLECTING THE EFFECTS OF DEFORESTATION 109

FIGURE 6.16 HEC-HMS SETUP FOR SOAPSTONE BRANCH CATCHMENT 112

FIGURE 6.17 SMA MODEL RESULT OF SOAPSTONE BRANCH CATCHMENT (OCTOBER 2009–SEPTEMBER 2016) 113

FIGURE 6.18 COMPARISON OF SMA MODEL WITH UNCALIBRATED EVENT-BASED CN MODEL FOR ARC CLASS I CONDITION WITH STORM EVENTS BEFORE 2011 (A) AND AFTER 2011 (B) 119

FIGURE 6.19 COMPARISON OF SMA MODEL WITH UNCALIBRATED EVENT-BASED CN MODEL FOR ARC CLASS II CONDITION WITH STORM EVENTS BEFORE 2011 (A) AND AFTER 2011 (B) 120

FIGURE 6.20 COMPARISON OF SMA MODEL WITH UNCALIBRATED EVENT-BASED CN MODEL FOR ARC CLASS III CONDITION WITH STORM EVENTS BEFORE 2011 (A) AND AFTER 2011 (B) 121

FIGURE 6.21 COMPARISON OF SMA MODEL WITH CALIBRATED CN MODEL FOR ARC CLASS I CONDITION WITH STORM EVENTS BEFORE 2011 (A) AND AFTER 2011 (B) 124

FIGURE 6.22 COMPARISON OF SMA MODEL WITH CALIBRATED CN MODEL FOR ARC CLASS II CONDITION WITH STORM EVENTS BEFORE 2011 (A) AND AFTER 2011 (B) 125

FIGURE 6.23 COMPARISON OF SMA MODEL WITH CALIBRATED CN MODEL FOR ARC CLASS III CONDITION WITH STORM EVENTS BEFORE 2011 (A) AND AFTER 2011 (B) 126

FIGURE 6.24 SEDIMENT YIELD AND PERCENTAGE INCREASE FOR EACH ARC CLASS CONDITION STORMS FROM THE SOAPSTONE BRANCH CATCHMENT IN 2011 AND 2015 SCENARIOS 129

FIGURE 6.25 SEDIMENT YIELD AND PERCENTAGE INCREASE FOR EACH ARC CLASS CONDITION STORMS FROM THE SOAPSTONE BRANCH CATCHMENT IN 2011 AND 2015 SCENARIOS BY NEGLECTING DEFORESTATION..... 130

LIST OF TABLES

TABLE 3.1 LAND COVER CLASSES AND THEIR RESPECTIVE COMPOSITION FOR DONOR CATCHMENT 23

TABLE 3.2 AVERAGE ANNUAL PRECIPITATION FOR RAINFALL STATIONS AROUND DONOR CATCHMENT 24

TABLE 3.3 LAND COVER CLASSES AND THEIR RESPECTIVE COMPOSITION FOR RECEIVER CATCHMENT 27

TABLE 3.4 CLASS VALUES AND DESCRIPTION FOR NLCD 2011 LAND COVER MAP 28

TABLE 3.5 MEAN MONTHLY PAN EVAPOTRANSPIRATION FOR MARTIN DAM 36

TABLE 4.1 CANOPY INTERCEPTION VALUES FOR DIFFERENT TYPES OF VEGETATION (BENNETT, 1998) 41

TABLE 4.2 SURFACE DEPRESSION STORAGE VALUES (BENNETT 1998) 43

TABLE 4.3 SOIL TEXTURE CLASSES AND SATURATED HYDRAULIC CONDUCTIVITIES 44

TABLE 4.4 GROUNDWATER PARAMETER VALUES FOR SELECTED STORMS AND THEIR AVERAGES 48

TABLE 4.5 SIMPLIFIED LAND COVER CLASSES FROM NLCD LAND COVER CLASSIFICATION 51

TABLE 4.6 CURVE NUMBER VALUES FOR CORRESPONDING LAND COVER AND HYDROLOGIC SOIL GROUP 53

TABLE 4.7 PARAMETER RANKING BASED ON THE VALUE OF SENSITIVITY PARAMETER FOR NSE AND PEV 62

TABLE 5.1 FINAL CALIBRATED PARAMETER VALUES FOR SMA MODEL OF DONOR CATCHMENT. 68

TABLE 5.2 SEMI-ANNUAL PARAMETER VALUES FOR DRY SEASONS AND WET SEASONS 73

TABLE 5.3 AREAL AVERAGE VALUE OF SMA PARAMETER FROM DONOR CATCHMENT 79

TABLE 6.1 LAND COVER CLASSES AND THEIR RESPECTIVE COMPOSITION FOR SOAPSTONE BRANCH CATCHMENT 84

TABLE 6.2 CURVE NUMBER AND BASIN LAG COMPUTATION AT SUBCATCHMENT SCALE FOR 2011 AND 2015 99

TABLE 6.3 EXPONENT M-VALUE IN LS FACTOR FOR DIFFERENT SLOPE 102

TABLE 6.4 AREAL AVERAGE C FACTOR VALUE AND PERCENT CHANGE FOR DIFFERENT SCENARIOS 110

TABLE 6.5 P FACTOR VALUES FOR DIFFERENT SOIL CONSERVATION PRACTICES 111

TABLE 6.6 ADJUSTMENT OF CURVE NUMBER FOR DRY CONDITION (I) AND WET CONDITION (III) 115

TABLE 6.7 RAINFALL LIMITS DEFINING THE ANTECEDENT RUNOFF CONDITION 116

TABLE 6.8 2011 CURVE NUMBER AND ADJUSTMENT FOR ARC CLASSES 117

TABLE 6.9 2015 CURVE NUMBER AND ADJUSTMENT FOR ARC CLASSES 117

TABLE 6.10 SELECTED STORM EVENTS 118

TABLE 6.11 CALIBRATED 2015 CN VALUES FOR ARC CLASS I, II, AND III 122

TABLE 6.12 CALIBRATED 2011 CN VALUES FOR ARC CLASS I, II, AND III 123

TABLE 6.13 PEAK RUNOFF AND VOLUME OF RUNOFF FOR THREE STORM EVENTS WITH 2011 AND 2015 SCENARIOS 127

TABLE 6.14 PERCENT CHANGES OF SEDIMENT YIELD FROM 2011 TO 2015 DUE TO DIFFERENT FACTORS 129

CHAPTER 1: INTRODUCTION

1.1 BACKGROUND

Soil erosion is the process of detachment of top layer of soils by mechanical forces of wind or water. Negative impacts of soil erosion include and not limited to severe draughts in arid and semi-arid regions, reduction in the conveyance of channel resulting in flood, and a decrease in agricultural productivity. In the world, around 80% of agricultural land experience severe to moderate erosion and 10% experience moderate erosion (Speth 1994). It costs the US economy about $30–$40 billion dollars annually due to on and off site effects such as loss in agricultural productivity, blockage of conveyance of irrigation channel, etc. (Morgan 2009). Unlike mountainous regions where soil erosion limits land use and impacts agricultural productivity, lowland areas are more affected by erosion that induces blockage of flow in streams, bridges, and culverts. Such aggradation problems if not treated develop exponentially over time and may risk the damage of such structures and cause flooding.

A serious aggradation problem has been identified in Soapstone Branch, a tributary of the Little Choctawhatchee River (USGS HUC 0314020105) located in Dale County, Alabama. Dean Road Bridge (Figure 1.1) was initially constructed in the 90's with a clearance of about 8 feet below the lower deck of the bridge. Aggradation problem was first identified in 2013, and aggravated over time reducing the conveyance of the bridge to couple inches by 2014. This aggradation problem reduced the conveyance of the bridge which threatens the durability of the

bridge and may cause severe damages during storm events (Figure 1.2). After identification of this aggradation problem, county engineers decided to excavate the sediment deposited below and near the bridge. Earlier in the year of 2015, sediment was excavated. However, this solution fixed the problem temporarily and sediment accumulated again in a short period of about eight months.

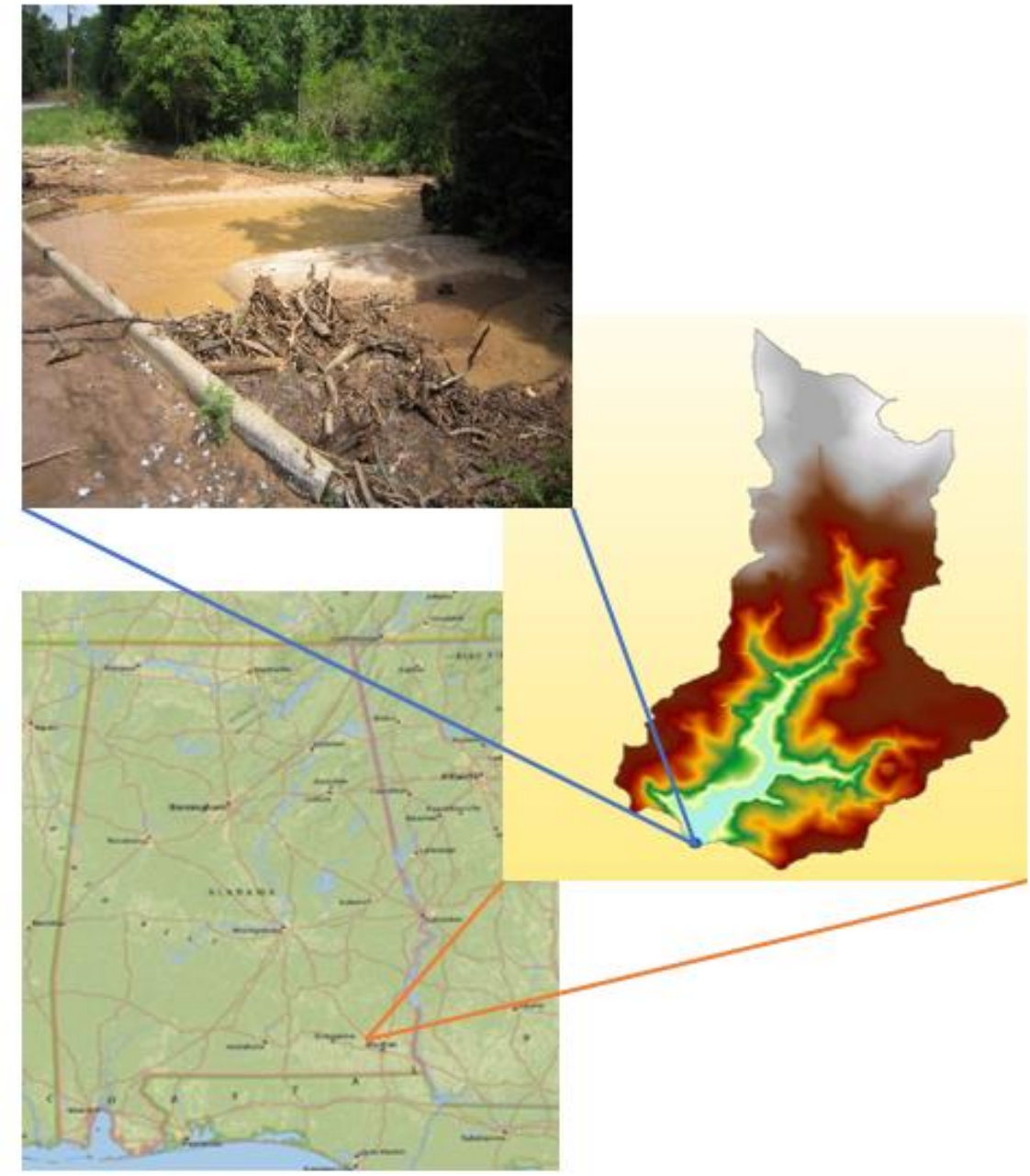

Figure 1.1 Location of Dean Road Bridge and Aggradation Problem

Figure 1.2 Overtopping at Dean Road Bridge during a storm event of 3rd February 2016

Figure 1.3 shows the historical annual precipitation data for the Dothan regional airport from 2006–2016. The average annual precipitation during this period was 51.35 in. with a standard deviation of 12.97 in. It is found that years 2009, 2013, 2014, and 2015 had significantly higher precipitation than the annual average whereas rest of the years had lower rainfalls than the annual average. Furthermore, aerial imageries of the catchment area for the Soapstone branch catchment (Figure 1.4) shows significant land cover changes over a period of several years. Change in landcover due to clear cutting of the trees in the vicinity of the stream channel is clearly visible for the period from 2011 to 2015 (Figure 1.4). For understanding these effects on the process of

aggradation and for quantifying the amount of sediments, a hydrological model needs to be developed.

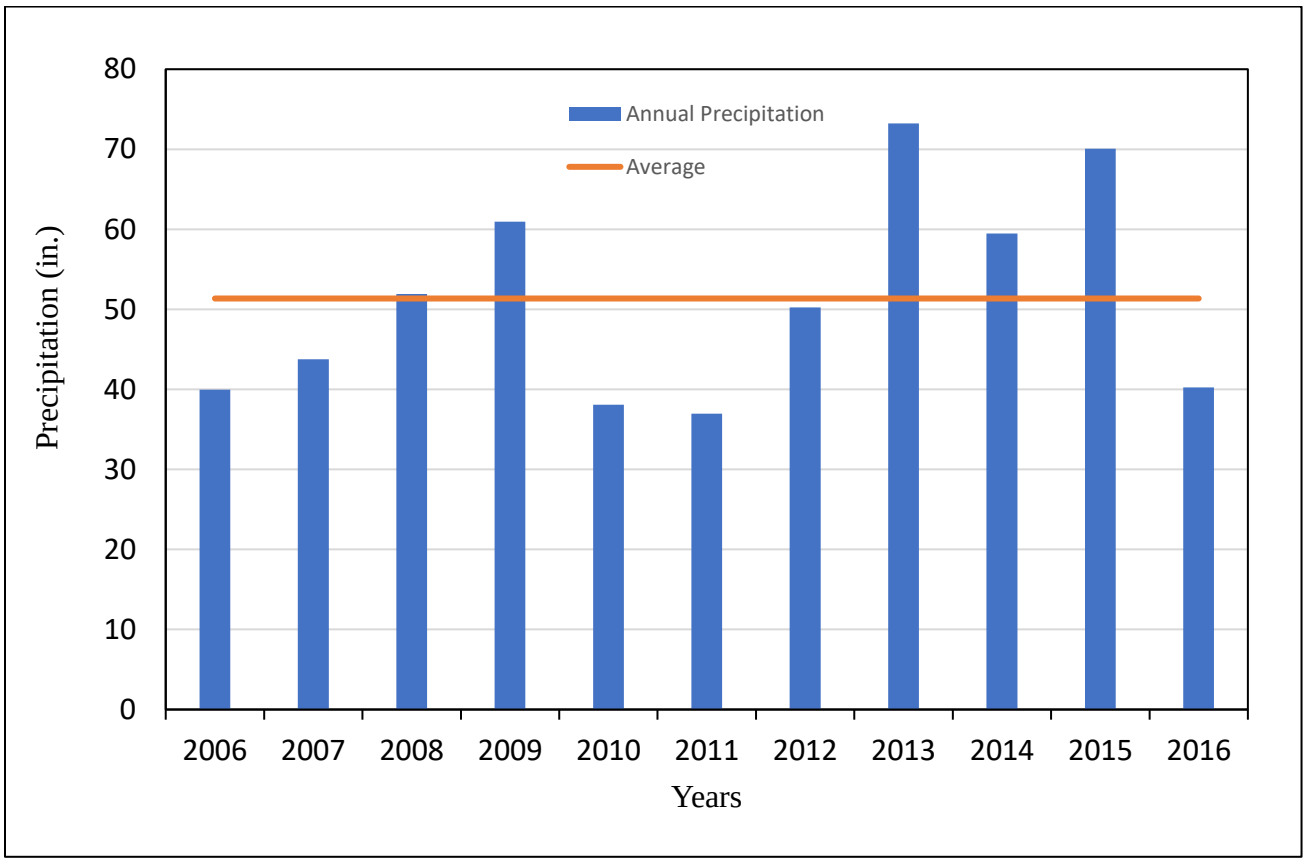

Figure 1.3 Annual Precipitation for Dothan Rainfall Station (2006–2016)

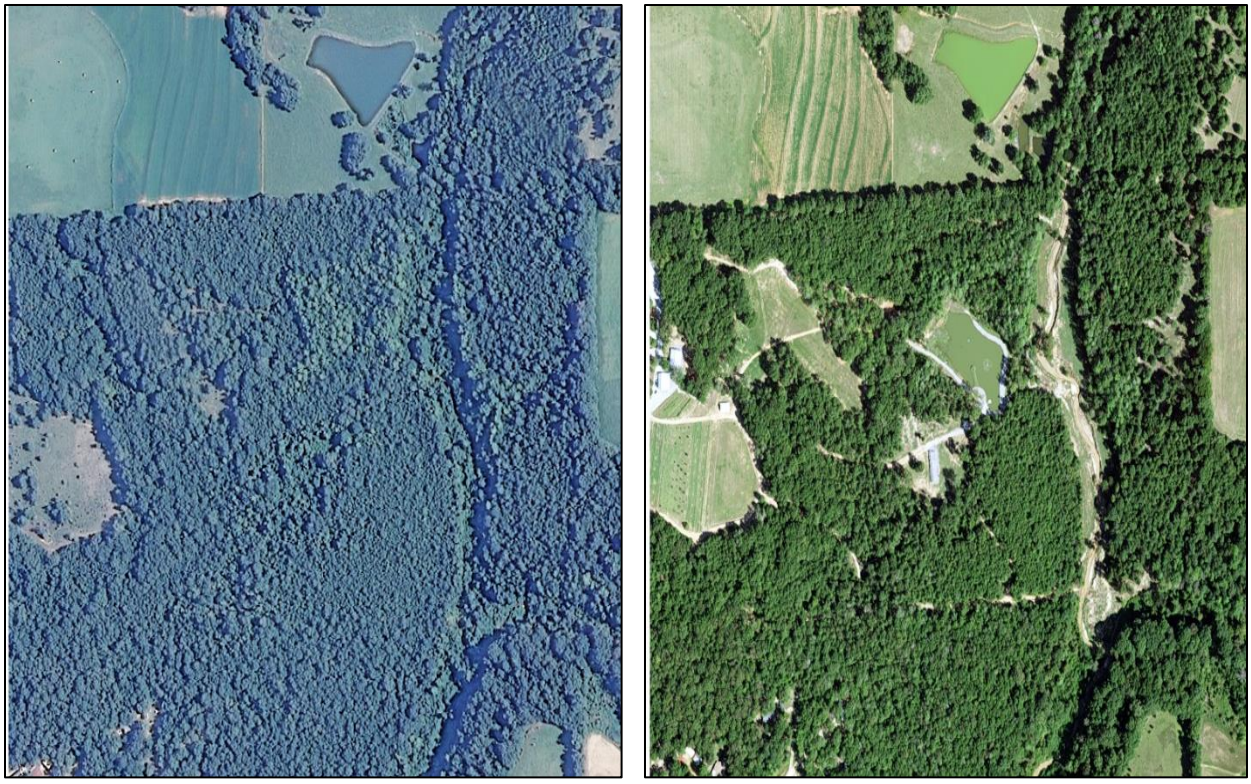

Figure 1.4 Aerial Imagery of a Portion of Soapstone Branch Catchment in 2011 (Left) and 2015 (Right)

1.2 HYDROLOGIC CYCLE AND HYDROLOGIC MODEL

The hydrologic cycle is defined as the process by which ocean water is transported to the atmosphere, then to the land and back to the ocean (Viessman and Lewis 2003). Earth's hydrologic cycle begins with the evaporation of water from the surface of ocean, sea or other water bodies (Figure 1.5). As the water vapor moves upward, it condenses to form clouds. These clouds carry the moisture around the world and fall to the earth's surface in the form of precipitation (rain, dew, snow, etc.). a part of this precipitation infiltrates into the ground whereas, the remaining precipitation appears as surface overland flow. Infiltrated volume of water is stored in the groundwater and then appears as groundwater flow to supplement the streams. These streams then

flow down to replenish seas and oceans. The process of transformation of precipitation into the overland flow, groundwater flow, and streamflow can be modeled using a hydrologic model.

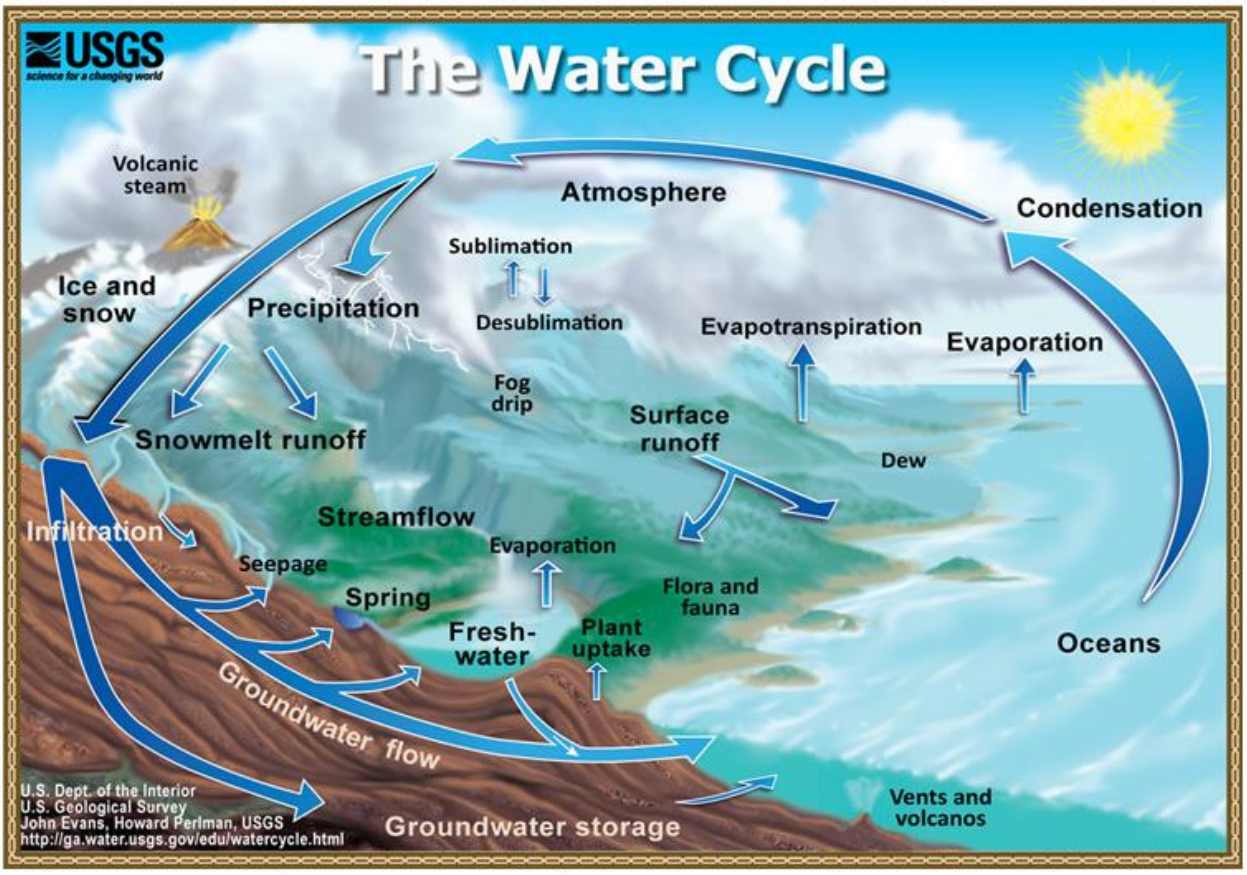

Figure 1.5 Earth's Hydrologic Cycle (Source: US Geological Survey)

The hydrologic model can be considered as an approximation of actual physical, chemical and biological processes going on in a catchment. The catchment is defined as the land area that drains to a specific point of interest in a stream. The physical process of interception, overland flow, infiltration, groundwater flow etc. are simplified by using model parameters which mimic the real physical phenomenon. Also, the processes of nutrient transfer, chemical yields from agricultural land, effects on the biotic composition, the function of riparian ecosystems, etc. can be simulated using hydrologic model. In terms of representation of reality, a hydrologic model can

be classified as a physical, analog or mathematical model (Feldman 2000). A physical hydrologic model is a miniature representation of real world system. This type of models when constructed at lab consists of surfaces altered to represent the land use, soil type, surface slope etc. of the watershed. The second type of hydrologic model, i.e., the analog model is developed to represent the flow of water with the flow of electricity in a circuit. This type of models has widespread use in computing subsurface flow. A mathematical hydrologic model consists of a set of equations to represent the flow of water with a change in a hydrometeorological variable. Further classification of a mathematical hydrologic model can be done based on whether it can simulate a single storm, i.e., an event-based model or it can simulate the hydrological response from a catchment for a longer period (both wet and dry), i.e., continuous hydrologic model.

1.3 SCOPE AND OBJECTIVES

Soapstone branch is an ungauged catchment with no discharge gauge installed within it. The prior attempts to install an Area-Velocity sensor were failed because of the higher degrees of aggradation and the sensor getting buried deep into the sand after each major rainfall event. Therefore, the parameter transfer from a hydrologic model developed for a donor catchment is needed for predicting streamflow in the Soapstone branch catchment.

The primary objectives of this study are:

1. Develop a hydrologic model for a donor catchment.
2. Transfer a set of parameters from the donor catchment to an assumed receiver catchment and validate the simulation by comparison with the observed flow data.
3. After validation of transfer process, transfer the parameters to the Soapstone branch catchment and simulate the hydrograph.

4. Estimate the increase in sediment yield from 2011 to 2015 due to land cover changes in the catchment

1.4 THESIS ORGANIZATION

This thesis is organized into seven different chapters. Chapter one covers the background, scopes and objectives of this study, and thesis organization. Chapter two provides information on literature review. Chapter three explains the selected study area and description of the data and its sources. Chapter four explains how HEC-HMS soil moisture accounting (SMA) model was developed for the donor and receiver catchments and describes the process of parameter transfer between the catchments. Chapter five includes and displays the results of the parameter transfer. Chapter six details the application of the SMA model to the Soapstone branch catchment and the determination of sediment yield. Chapter seven contains summary, conclusions, and scope for future studies.

CHAPTER 2: LITERATURE REVIEW

2.1 PREDICTION IN UNGAUGED CATCHMENT

All hydrologic models used so far are developed from classical theories which assume homogeneity despite the heterogeneity exhibited by nature. The only way to increase the resemblance of the model to reality is through calibration with the existing gauged data (Sivapalan 2003). Parameter calibration procedure has multiple advantages. Due to the dependence of empirical model equations on hydrologic settings, the calibration can include the effects of hydrological setting on a particular catchment. It can also help in adjusting the input biases such as orographic effects and instrumental errors. Furthermore, the calibration procedure is known to improve the performance of a rainfall-runoff model of a catchment with high spatial heterogeneity (Blöschl 2005). However, the existing gauged data required for such calibration process is not available at all required locations. Even after 3000 years from when first river gauging began on the Nile, there are a large number of catchments around the world, especially in developing countries where no flow data is available. Such catchments are termed as ungauged catchment Predicting runoff response in such catchments remains a complex, unsolved problem needing urgent resolution. Considering the scope and importance of the prediction in the ungauged basin (PUB), the International Association of Hydrological Sciences put forward PUB as an initiative for the decade of 2003-2012.

Ungauged catchments can be modeled well by borrowing parameters from an analogue donor catchment. There exist three popular regionalization procedures to transfer the parameter from a donor gauged catchment to a target ungauged catchment: regression, spatial proximity, and physical similarity. In regression analysis, the regression equation is used to relate stream and

catchment characteristics with the model parameters. Generally, multiple linear regression is used in which catchment attributes are treated as independent variables and model parameter as a dependent variable. This approach assumes that the relationship between catchment attributes and model parameters is well-behaved, however, it has been found that model parameters are significantly affected by the calibration period and input accuracies. Furthermore, it assumes that the selected catchment attribute provides enough information on the behavior of ungauged catchment (Oudin et al. 2008). In physical similarity approach, parameters from donor (gauged) catchments that are "physically" similar to ungauged catchments are transferred. The rationale behind this approach is that catchments with similar physical properties behave hydrologically similar. Generally, this approach includes defining several physical properties and then ranking them based on similarity to identify the donor catchment. In spatial proximity approach, parameters from donor (gauged) catchments that are near to ungauged catchments are transferred. It follows the assumption that the catchments nearby have similar climatic and catchment condition. It has been found that this approach performs better than physical similarity and regression analysis (Oudin et al. 2008; Zhang and Chiew 2009).

Prediction in ungauged catchments has been performed by using different hydrologic models such as McMaster University-Hydrologiska Byrans Vattenbalansavdelning (MAC-HBV) (Samuel et al. 2011), Xinanjiang and SIMHYD (Zhang and Chiew 2009), Soil Water Assessment Tool (SWAT) (Srinivasan et al. 2010), etc. MAC-HBV, Xinanjiang, and SIMHYD models are lumped conceptual models, therefore, they are not suitable for larger catchments. SWAT developed by the US Department of Agriculture-Agriculture Research Service (USDA-ARS) is capable of simulating flow in a stream operating on a daily time step (Santhi et al. 2001). Since the size of Soapstone branch catchment is small resulting in a smaller time of concentration, the

daily time step of SWAT is not recommended. Other hydrologic models which can be used for prediction in the ungauged catchment are Hydrological Simulation Program Fortran (HSPF), Hydrologic Engineering Center's-Hydrologic Modeling System (HEC-HMS), etc. HSPF is a semi-distributed, conceptual model based on Stanford watershed model and can simulate the hydrological response of a catchment (Johnson et al. 2003). However, it contains a large number of parameters which cannot be obtained from field data and needs to be determined through calibration (Singh et al. 2005). Since the complexity of parameter transfer increases with the increased number of parameters, HSPF is not suitable for parameter transfer process. HEC-HMS developed by US Army Corps of Engineers is a mathematical hydrologic model capable of simulating runoff processes in a dendritic watershed system (Feldman 2000). HEC-HMS, unlike SWAT, can simulate for time steps ranging from 1 minute to 1 day and, has fewer parameters than HSPF, most of which can be obtained from field data. Furthermore, HEC-HMS has been found to perform better than SWAT and HSPF in simulating both streamflow and total suspended solids (Pak et al. 2015). Therefore, HEC-HMS model was used in this study for the parameter transfer to ungagged watershed.

2.2 HEC-HMS MODEL

HEC-HMS is an advancement of prior HEC-1 software developed by Leo R. Beard in 1967. HEC-1 software was revised multiple times after that, including major revision in 1973 and 1981. HEC-HMS was developed from HEC-1 in 1998 by adding graphical user interface as well as improving the quality of simulation results by utilizing modern computation techniques. Figure 2.1 represents the simple conceptualization of HEC-HMS for simulating watershed runoff.

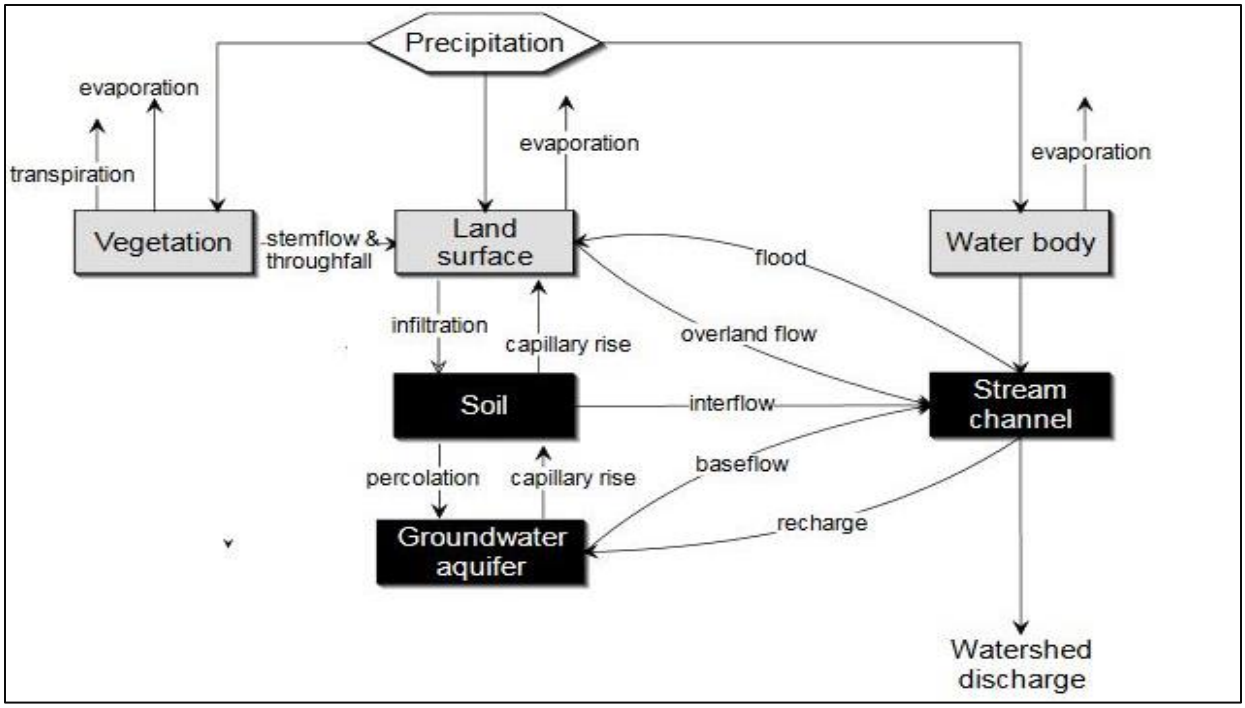

Figure 2.1 Systems Processes in HEC-HMS for Simulating Watershed Runoff (Feldman 2000)

The precipitation occurring during a storm event is intercepted by vegetation, falls into a waterbody or on the land surface. The part of precipitation intercepted by vegetation is removed by the process of evapotranspiration, whereas, the precipitation falling on the land surface is either lost through evaporation and infiltration or gets converted into the overland flow to reach out to stream channels. The remaining small portion of rainfall falling on a waterbody is lost through evaporation or reaches the main stream channel. The portion of infiltrated precipitation is either discharged comparatively quicker through the interflow or gets percolated down to the groundwater and then reaches the stream channel through the slow process of baseflow.

HEC-HMS consists of four different models to represent each component of the runoff process viz. model to compute runoff volume, model of direct runoff, model of baseflow, and model of channel flow. Each of these models has several options within HEC-HMS for the choice of the user depending upon the watershed of interest and the tasks to be performed. Furthermore,

its model setup consists of four main model components viz. basin model, meteorological model, control specifications, and input data. A basin model within HEC-HMS is the physical representation of the watershed using hydrologic elements and their connectivity such as subbasins, reservoirs, streams, etc. The computation process in the basin model always proceeds from upstream to downstream direction. The meteorological component consists information on meteorological boundary conditions for each of the subbasins. Control specifications allow the user to define the start, stop, and the time interval for each simulation. Input data for HEC-HMS can take any of these three forms: time series, paired data, and grid data.

HEC-HMS is capable of simulating both event and continuous hydrologic simulations. Soil conservation services curve number method (Knebl et al. 2005), initial loss and constant rate method (Arekhi 2012) etc. included in HEC-HMS have been widely used to simulate a single storm event. For continuous simulation within HEC-HMS, the soil-moisture accounting algorithm (SMA) is available.

2.2.1 SOIL MOISTURE ACCOUNTING ALGORITHM

The SMA algorithm is a continuous, semi distributed and empirical loss method available within HEC-HMS. It is based on Leavesley's Precipitation Runoff Modeling System (PRMS). It consists of series of different layers for the movement of water within the land based components (Figure 2.2). This algorithm allows HEC-HMS to compute the rainfall excess, groundwater flow, and deep percolation; and then updates the moisture content within different storages during each time step. The one-dimensional SMA loss model allows the water to flow in only one direction during each time step. This introduces errors in the model at larger spatial scales. Complex behavior of flow due to heterogeneity in landscape and soil properties cannot be well accounted

by a one-dimensional hydrologic model. An improvement over this error in HEC-HMS is achieved by including separate storage compartments and semi-distributed modeling capabilities (Holberg 2015).

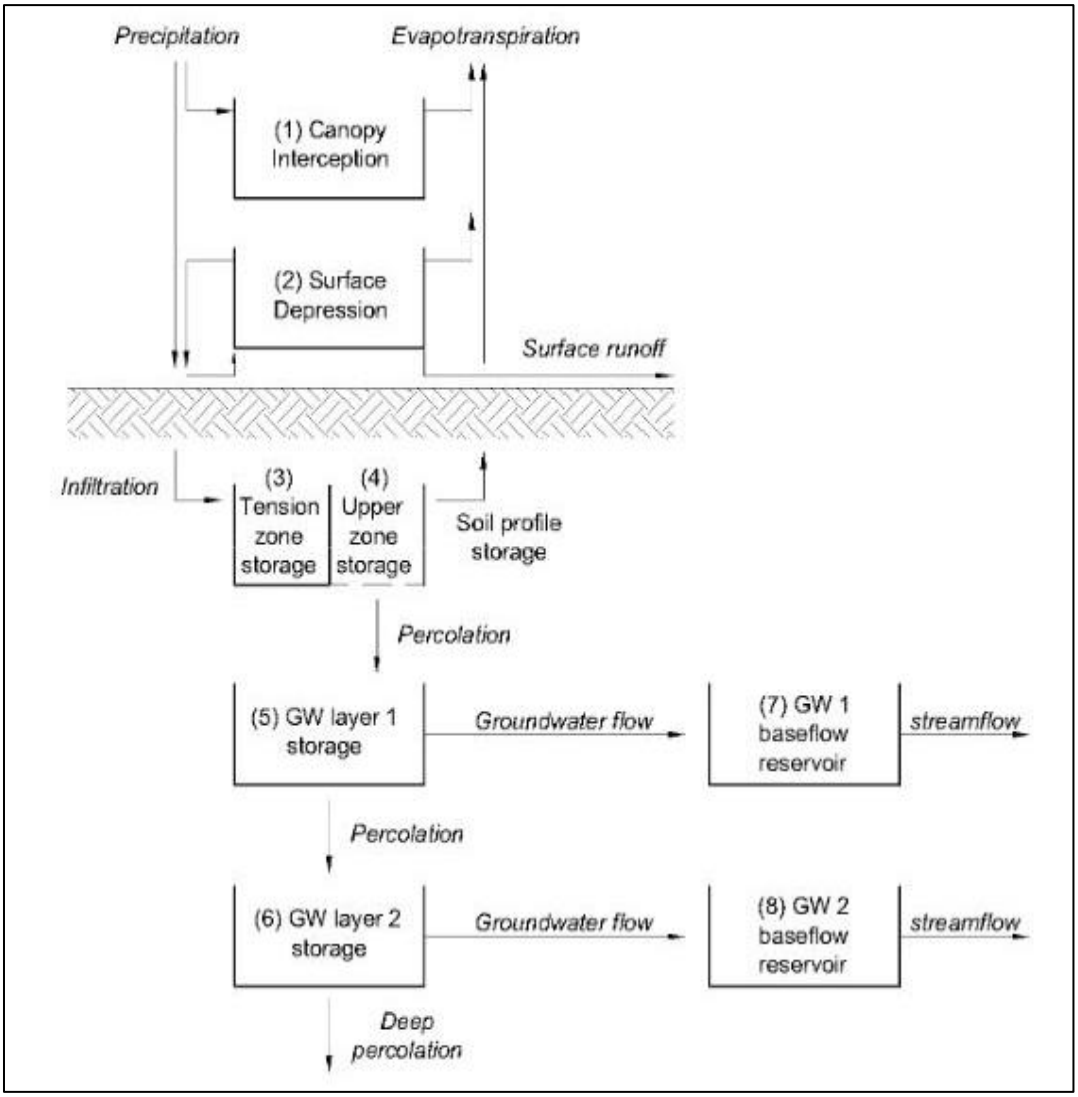

Figure 2.2 Schematic of HEC-HMS SMA Model (Feldman 2000)

The layers in SMA model includes canopy storage representing interception by trees and shrubs, surface storage accounting for depressions in the soil surface, soil storage for water held in a top layer of the soil and two groundwater layers for representing interflow and baseflow. The

soil storage is further divided into an upper zone storage and tension zone storage. The upper zone represents the amount of water held in the soil pores whereas the tension storage represents water attached to the soil particles. Therefore, the upper zone loses water through both percolation and evapotranspiration whereas the tension storage zone loses water only through the process of evapotranspiration.

Model computation is decided based on whether it is a period of precipitation (wet) or evapotranspiration (dry). During the precipitation period, canopy storage is first filled. Precipitation in excess of canopy storage together with water in surface depression is available for infiltration. If the volume of water available for infiltration is greater than the potential infiltration volume then excess water is stored in the surface depression storage. Runoff occurs when the surface storage is filled. The infiltrated volume of water then fills the soil storage. Water in the soil storage percolates down to the first groundwater layer where a part of it is routed out of the layer or further percolates down to the second groundwater layer. Depending upon the size of the second groundwater layer and the coefficient, routing and percolation process occurs. Deep percolation from the second groundwater layer is considered a loss from the model.

The model computes evapotranspiration (ET) only during the period of no precipitation. ET occurs first from the canopy storage. ET is then satisfied from the surface depression storage when the canopy storage becomes empty. After the surface depression storage is completely depleted then water is lost through the upper soil zone storage at the potential infiltration rate. If the water available in the these mentioned storages is not sufficient to satisfy the ET, then water is removed from the tension zone storage. The ET rate from the tension zone storage is based on water available in storage to the maximum tension zone storage capacity.

The equations in the SMA model are used to define the rate of rainfall loss at each time step and then at the end of time step it is converted to volume by multiplying the current rate with the simulation time step.

The soil infiltration rate at each time step is a linear function of the maximum soil infiltration rate provided by the user, the current soil storage, and the maximum soil storage (Eqn. 2.1). The actual infiltration rate is the minimum of the potential infiltration rate and water available for infiltration.

$$\text{PotSoilInfil} = \text{MaxsoilInfil} - \frac{\text{CurSoilStore}}{\text{MaxSoilStore}}\text{MaxsoilInfil} \qquad (2.1)$$

Where,

PotSoilInfil = potential soil infiltration rate at a time step

MaxsoilInfil= maximum rate of infiltration entered by the user

CurSoilStore = current moisture level in the soil storage

MaxSoilStore = maximum soil storage capacity

Potential percolation from the soil storage to the first groundwater layer, from the first to the second groundwater layer and the deep percolation is a function of specified maximum percolation rate and the fraction of storage filled in the participating storages (Eqn. (2.2)).

$$\text{Potperc} = \text{Maxperc} * (\text{Frus}) \ * (1 - \text{Frls}) \qquad (2.2)$$

Where,

Potperc = potential percolation rate at a time step

Maxperc= maximum percolation rate entered by the user

Frus = fraction of storage filled in upper storage

Frls = fraction of storage filled in lower storage

For the deep potential percolation rate, the lower storage is considered infinite, thus the deep percolation rate only depends on the water filled in the groundwater layer 2 and the maximum deep percolation rate.

HEC-HMS has been effectively used to predict streamflow in ungauged catchments using loss methods such as the initial and constant-rate method (Song et al. 2011) and the deficit and constant rate (Halwatura and Najim 2013). The SCS Curve Number (CN) method is a simple method for predicting runoff because of a fewer number of parameters. However, CN is one of the most sensitive parameters and a 15–20% change in its value, doubles or halves the volume of runoff. Furthermore, CN is highly sensitive to the land cover type of the catchment. Since it is very complicated to find a donor catchment with the exact land cover composition as that of the Soapstone branch, it cannot be efficiently used for estimating runoff in the ungauged catchment. On the other hand, SMA model is least sensitive to land cover parameters and is mostly affected by the soil parameters. However, continuous simulation in ungauged catchments using full parameter transfer of SMA algorithm has never been tried due to a large number of parameters included within it.

2.2.2 CALIBRATION IN HEC-HMS AND PERFORMANCE CRITERIA

The model calibration refers to the tuning of model parameters until model output matches reasonably with the observed data. The degree of match between model output and observed data is described quantitatively with the help of objective function such as Nash-Sutcliffe efficiency

(NSE), percent error in volume (PEV), percent error in peak (PEP), etc. The main purpose of the calibration procedure is to maximize or minimize these objective functions based on their type. There exist two calibration techniques in HEC-HMS viz. manual calibration and automatic calibration (Feldman 2000). The manual calibration refers to the time-consuming process of changing parameter values by the user itself and is highly dependent on user's understanding of physical properties of the catchment and expertise in hydrologic modeling. In automated calibration, parameters are iteratively changed in the range defined by the user until the value of the objective function is minimized or maximized. Two methods for automated calibration exists in HEC-HMS, i.e., the univariate gradient method and the Nelder and Mead (NM) method. In the univariate gradient method, the parameter is changed one at a time and other parameters are held constant whereas, in the NM method, a downhill simplex algorithm is used to evaluate all parameters simultaneously and determining which parameters to adjust (Feldman 2000).

After the calibration, HEC-HMS output can be used for various tasks ranging from regulation to research if it is scientifically sound and strong. For a model to be considered fit for further usage, a comparison between model computed flow and measured flow using both visual and statistical approach is needed. The visual comparison allows the user to have a general overview of model performance whereas the statistical comparison provides a quantitative measurement of goodness-of-fit. An ASCE task committee (1993) suggests Nash Sutcliffe efficiency (NSE) (Eqn. (2.3)) as a goodness-of-fit criterion for evaluating the continuous hydrologic model. NSE measures the relative magnitude of residual variance to the variance of flows. Its value varies from $-\infty$ to +1 (inclusive), 1 being the best fit where computed model discharge matches with the observed discharge for the entire simulation period. A negative value

suggests the model is biased and is not predicting better than using the average of the observed data (McCuen et al. 2006; Nash and Sutcliffe 1970).

$$NSE = 1 - \frac{\sum_{i=1}^{n}(Q_{sim} - Q_{obs})^2}{\sum_{i=1}^{n}(Q_{obs} - \overline{Q_{obs}})^2} \quad (2.3)$$

Where,

Q_{sim}=simulated model discharge

Q_{obs}= observed streamflow discharge

$\overline{Q_{obs}}$= mean of the observed streamflow discharge

Apart from NSE, the percent bias was used for evaluating the performance of the HEC-HMS model. The percent bias (Eqn. (2.4)) measures the average tendency of simulated data to be larger or smaller than the observed ones. The value ranges from 0 to $\pm$100%, 0 being the optimal value. A negative value indicates that the model is biased with overestimation whereas a positive value suggests that the model is biased with underestimation (Gupta et al. 1999).

$$PBIAS = \frac{\sum_{i=1}^{n}(Q_{obs} - Q_{sim}) * 100}{\sum_{i=1}^{n}(Q_{obs})} \quad (2.4)$$

A standardization technique is required to recommend the applicability of a watershed model based on the range of values for the performance criteria mentioned. A study performed by Moriasi et al. (2007) provides a general performance rating for recommended statistics for a monthly time step which can be used for performance rating for daily time step too.

2.3 MODIFIED UNIVERSAL SOIL LOSS EQUATION

The Universal Soil Loss Equation (USLE) is one of the most widely adopted methods for estimating soil erosion worldwide. Mathematical equations used to estimate the amount of soil erosion began in the 1940's. The first equation ever developed related to USLE, tried to quantify the effects of soil slope length and steepness, and was published by Zingg (1940). This study was followed by the development of crop and support practice factors by Dwight D. Smith, an employee of USDA-SCS at the University of Missouri in Columbia (Smith 1941). Smith further introduced tolerable soil loss limits. This developed tolerable soil loss limit equation was then used in Iowa by G.M. Browning and his workers who added soil erodibility factor. A national committee in Ohio in 1946 developed a rainfall factor. A combination of all these studies helped in the development of USLE. The mathematical expression for USLE is given in

$$A = R * K * LS * C * P \tag{2.5}$$

Where,

A = soil loss per unit area with units depending on the units selected for K and R

R= rainfall erosivity factor

K= Soil erodibility factor

LS = topographic factor considering the effect of slope length and steepness of the slope

C = cover and management factor

P = support practice factor

After the development of USLE, additional researches were carried out which included revised isoerodent maps (spatial distribution of R factor), a new equation to reflect slope length and steepness, etc. All these improvements to the original USLE were incorporated into the Revised Universal Soil Loss Equation (RUSLE). However, there were two main issues with USLE and RUSLE viz. determination of sediment yield and failure to consider the runoff effect on soil erosion. Sediment yield at a specific point on watershed is defined as the total amount of eroded soil reaching that point, regardless of the origin of detached soil particle. Since USLE and RUSLE only provided an annual estimate of soil erosion occurring on a watershed, determination of sediment yield required further estimation of sediment delivery ratio (SDR, Eqn. (2.6)). Also, as the overland flow moves downstream, it gains energy and erodes more particles. Both USLE and RUSLE lacked any consideration of runoff producing sediments which leads to the wrong estimate in the event based calculation and thus, the annual soil erosion amount (Kinnell 2005).

$$SDR = \frac{Y}{E} \tag{2.6}$$

Where,

SDR= Sediment Delivery Ratio

Y = Average annual sediment yield per unit area

E = Average annual erosion over the same area

The Modified Universal Soil Loss Equation (MUSLE) is an advancement over both originally developed USLE and RUSLE, developed by replacing the rainfall erosivity factor with the runoff energy factor (Williams 1975). Unlike USLE and RUSLE, it is an event based soil loss model which considers the effect of runoff energy on generating sediment. Furthermore, it can provide an estimation of sediment yield. Apart from the runoff energy factor, other factors used in

MUSLE are same as those of USLE which include the soil erodibility factor *R*, topographic factor *LS* (slope length and slope steepness), soil cover factor *C*, and conservational practice factor *P*. It was developed by collecting the data from 18 small watersheds with areas ranging from 132 to 4380 acres. Several combinations of the volume of runoff and peak discharge were tried and the most accurate sediment prediction equation was finalized. The mathematical expression for MUSLE is given in Equation (2.7).

$$S = 95 * (Q * q_p)^{0.56} * K * LS * C * P \quad (2.7)$$

Where,

S = Sediment yield in tons

Q = Volume of runoff in acre-feet

q_p = peak flow rate in cubic feet per second

CHAPTER 3: STUDY AREA AND INPUT DATA

3.1 STUDY AREA

3.1.1 DONOR CATCHMENT

Choctawhatchee river catchment draining near Newton, Alabama covers an area of 686 sq. miles (Figure 3.1) and is spread across Dale, Barbour and Henry County of Alabama. It was selected as donor catchment for the parameter transfer of the SMA model to the Soapstone branch catchment. The catchment outlet is 15 miles northeast of Dothan and 39 miles southeast of Troy city. The catchment is primarily comprised of five land cover classes viz. forest, rangeland, agricultural land, wetlands, and developed area. Their respective composition is shown in Table 3.1. The elevation of the catchment ranges from 142 ft. to 636 ft. with average basin elevation of 375 ft. above the mean sea level. The average basin slope is 6.67%. The average basin precipitation is 54.72 inches which is computed as an average of normal annual precipitation for four rainfall stations viz. Abbeville, Dothan, Troy and Union Springs (Arguez et al. 2012) around the catchment. Average annual precipitation for these four rainfall stations is presented in Table 3.2. Soils of different textures viz. loamy sand, sandy loam, sand, etc. are present within the catchment with the highest composition of loamy sand (Service 1995).

Table 3.1 Land Cover Classes and their Respective Composition for Donor Catchment

Land Cover	Composition
Forest	48.5%
Rangeland	28.4%
Agricultural land	11.8%
Wetland	6.0%
Developed Area	4.5%

Table 3.2 Average Annual Precipitation for Rainfall Stations around Donor Catchment

Rainfall station	Average annual precipitation (in inches)
Abbeville	55.51
Dothan	55.91
Troy	52.05
Union Springs	55.42

„

3.1.2 RECEIVER CATCHMENT

Double Bridges Creek draining near Enterprise, Alabama covers an area of 21.34 sq. miles (Figure 3.2) and is spread across Coffee County of Alabama. It was used as an assumed receiver catchment to verify the parameter transfer of the SMA model. The catchment outlet is about 36 miles South of Troy and 34 miles West of Dothan city. The catchment consists of five landcover classes viz. Forest, agricultural land, developed area, wetland, and rangeland. Their respective composition is shown in Table 3.3. The elevation of the catchment ranges from 61 ft. to 144 ft. with average catchment elevation of 102 ft. above the mean sea level. The average basin slope is 1.77%. The average basin precipitation is 53.98 inches which is computed as an average from data involving two rainfall stations viz. Troy and Dothan. Average annual precipitation of these two rainfall stations is provided in Table 3.2.

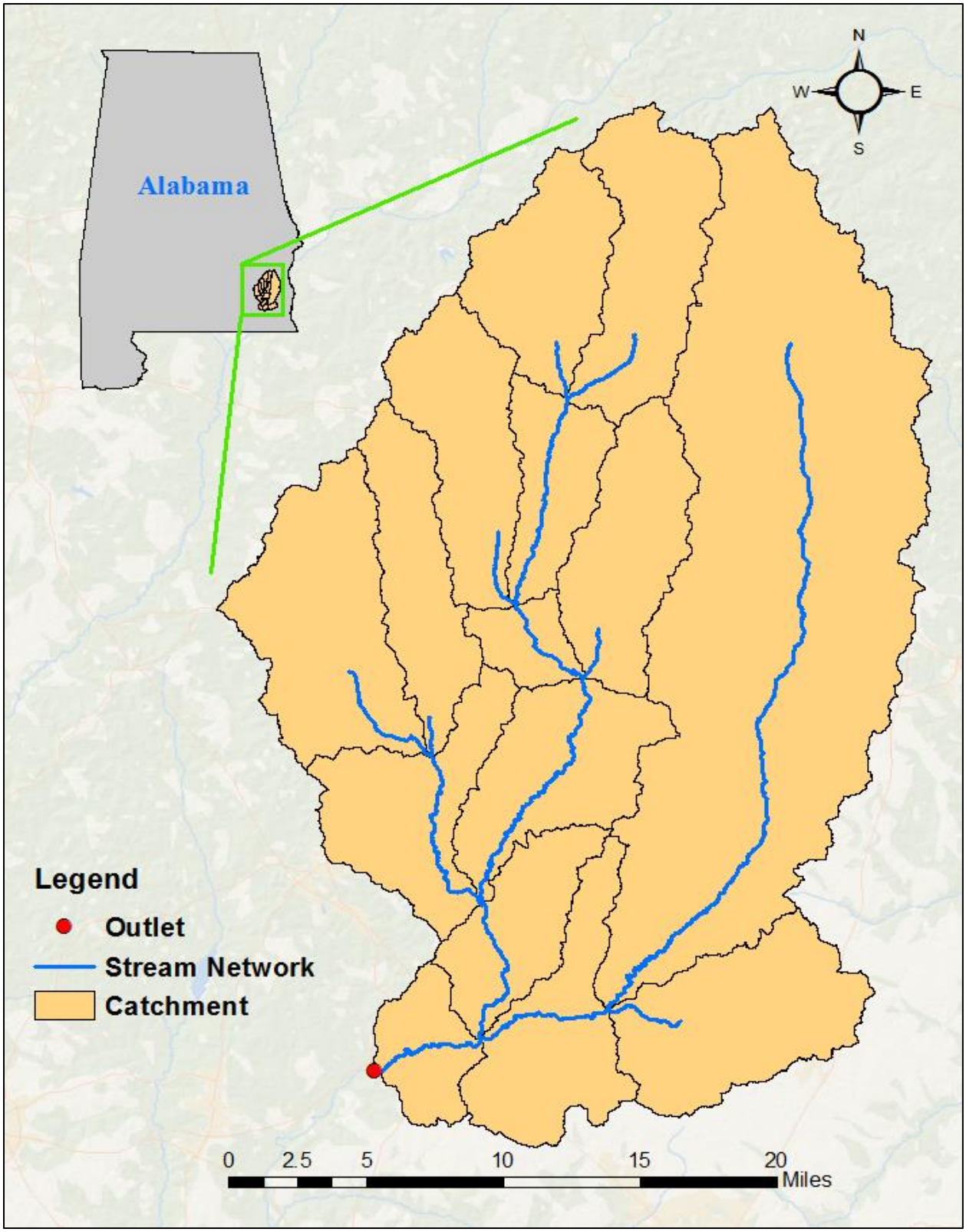

Figure 3.1 Location of Donor Choctawhatchee River Catchment

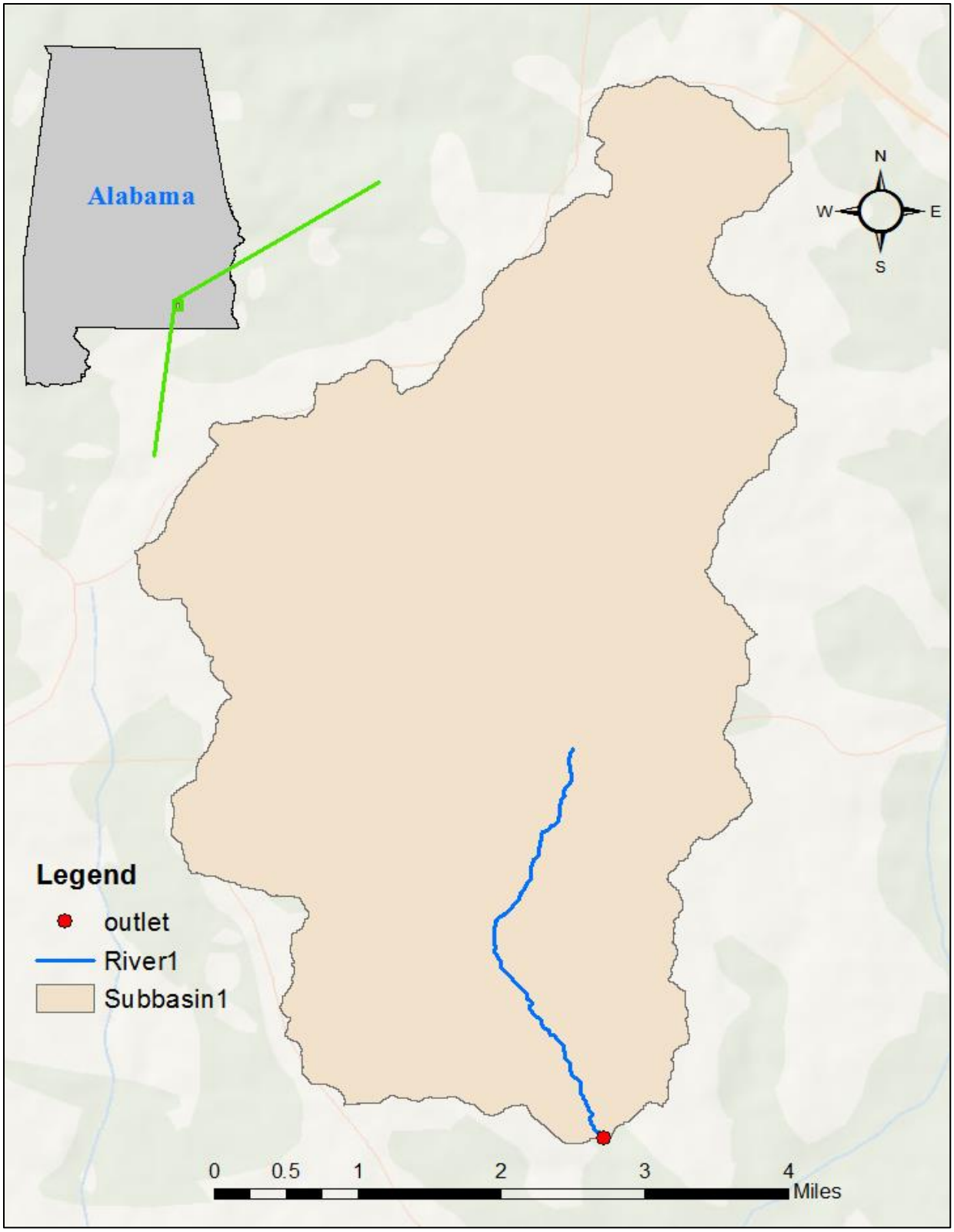

Figure 3.2 Location of Double Bridges Creek Receiver Catchment

Table 3.3 Land Cover Classes and their Respective Composition for Receiver Catchment

Land Cover	Composition
Forest	55.6%
Agricultural land	37.1%
Developed area	5.0%
Wetland	1.3%
Rangeland	0.8%

3.2 INPUT DATA

3.2.1 DIGITAL ELEVATION MODEL

Digital elevation model (DEM) provides information about the elevation of the land surface in a pixel based format. It can be effectively used in catchment delineation and provides important information on the slope of the land surface. Elevation information is obtained first through the process of photogrammetry, Light Detection and Ranging (LIDAR) or land surveying and then processed to create DEM. The 10 m spatial resolution DEM were obtained from AlabamaView (http://www.alabamaview.org/) for the counties where both the donor and receiver catchments are spread and then clipped using ArcGIS. DEM for the donor and receiver catchments is shown in Figure 3.3.

3.2.2 LAND COVER DATA

Land cover data is available from National Land Cover Database (NLCD) created by Multi-Resolution Land Characteristics (MRLC) Consortium for the entire United States at a spatial resolution of 30 m and 5 years temporal resolution (Homer et al. 2015). It was developed using the Landsat 5 Thematic Mapper (TM) imagery and is based on Modified Anderson Land Cover classification scheme. Grid values and class description for NLCD 2011 Landcover map is

presented in Table 3.4. The 2011 land cover map was obtained for the entire United States and was clipped for both donor and receiver catchments as shown in Figure 3.4.

Table 3.4 Class Values and Description for NLCD 2011 Land Cover Map

Class\Values	Classification Description
Water	
11	Open water
12	Perennial Ice/Snow
Developed	
21	Developed, open space
22	Developed, low intensity
23	Developed, Medium intensity
24	Developed, High intensity
Barren	
31	Barren Land
Forest	
41	Deciduous Forest
42	Evergreen Forest
43	Mixed Forest
Shrubland	
51	Dwarf Scrub
52	Shrub/Scrub
Herbaceous	
71	Grassland/Herbaceous
72	Sedge/Herbaceous
73	Lichens
74	Moss
Planted/Cultivated	
81	Pasture/Hay
82	Cultivated Crops
Wetlands	
90	Woody Wetlands
95	Emergent Herbaceous Wetlands

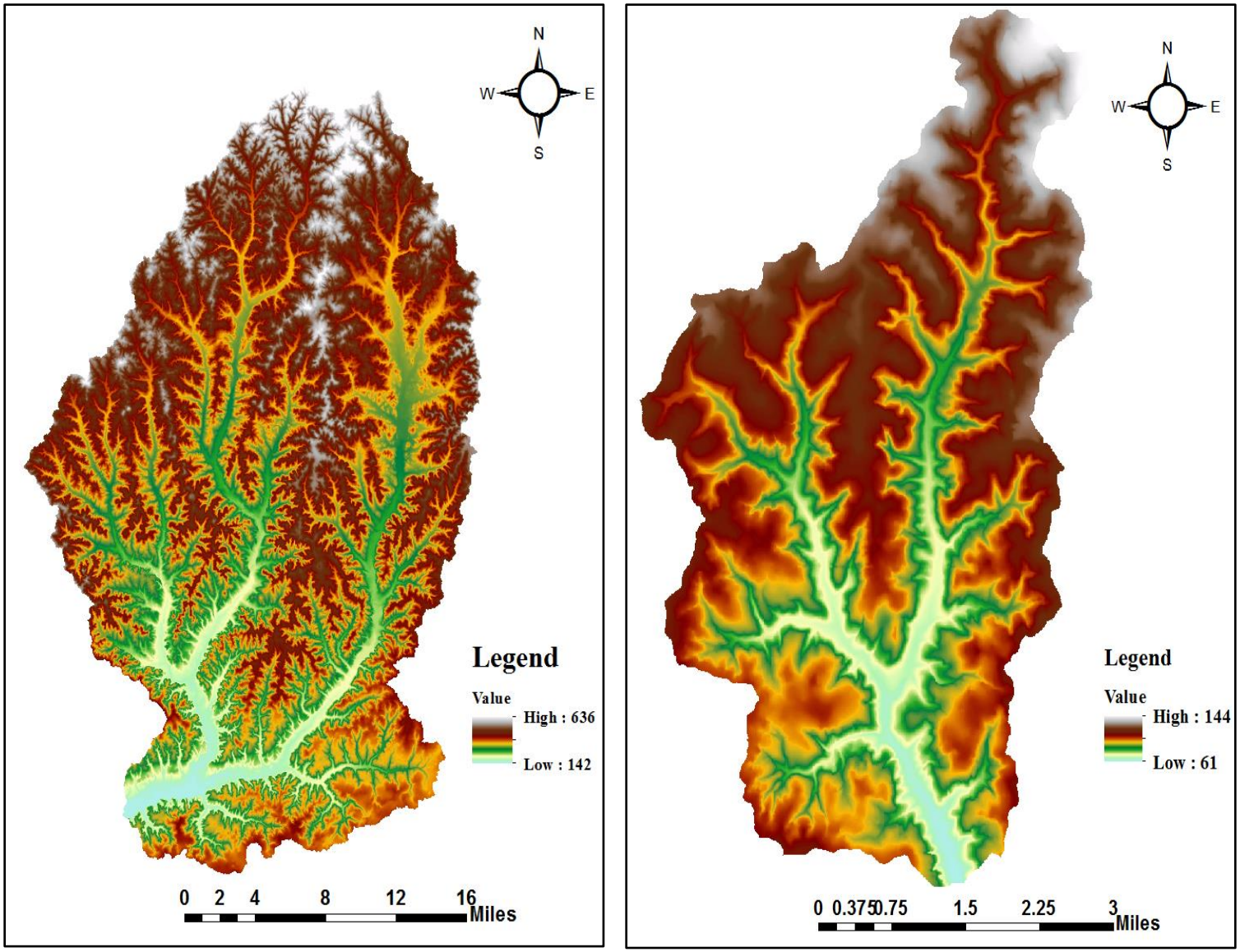

Figure 3.3Digital Elevation Model of Donor Catchment (Left) and Receiver Catchment (Right)

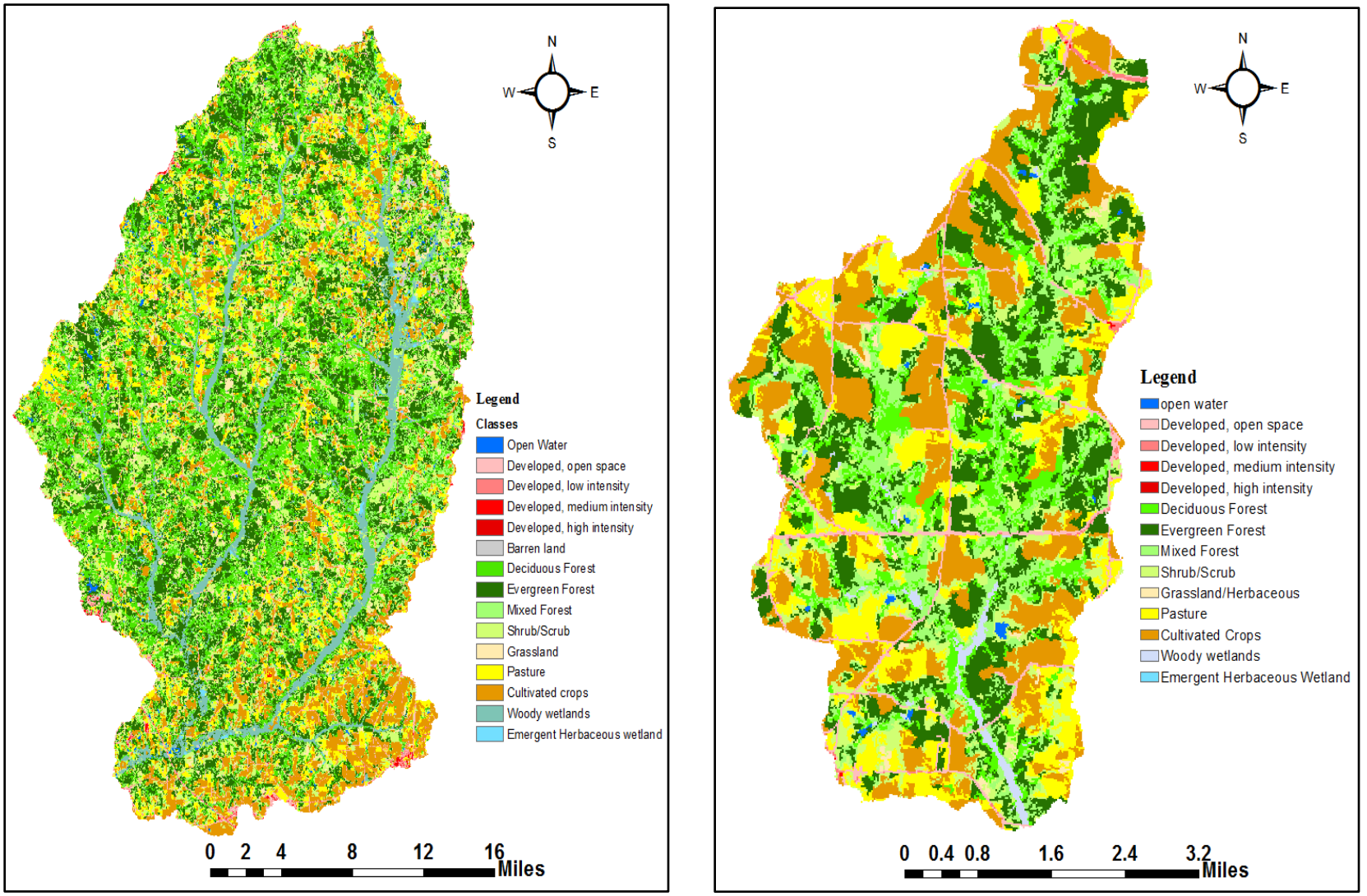

Figure 3.4 NLCD 2011 Land Cover map of Donor Catchment (Left) and Receiver Catchment (Right)

3.2.3 SOIL DATA

Fine-scale soil data are available in the Soil Survey Geographic Database (SSURGO) collected over a century by the National Cooperative Soil Survey for almost all areas of the country. The source of soil information comes from field observations and laboratory testing of the collected soil samples. The scale of information ranges from 1:12000 to 1:63360. It was designed to be used for county and parish, and watershed resource planning and management. It is much more detailed than State Soil Geographic (STATSGO) which was originally designed for planning, management and monitoring of regional, multiscale, river basin, state and multiple counties (Reybold and TeSelle 1989; Service 1995). SSURGO dataset includes map data, tabular data and a metadata file containing information on how tables and maps were created for each different county of all 50 states.

Soil data was obtained from SSURGO database for three different counties, i.e., Dale, Barbour and Henry County for the donor catchment. As the soil data were available from three different counties, it was merged and then clipped for the catchment. Different information on soil data such as surface texture (Figure 3.6), hydrologic soil group, bulk density, etc. is available and can be plotted with the help of US Department of Agriculture (USDA) Soil Data viewer. The USDA Soil Data viewer is an ArcGIS extension which helps the user to create soil-based thematic maps. Soil information in SSURGO database is distributed among more than 50 tables. Extraction and usage of soil information from these tables is a cumbersome and time-consuming task. With the development of the Soil Data viewer, the user can easily extract required information without going through the database and linking it to the spatial map.

In Alabama, SSURGO data of 16 counties is available only from a survey performed prior to 1965 (Figure 3.5). For the donor catchment, Dale County is among those 16 counties for which recent soil information is not available.

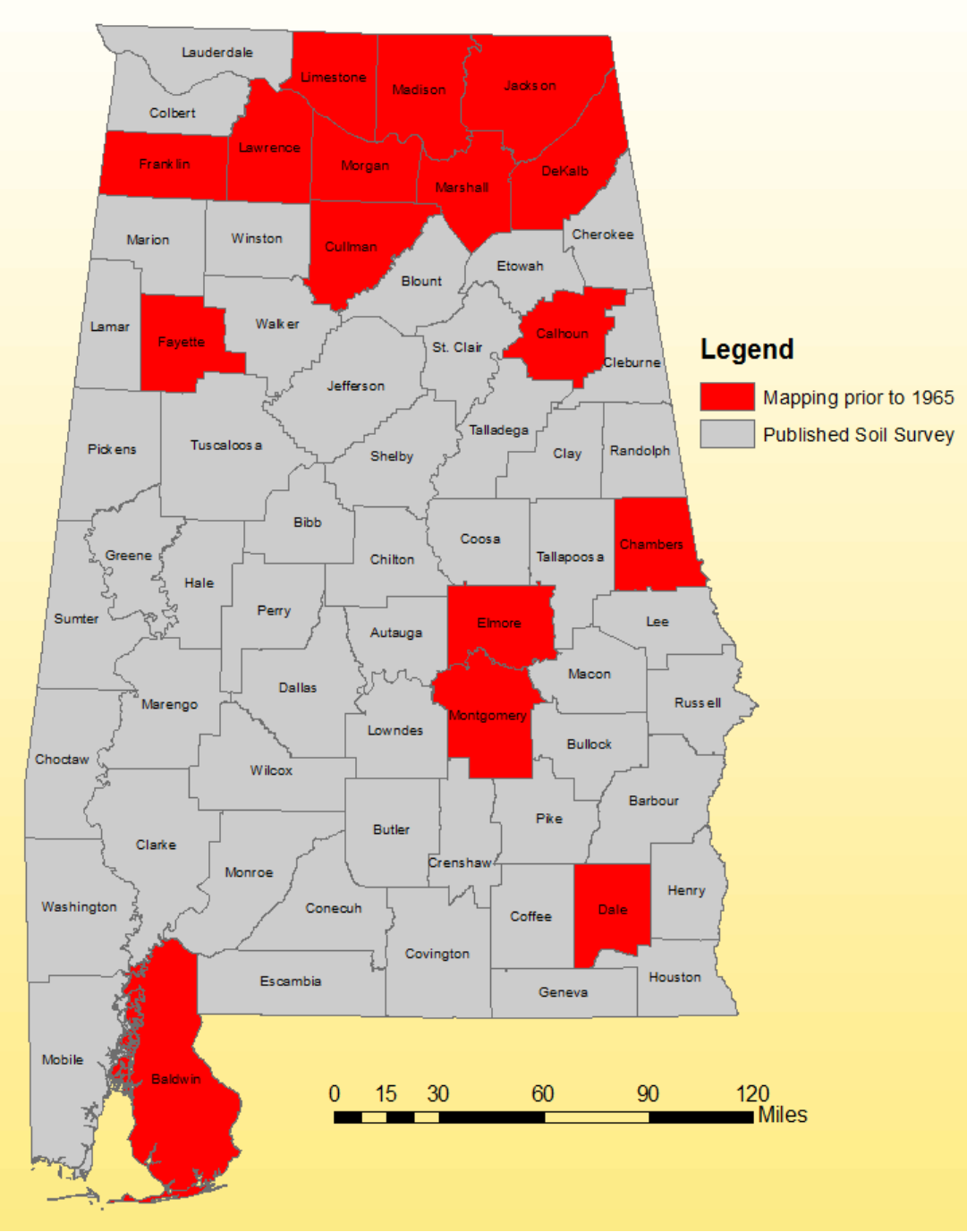

Figure 3.5 Status of Soil Survey in Alabama

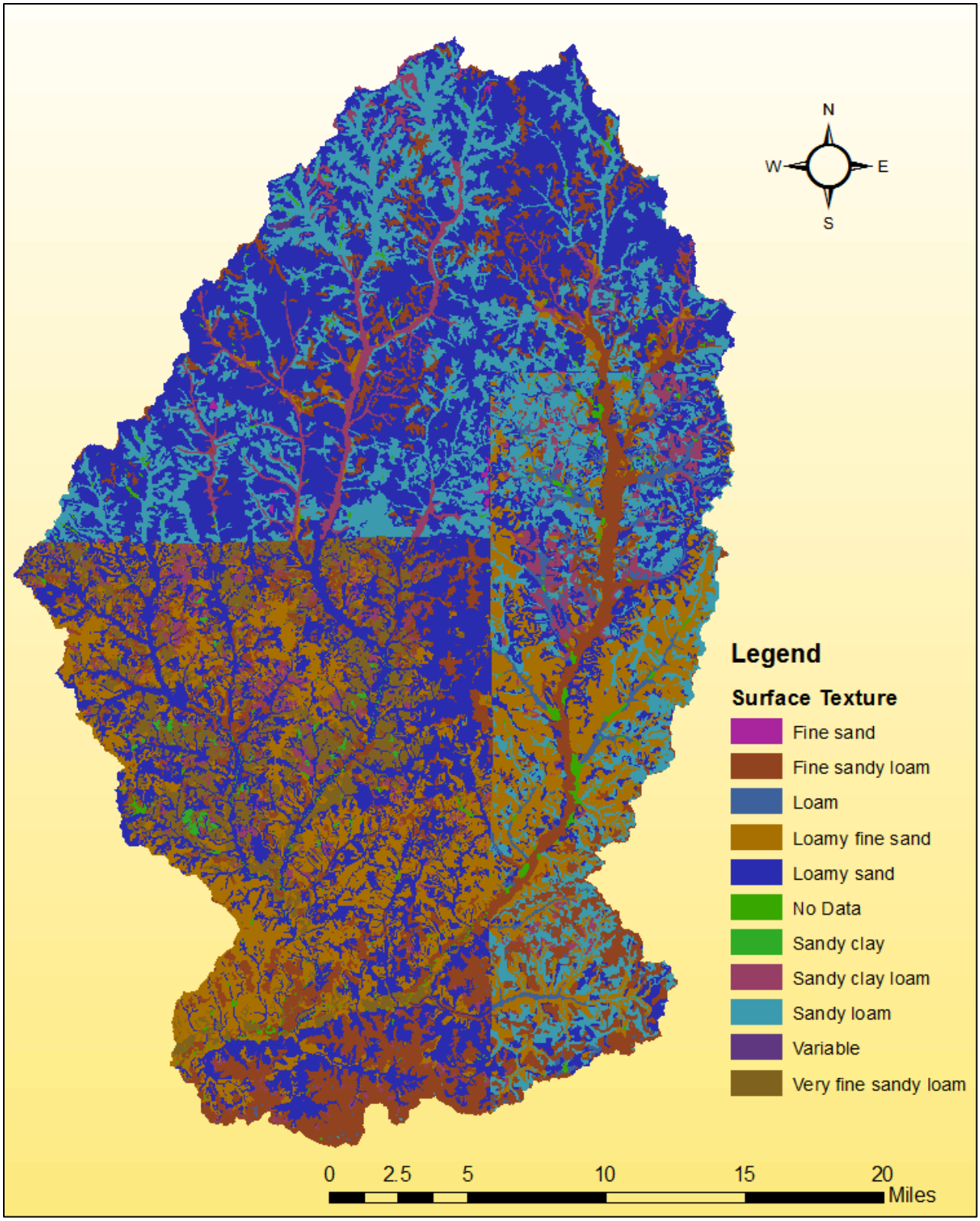

Figure 3.6 Soil Surface Texture of Donor Catchment

3.2.4 PRECIPITATION DATA

Precipitation data is one of the most important inputs for hydrologic modeling. Hourly precipitation data were used for the calibration, validation and as well as simulation of streamflow discharge in the ungauged receiver catchment. Hourly precipitation data were collected from variable sources which include the US Climate Reference Network's quality controlled dataset (Diamond et al. 2013) and the local climatological data (LCD) from the National Oceanic and Atmospheric Administration (NOAA) and Auburn University Mesonet. The precipitation data cover the years from 2009–2015 (Figure 3.8). For the donor catchment, three rainfall stations viz. Troy, Union Springs, and Dothan were used whereas for the receiver catchment hourly rainfall data from Dothan were used. It was found that there were errors and a large number of missing values in precipitation data for Dothan collected from LCD. As an attempt to correct Dothan data, precipitation data for Ozark (22 mi. from Dothan and closer to the catchment) was collected for some of the storm events from Weather Underground (https://www.wunderground.com/). Example precipitation data for Troy is shown in Figure 3.7.

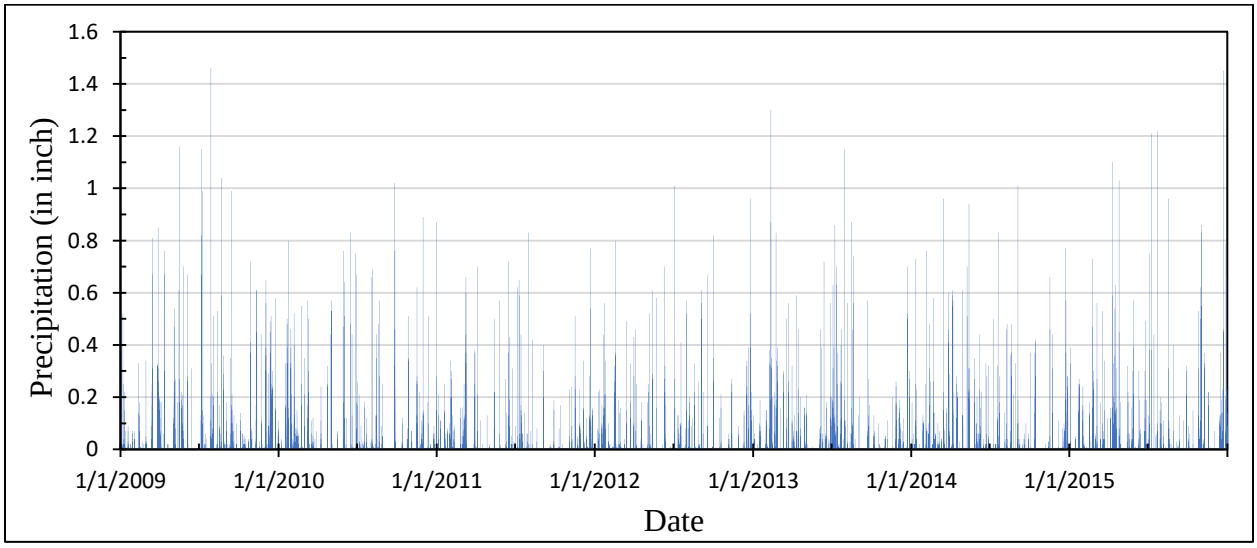

Figure 3.7 Hourly Precipitation Values for Troy (2009–2015)

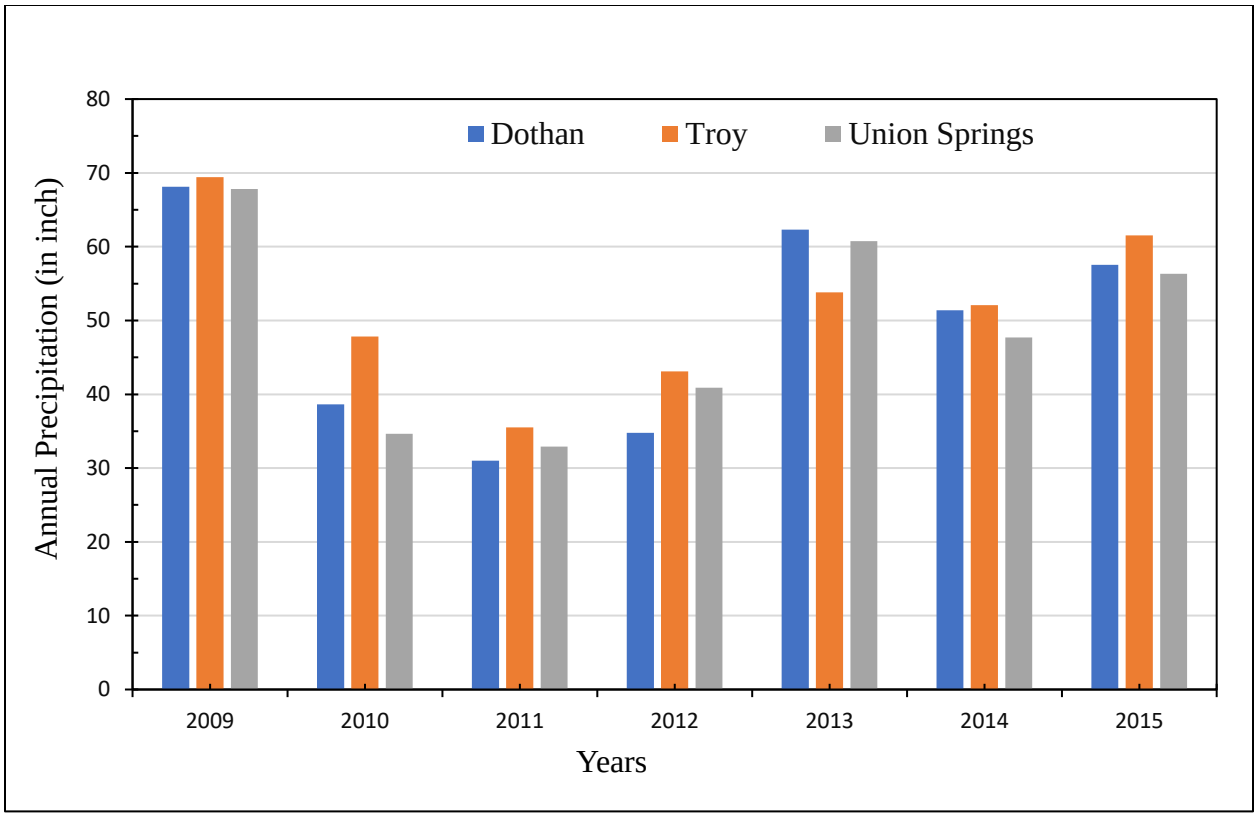

Figure 3.8 Annual Precipitation for Rainfall Stations (2009–2015)

3.2.5 EVAPOTRANSPIRATION DATA

Daily pan evapotranspiration data are available from the NOAA website for selected stations within the United States. Daily pan evapotranspiration data were obtained for stations located in Headland, Alabama for the period of 2009–2013 (Figure 3.9). For years 2014–2015 and days with missing value, monthly average pan evapotranspiration data from Class A pans for Martin Dam (Table 3.5) provided by NOAA (Farnsworth and Thompson 1983) were used. A correction factor of 0.7 is applied to convert pan evapotranspiration to potential evapotranspiration (Hamon 1960).

Table 3.5 Mean Monthly Pan Evapotranspiration for Martin Dam

Month	Mean monthly Pan ET (in inches)
January	1.9
February	2.43
March	4.06
April	5.04
May	6.21
June	6.38
July	6.28
August	6.21
September	4.96
October	4.01
November	2.53
December	2.09

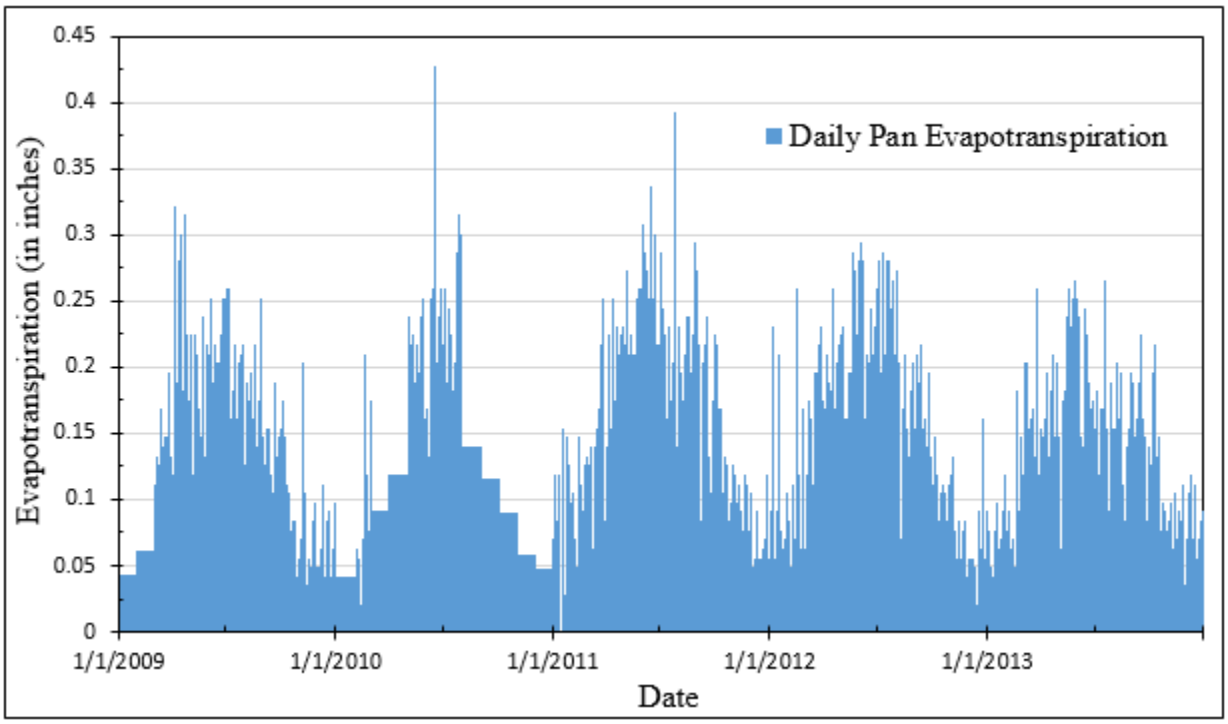

Figure 3.9 Pan Evapotranspiration Data for Martin Dam (2009–2013)

3.2.6 STREAMFLOW DATA

Hourly streamflow data for the donor catchment were obtained from the United States Geological Survey (USGS) for calibration and validation purposes for the period of 2009–2015 (Figure 3.10). For the receiver catchment, 30-minute interval streamflow data were obtained for the period of 2009–2012 (Figure 3.11). For the donor catchment, available USGS gauge station is USGS 02361000 at Choctawhatchee River near Newton, AL. For the receiver catchment, available USGS gauge station is USGS 02362240 at Little Double Bridges Creek near Enterprise, Alabama. For determining groundwater parameters, daily streamflow records were collected for the donor catchment.

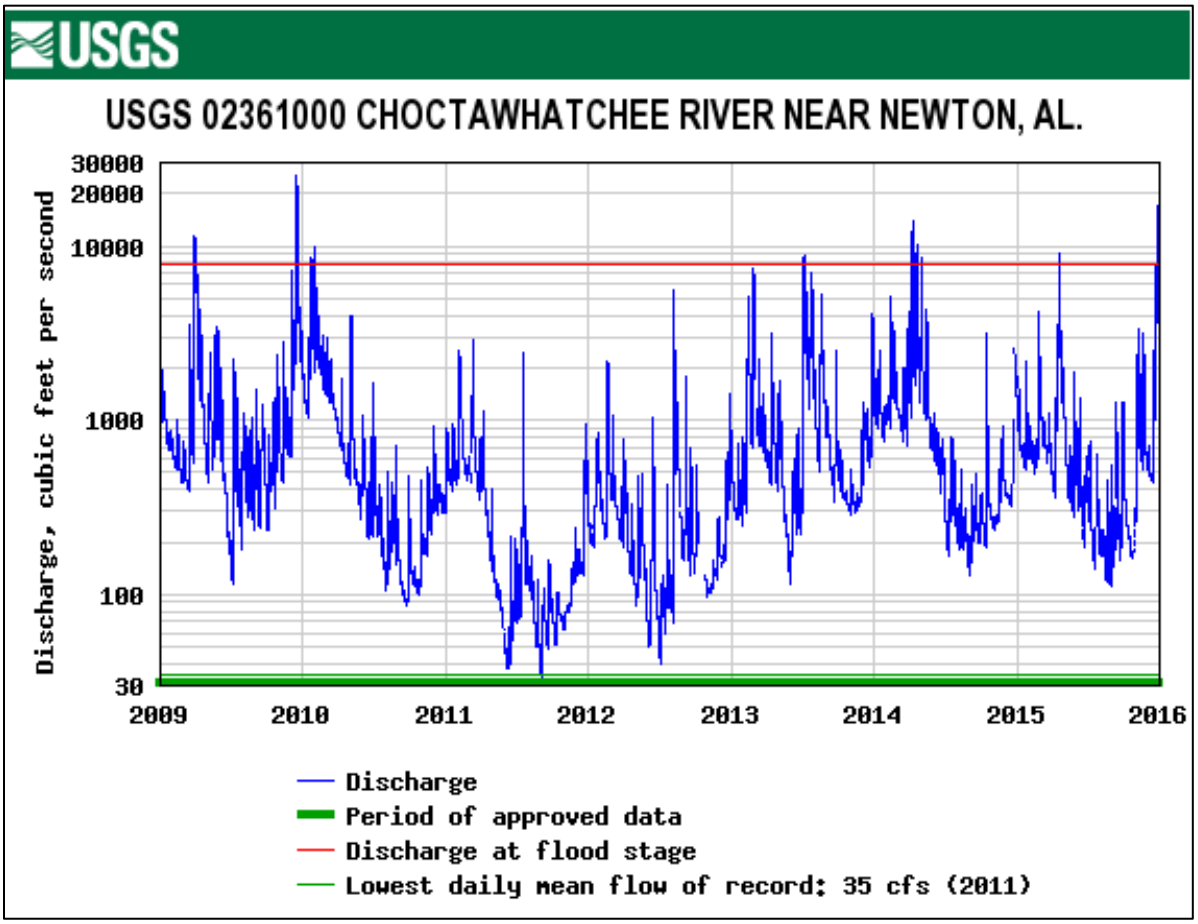

Figure 3.10 Streamflow Hydrograph for Donor Catchment

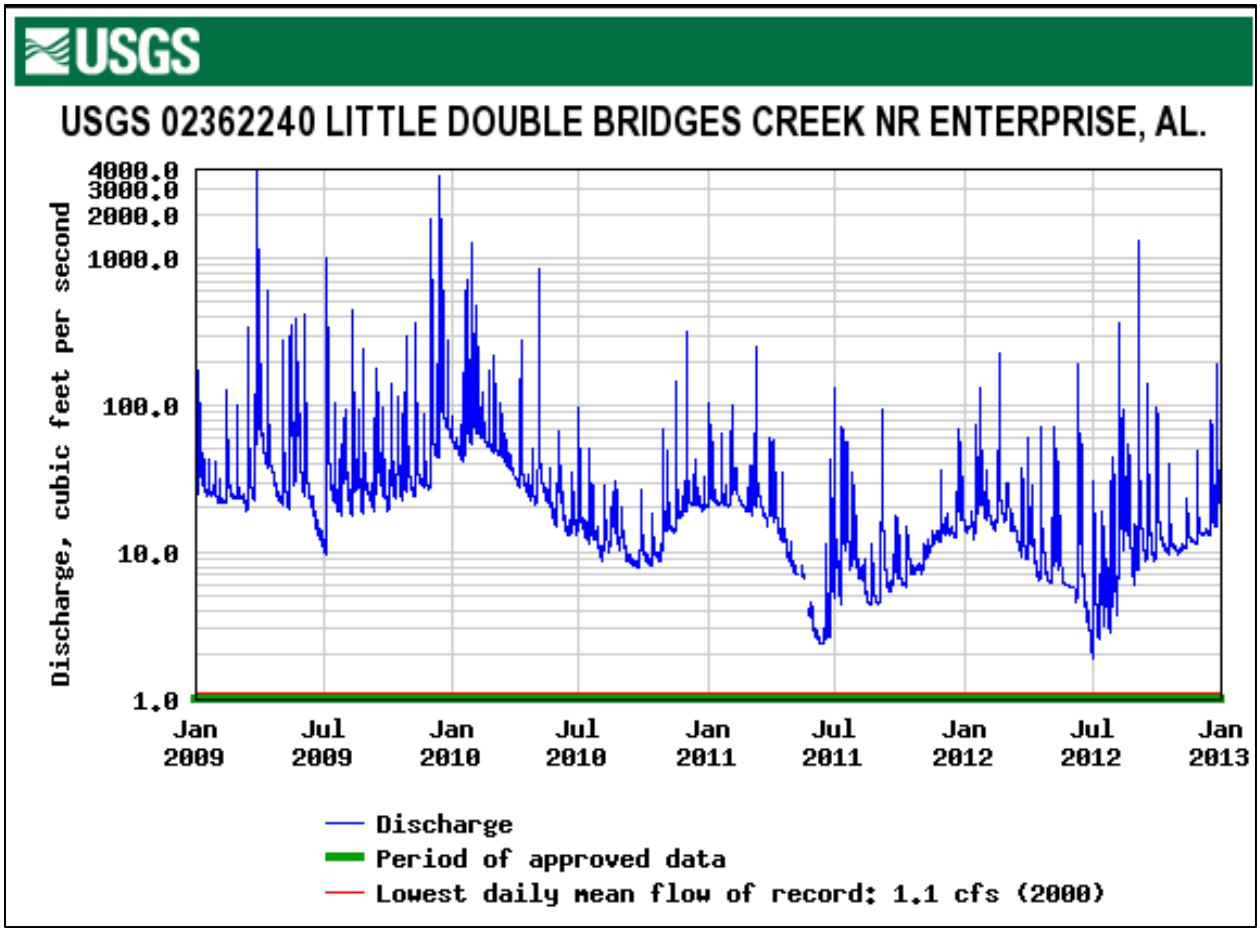

Figure 3.11 Streamflow Hydrograph for Receiver Catchment

CHAPTER 4: METHODOLOGY

4.1 CATCHMENT DELINEATION AND STREAM DEFINITION

Catchment delineation and stream processing for both donor and receiver catchments were done with the help of Hydrologic Engineering Center's Geospatial Hydrologic Modeling System (HEC-GeoHMS). HEC-GeoHMS is an extension developed by USACE as a set of tools within ArcGIS to process and create input files for HEC-HMS. It consists of several tools such as fill, flow direction, flow accumulation, etc. which help the user in deriving the boundary area for an outlet using the elevation information from DEM. It can be further used for partitioning a catchment into subcatchments using stream definition. Stream definition refers to defining a threshold for a grid cell within the catchment which can be treated as a stream. For example, a stream definition of 1 sq.km means that if any DEM grid cell is receiving flow from 1 sq. km. upstream area then, it is a stream. There is no available guideline for selection of stream definition and completely depends on the experience and expertise of modeler and modeling purpose. For the donor catchment, the catchment area was divided into 15 subcatchments using a stream definition of 75 sq. km. Using a smaller value of stream definition will increase the number of subcatchments. For example, a new stream definition of 45 sq.km. produces 21 subcatchments.

4.2 PARAMETER ESTIMATION FOR SMA MODEL

Twelve parameters of the SMA model mimic the natural process of the interception, surface depression, surface runoff and groundwater flow. Each of these parameters requires an initial value before it can be calibrated. Five of these parameters, i.e., the maximum surface

depression storage, maximum infiltration rate, soil percolation rate, maximum soil profile storage and maximum tension zone storage were derived from soil data, four parameter values, i.e., the groundwater layer 1 storage, groundwater layer1 coefficient, groundwater layer2 storage and groundwater layer 2 coefficient were obtained using streamflow data, the canopy interception value was obtained from landcover data, and the groundwater layer 1 percolation was determined during the calibration.

4.2.1 PARAMETER ESTIMATION FROM LAND COVER

Interception refers to the amount of precipitation held by the objects present above the ground and is only returned to the atmosphere through evaporation. Interception is an important part of the hydrologic cycle as around 10-20 percent of precipitation is intercepted during the growing season (Viessman and Lewis 2003). Interception loss is high during the initial storm period, however, drops down to zero very rapidly during a storm event. Various factors such as precipitation type, rainfall intensity, volume, wind condition, season etc. affect the canopy interception. Bennett (1998) has provided interception values for different types of vegetation which are shown in Table 4.1. Land cover classes from NLCD 2011 were categorized into three types of vegetation and each was assigned respective canopy interception values.

Table 4.1 Canopy Interception Values for Different Types of Vegetation (Bennett, 1998)

Types of Vegetation	Canopy Interception (in.)
General Vegetation	0.05
Grasses and Deciduous Trees	0.08
Trees and Coniferous Trees	1

4.2.2 PARAMETER ESTIMATION FROM SOIL DATA

The information about the soil components and their properties is linked in the SSURGO database for each map unit which represents a geographical area with dissimilar soil properties than the nearby soil areas. A map unit may include major components and minor components which are a single soil series. Each of these components is further classified into horizons or horizontal layers of soil as shown in Figure 4.1. Initial estimates for five different SMA parameters viz. the maximum surface depression storage, maximum infiltration rate, soil percolation rate, maximum soil profile storage, and maximum tension zone storage were obtained from SSURGO database. A single value for each parameter was calculated for each map unit which was then converted into raster format using ArcGIS.

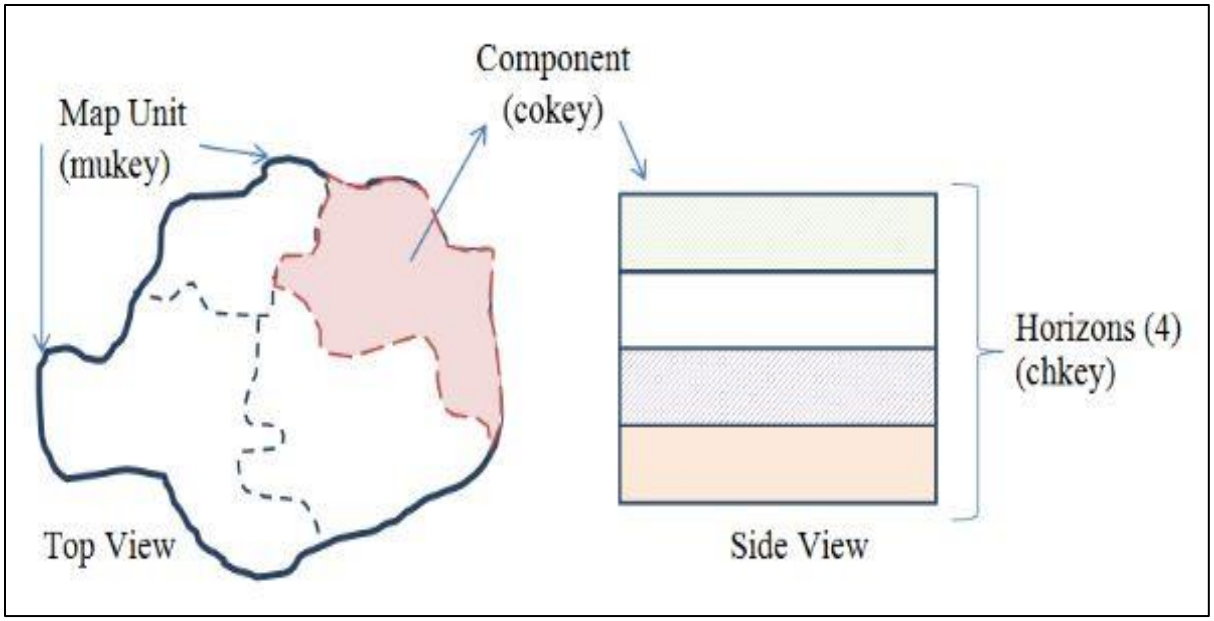

Figure 4.1 Organization of SSURGO Map Data (Holberg 2015)

4.2.2.1 MAXIMUM SURFACE DEPRESSION STORAGE

Initial estimates for surface depression storage have been suggested using the information on the slope of the land surface (Bennett 1998). Land areas with steeper slopes have less depression storage as the water flows out of them quickly due to higher energy gradient whereas flat lands can store more water. Slope information for each component is available from SSURGO database which is then averaged for map units and then associated with the maximum surface depression storage using Table 4.2.

Table 4.2 Surface Depression Storage Values (Bennett 1998)

Description	Slope (%)	Surface Storage (in)
Paved Impervious Areas	NA	0.125-0.25
Steep, Smooth Slopes	>30	0.04
Moderate to Gentle Slopes	5-30	0.25-0.5
Flat, Furrowed Land	0-5	2

4.2.2.2 MAXIMUM INFILTRATION RATE

Soil Infiltration rates are defined as the rate at which the soil can absorb rainfall or irrigation. Previous studies (Bennett 1998) have suggested that the initial estimates for maximum infiltration rate can be considered equal to the saturated hydraulic conductivity. Saturated hydraulic conductivity for a soil can be obtained from its texture class (12 soil texture classes defined by USDA). It has been found that the soil texture class is the most significant soil property related to the soil moisture parameters (Cosby et al. 1984). A previous study (Rawls et al. 1982) suggests the value of saturated hydraulic conductivity for each of the soil texture classes which is presented in Table 4.3.

Table 4.3 Soil Texture Classes and Saturated Hydraulic Conductivities

Soil Texture Class	Saturated Hydraulic Conductivity (in/hr)
Sand	8.27
Loamy Sand	2.41
Sandy Loam	1.02
Loam	0.52
Silt Loam	0.27
Sandy Clay Loam	0.17
Clay Loam	0.09
Silty Clay Loam	0.06
Sandy Clay	0.05
Silty Clay	0.04
Clay	0.02

4.2.2.3 MAXIMUM PERCOLATION RATE

Percolation rate defines the rate at which water is transferred through soil and groundwater layers under the force of gravity or sometimes even due to capillary forces. Previous studies (Bennett 1998; Fleming 2002) have shown that vertical average value of saturated hydraulic conductivity can reasonably estimate the maximum percolation rate. Therefore, saturated hydraulic conductivity values were associated with respective soil texture classes (Table 4.3) for each of the soil horizons and then averaged vertically to obtain a single percolation value for each component. Percolation rate thus obtained is then finally converted into raster format using ArcGIS.

4.2.2.4 MAXIMUM SOIL PROFILE STORAGE

Soil profile storage represents the amount of water held within soil pores which can be removed by the process of percolation and evapotranspiration (Feldman 2000). It is obtained by multiplying soil depth to the deepest soil horizon with the porosity of the soil. Porosity is defined as the ratio of the volume of the void to the volume of soil. The obtained soil storage for each soil component is then converted into raster file format using ArcGIS.

4.2.2.5 MAXIMUM TENSION ZONE STORAGE

Tension zone storage represents the volume of water attached to the soil particles (Feldman 2000) and can be related to the field capacity of the soil (Fleming 2002). The field capacity is defined as the soil moisture content in field conditions with uninterrupted subsurface drainage (Colman 1947). It is obtained by multiplying soil depth to the deepest soil horizon with the field capacity. The obtained tension zone storage for each soil component is then converted into raster file format using ArcGIS. The upper zone storage is not required to be entered by the user as it is calculated as the difference of the soil profile storage and the tension zone storage by HEC-HMS in each simulation time step.

4.2.3 PARAMETERS ESTIMATION FROM STREAMFLOW DATA

Any streamflow is comprised of surface runoff, interflow, and groundwater flow. The lines of decreasing slope on recession curve of streamflow hydrograph can help derive different contributing storage volumes when it is plotted on semi-logarithmic graph (Fleming 2002). Two

parameters within the simplified SMA loss method, i.e., the groundwater 1 storage and the groundwater 1 recession constant can be derived from streamflow hydrograph.

The lower end of the recession curve in streamflow hydrograph represents only the groundwater flow as surface flows and interflows have subsided. To separate the groundwater flow from streamflow, a line is projected backwards from the tail end to the time of peak with the same slope as the tail end of streamflow hydrograph. From the rising head of the streamflow hydrograph, a similar line is projected towards the time of peak. The combination of these two lines represents the groundwater flow. The recession curve of hydrograph can be represented by Eqn. (4.1).

$$q_t = q_0 \times K^t = q_0 \times \exp(-\propto t) \tag{4.1}$$

where,

q_t = future flow in time t

q_0 = initial flow

K = recession constant

$\propto$ = -ln(K)

The value of $\propto$ is calculated at each step and the average value of $\propto$ is calculated. The groundwater recession coefficient is then given by

$$\text{Groundwater recession coefficient} = \frac{1}{\propto} \tag{4.2}$$

Integration of Eqn. (4.3) gives an expression for groundwater storage (S_t) at time t for basin area A:

$$S_t = \frac{q_t}{\propto \times A} \tag{4.3}$$

The maximum value of storage is the most accurate value of groundwater storage that can be obtained from streamflow regression analysis (Holberg 2015). The value of groundwater layer 1 recession coefficient and storage were computed from baseflow for each of the four storms.

Figure 4.2 shows streamflow hydrograph for an isolated storm of 15th March 2009 plotted on a semi-logarithmic scale. The parameters derived from streamflow data are highly variable and therefore, were obtained after isolating the streamflow from storms in various months. Four different storms of 1st September 2005, 15th December 2007, 15th March 2009, and 28 June 2010 were selected, and the average values of groundwater parameters derived from the four storms were used as initial estimates of these parameters. The value of groundwater parameters for each storm and their average values are given in Table 4.4.

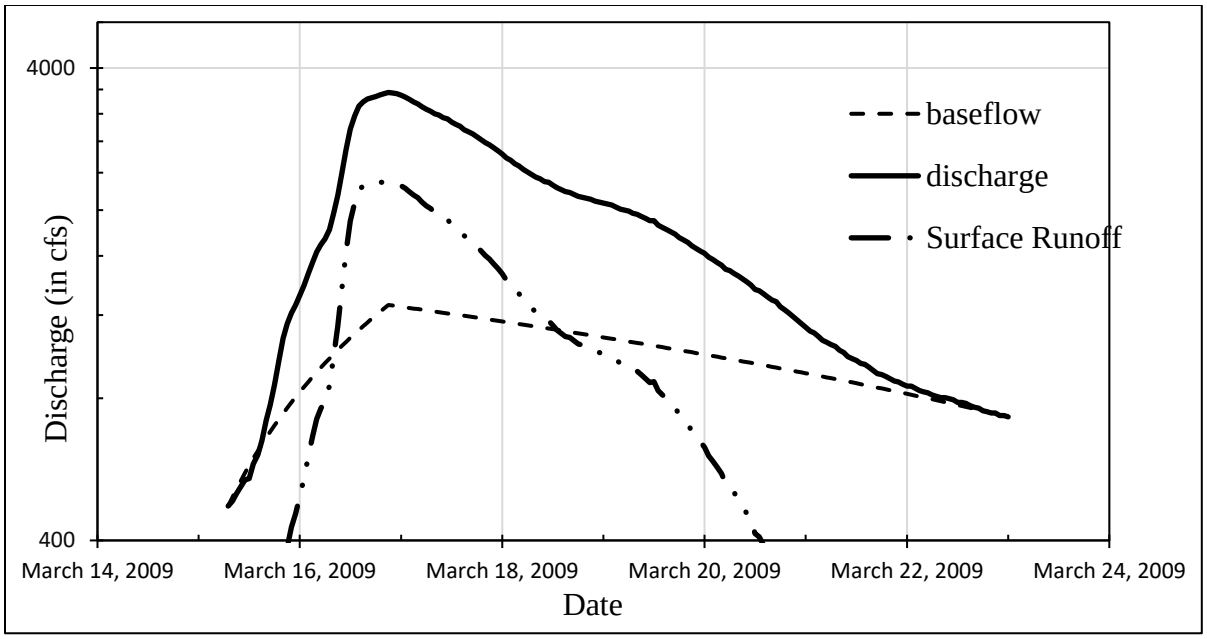

Figure 4.2 Baseflow Separation for Storm of 15th March 2009

Table 4.4 Groundwater Parameter Values for Selected Storms and their Averages

Storm event	Groundwater1 Coefficient (hr)	Groundwater1 storage (in.)	Groundwater2 Coefficient (hr)	Groundwater2 storage (in.)
28th June 2010	49.7	0.04	285.3	0.30
11th Nov 2009	47.9	0.01	449.3	0.55
15th March 2009	55.5	0.31	296.2	0.43
17th July 2011	35.0	0.05	162.8	0.05
Average	47.0	0.1	298.4	0.33

4.3 CURVE NUMBER DEVELOPMENT AND BASIN LAG

Soils are divided into four different hydrologic soil groups (HSGs) viz. A, B, C, and D depending on their runoff potential and infiltration rates. The classification of soil into these classes

is dependent on intake and transmission of water, freezing condition of soil etc. (USDA 1972). Soils in the group A have low runoff potential when they are wet and typically have a composition of <10% clay and >90% sand. Soils in the group B have moderately low runoff potential. The composition of this group of soils has 10%–20% clay and 50%–90% sand. Soils with moderately high runoff potential are placed in the group C and have a composition of about 20%–40% clay and <50% sand. Soils in the group D have high runoff potential and water movement is restricted. The composition of soils in this group is >40% clay and <50% sand. Hydrologic soil group in combination with land cover data can help calculate the curve number (CN). The Soil Data Viewer can map HSGs based on the SSURGO data of county provided by the user. Hydrologic soil group for the donor and receiver catchments is shown in Figure 4.3.

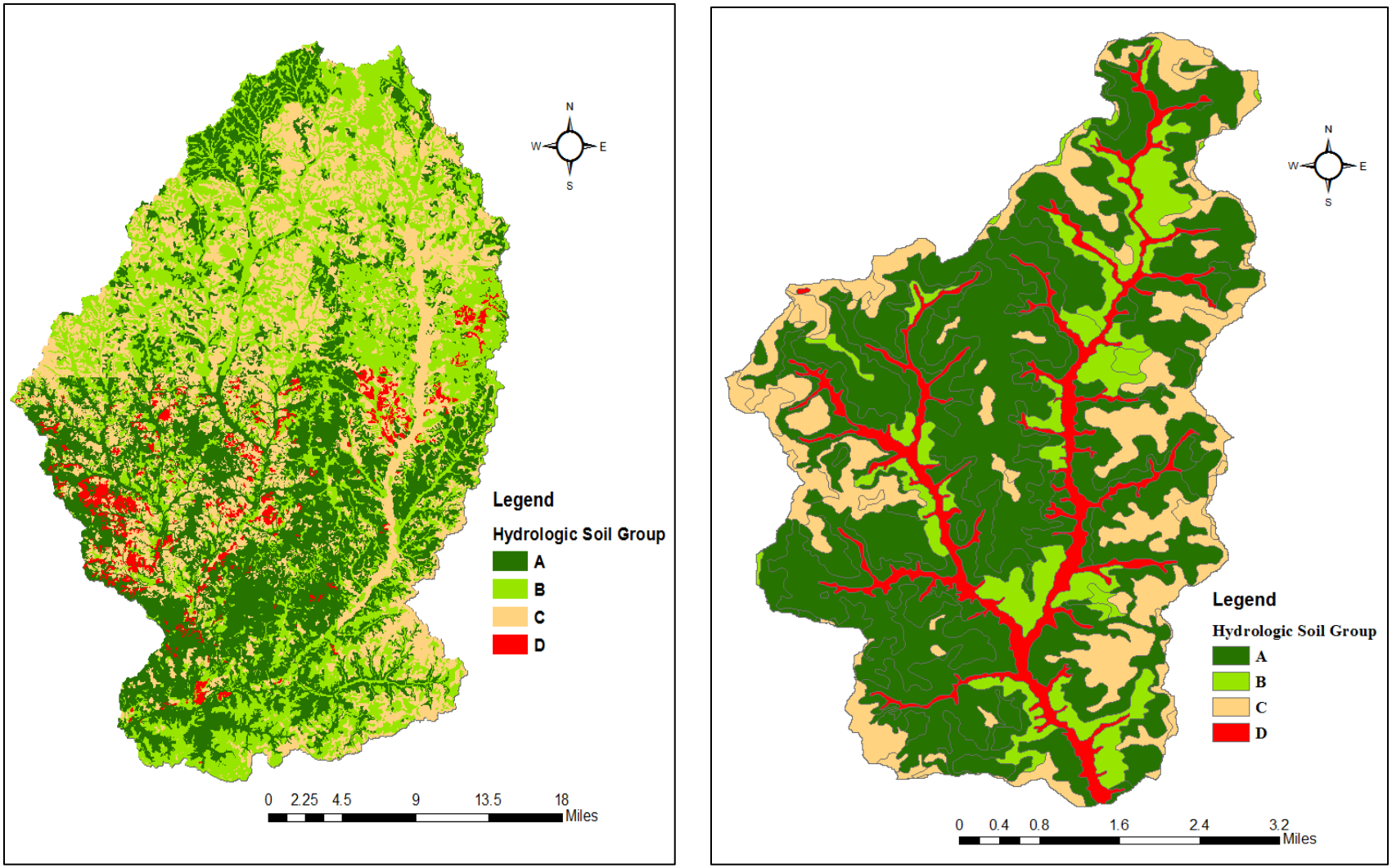

Figure 4.3 Hydrologic Soil Group of Donor Catchment (Left) and Receiver Catchment (Right)

The curve number is an empirical parameter which provides information on the amount of runoff from a given precipitation and was developed by the Soil Conservation Services (SCS) (now the National Resources Conservation Service or NRCS) for application in small rural catchments. Apart from land cover and HSG, different conditions such as antecedent moisture condition, hydrologic condition, etc. affect the value of curve number. To avoid complexity in the determination of curve number, available landcover classes were merged together to form four land cover classes (Table 4.5). Figure 4.4 shows the simplified land cover map of the donor and receiver catchments. Table 4.6 was then developed to assign CN for each of the four HSGs and the four land cover classes. Combining the information from land cover, HSG and Table 4.6, curve number grids were created for both the donor and receiver catchments (Figure 4.5). Curve number is an important precipitation loss computing parameter in event-based modeling. In the continuous modeling, it can be used for calculation of the basin lag which is defined as the time difference between the center of mass of rainfall excess and unit hydrograph peak.

Table 4.5 Simplified Land Cover Classes from NLCD Land Cover Classification

Grid Code	Description	Grid Code	Description
11 90 95	Open water Woody wetlands Emergent herbaceous wetlands	1	Water
21 22 23 24	Developed, open space Developed, low intensity Developed, medium intensity Developed, high intensity	2	Medium residential
41 42 43	Deciduous forest Evergreen forest Mixed forest	3	Forest
31 52 71 81 82	Barren land Shrub/Scrub Grassland/herbaceous Pasture/hay Cultivated crops	4	Agricultural land

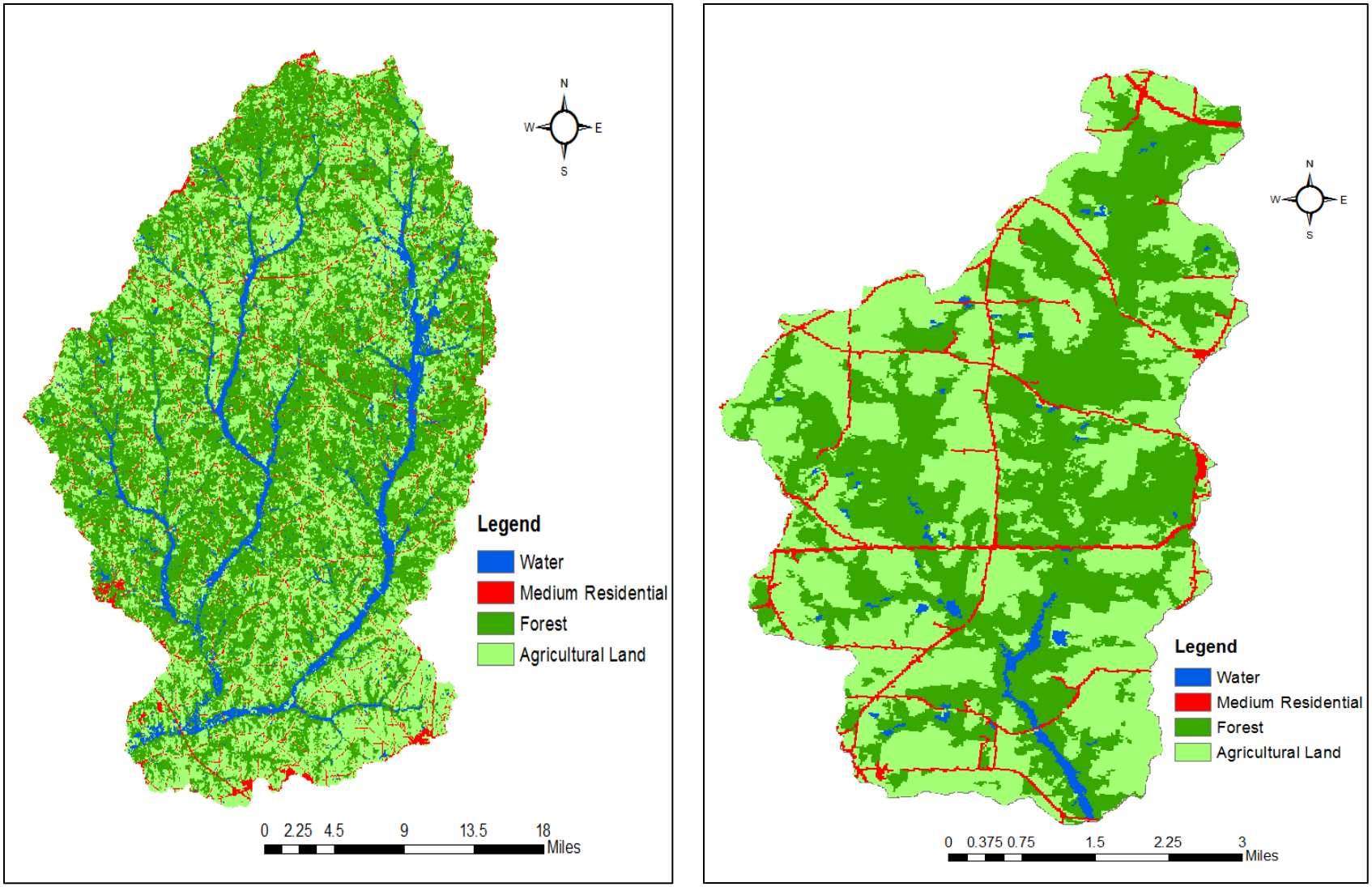

Figure 4.4 Simplified Land Cover Map of Donor Catchment (Left) and Receiver Catchment (Right)

Table 4.6 Curve Number Values for Corresponding Land Cover and Hydrologic Soil Group

Land Cover Classes\ HSG	A	B	C	D
Water	100	100	100	100
Residential	57	72	81	86
Forest	30	58	71	78
Agricultural	67	77	83	87

The SMA model is a loss model which calculates the volume of water that has intercepted, infiltrated, evaporated, and stored in different zones. It does not provide the discharge which is the model output of HEC-HMS. The calculation of transforming the runoff volume (rainfall excess) to discharge is done by suitable transform methods available within HEC-HMS. For this study, the SCS unit hydrograph method was used because of required minimum number of parameters. The SCS unit hydrograph method requires the user to enter only one parameter, i.e., lag time. Based on lag time, the program computes time of concentration and rescales the SCS dimensionless unit hydrograph. Basin lag can be calculated from curve number using Eqn. (4.4).

$$\text{Basin Lag} = \frac{(L^{0.8} \times (S+1)^{0.7})}{(1900 \times Y^{0.5})} \tag{4.4}$$

Where,

L= Hydraulic length in feet

Y= slope of watershed in percentage

$$S = \frac{1000}{CN} - 10 \tag{4.5}$$

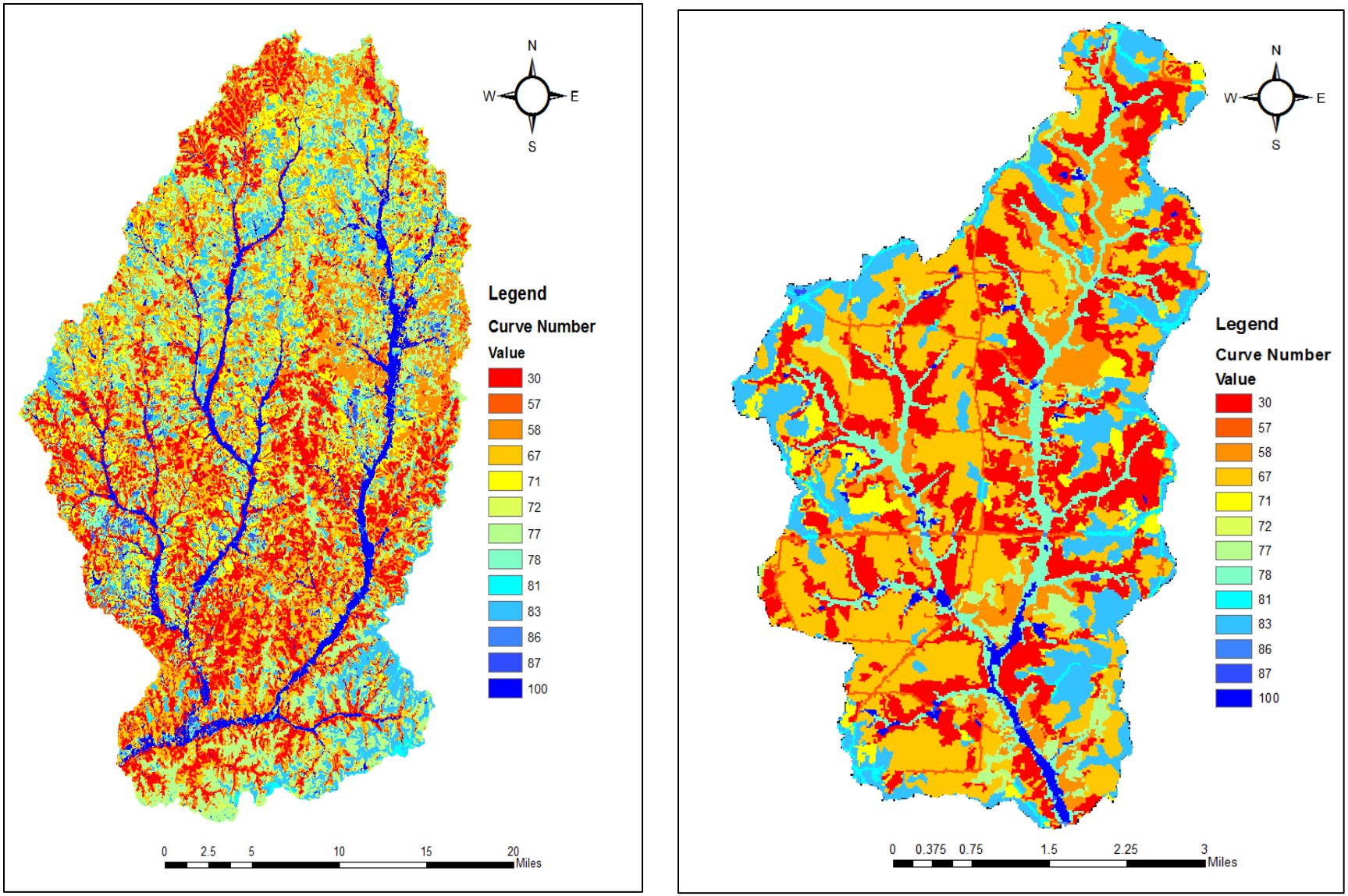

Figure 4.5 Curve Number Grid for Donor Catchment (Left) and Receiver Catchment (Right)

4.4 HEC-HMS MODEL SETUP

After all the soil and streamflow parameters required for HEC-HMS model have been calculated, HEC-GeoHMS was used for transferring both the spatial information and information on parameter values for each subcatchment to HEC-HMS. HEC-GeoHMS also develops the background map file and distributed-basin schematic model file. It performs the tasks of the automatic naming of reaches and subcatchments, checks for errors in the catchment and connectivity of streams. HEC-HMS model setup for the donor catchment is shown in Figure 4.6.

4.4.1 THIESSEN POLYGON METHOD

Thiessen polygon method is one of the most common methods of determining average precipitation over a catchment. In this method, the catchment (or subcatchments in our study) is divided into a number of polygons utilizing rain gauges as centers. These polygons are then assigned a precipitation value corresponding to their respective gauges and then a weighted average of precipitation value is computed for hydrologic modeling. For the donor catchment, three rainfall stations viz. Dothan, Troy, and Union Springs were used for creating Thiessen polygons and subsequent calculation of the areal average value of precipitation. For the receiver catchment, only rainfall data from Dothan were used. Figure 4.7 shows the location of rain gauges near the donor catchment and three Thiessen polygons created using those rain gauges.

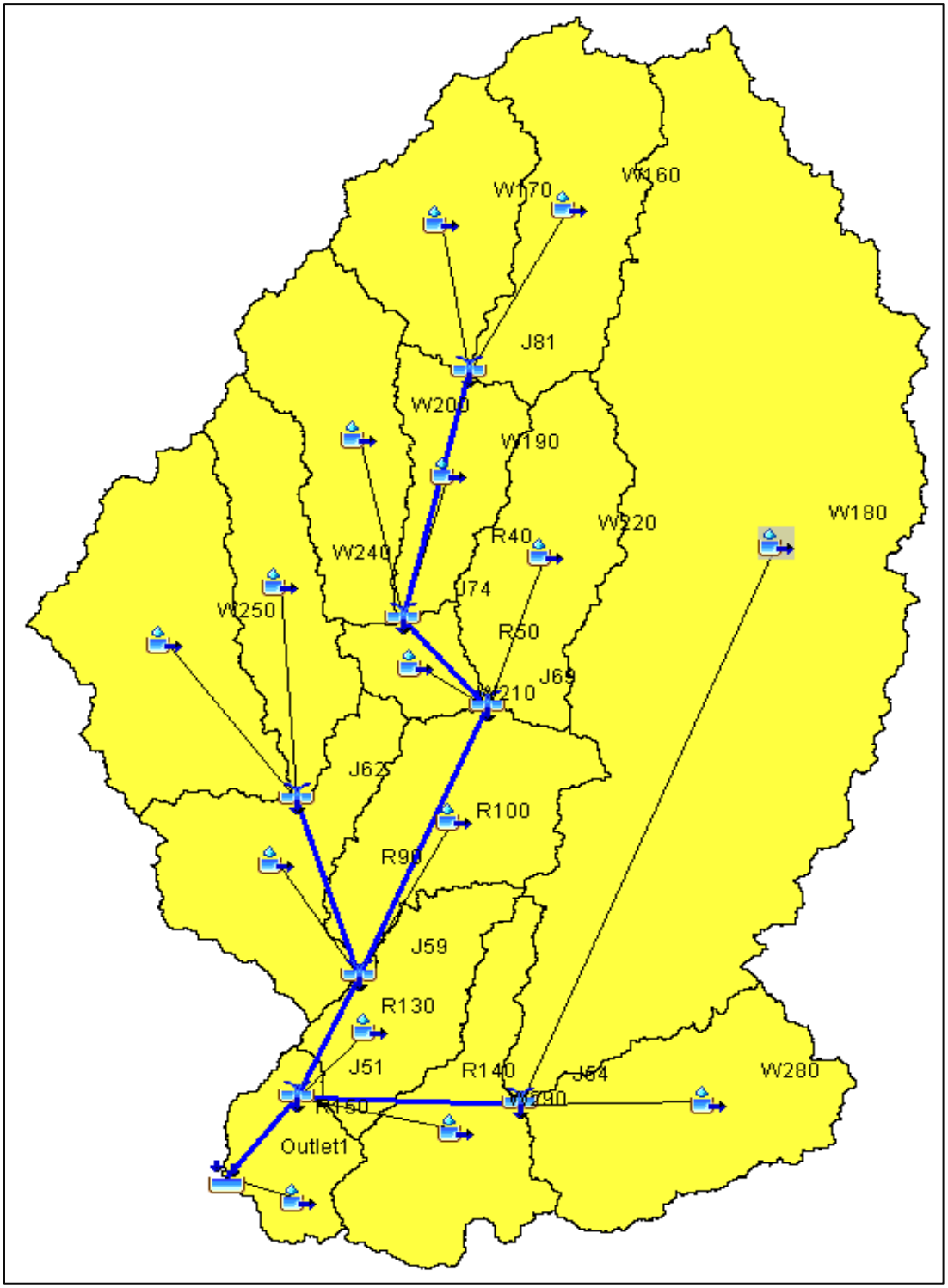

Figure 4.6 HEC-HMS Model Setup for Donor Catchment

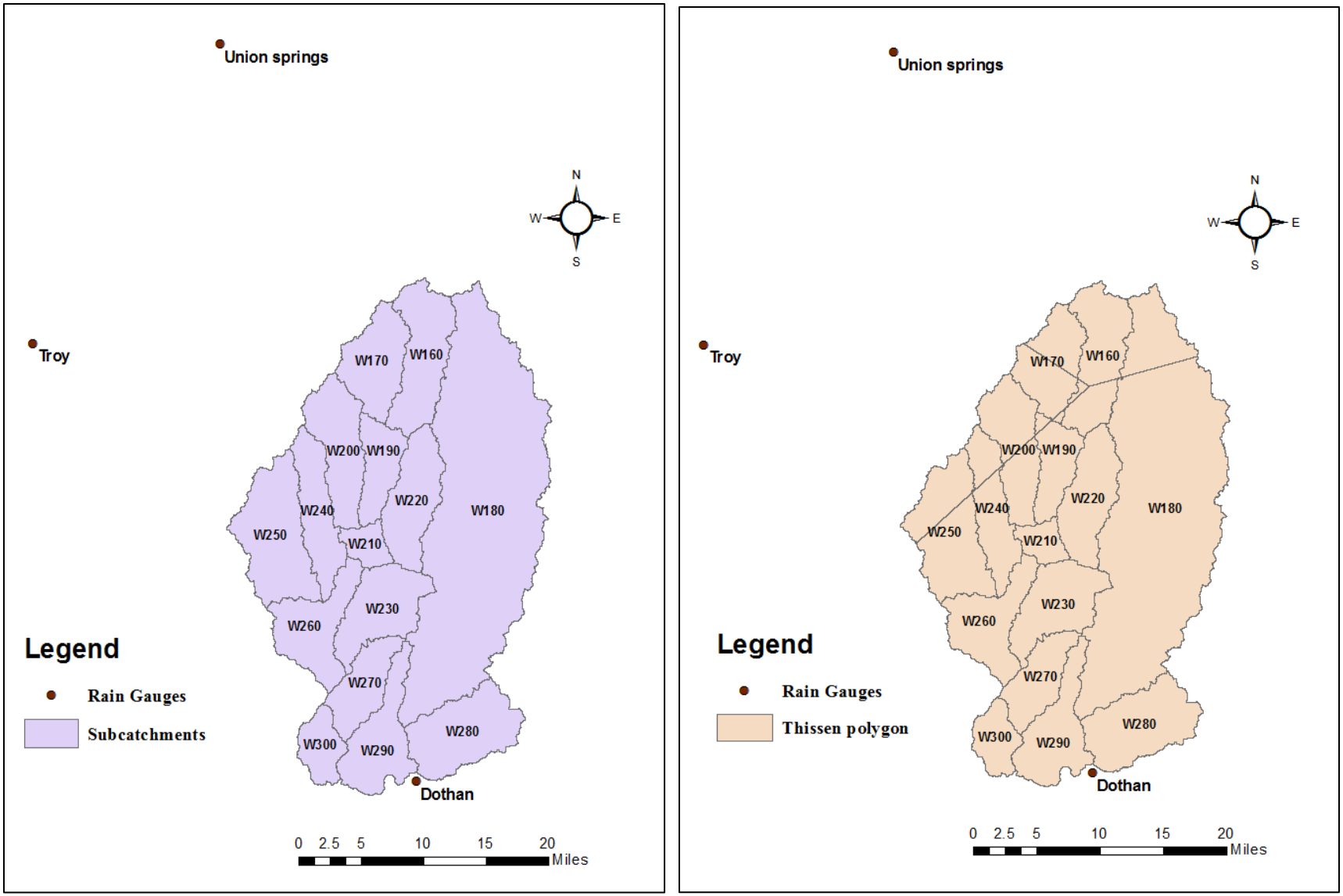

Figure 4.7 Location of Rain Gauges near the Donor Catchment (Left) and Thiessen Polygon for Donor Catchment (Right)

4.4.2 INITIAL WARMUP PERIOD

The model warmup period is defined as an initial length of simulation time at the end of which model parameters are converged to values independent of initial estimated values (Johnston and Pilgrim 1976). HEC-HMS SMA model consists of five separate zones viz. canopy, surface depression, soil, Groundwater 1 (GW1), and Groundwater 2 (GW2). Apart from the parameters developed so far, the model setup requires defining initial moisture content in each one of the five storage zones. As an attempt to find the warmup period, the model was run by increasing moisture content for each zone to 90% one at a time and then, resulting hydrographs were compared with the initial model run with 10% moisture content for each zone. Figure 4.8 shows the effect of variation of initial moisture level on modeled output streamflow. It was found that except soil storage, initial moisture content in other storage zones doesn't affect the streamflow hydrograph and tend to overlap with each other.

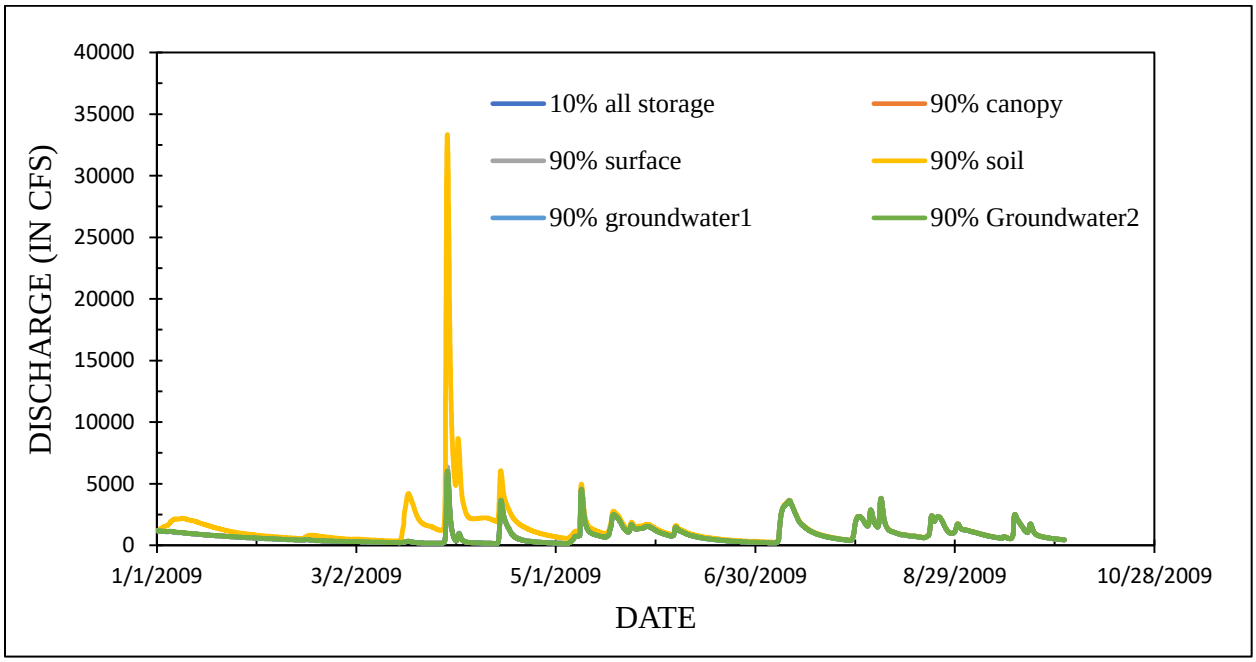

Figure 4.8 Effect of Variation of Initial Moisture in Different Storage Zones on Model Output

It can be seen from Figure 4.8 that variation of initial moisture seizes to affect streamflow after five months of the model run. A warmup period of nine months was selected to be on the conservative side.

4.5 SENSITIVITY ANALYSIS

Any model parameter is subjected to unprecedented changes and errors. Sensitivity analysis is the investigative procedure of identifying the effects of changes or errors in model parameter to the model output. A large number of uses of sensitivity analysis includes but not limited to allowing the decision maker to select assumptions, identifying sensitive or important variables, testing optimal solutions' robustness, etc. (Pannell 1997). The goal of sensitivity analysis in this study was to identify the order of sensitivity of key model parameters which would further help in calibration of the model. There are two types of sensitivity analysis, i.e., global and local. In the global sensitivity analysis, all model parameters are varied over their ranges at the same time. While in the local sensitivity analysis, each model parameter is varied separately by keeping all other model parameters constant.

As identified by Fleming (2002), changing either soil storage or tension zone storage produces same results, so that the soil storage was eliminated for sensitivity analysis. Furthermore, since GW2 percolation rate can only be calculated during calibration, it was not included in the sensitivity analysis. For this study, a local sensitivity analysis was performed where model parameters were varied within the range of ± 40% (at an interval of 10%) of initial estimates individually by keeping remaining parameters constant. The effect of model parameter variation in NSE and PEV were plotted as shown in Figure 4.9 and Figure 4.10.

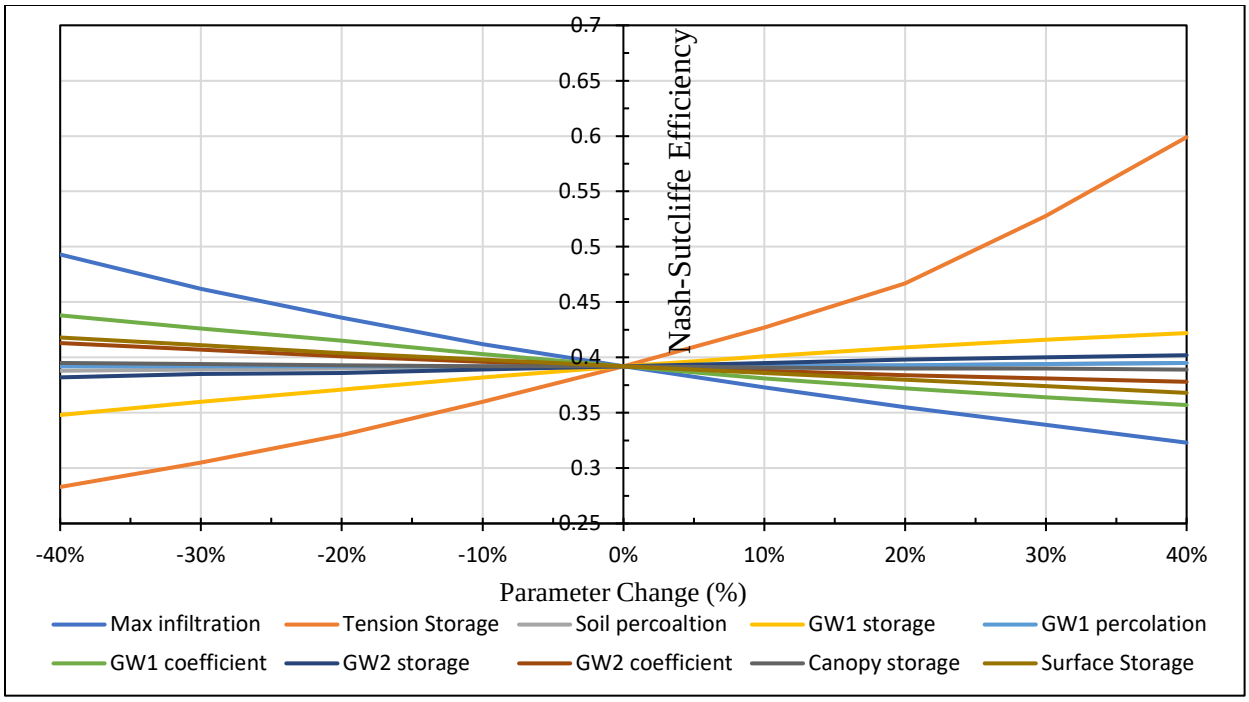

Figure 4.9 Nash-Sutcliffe Efficiency of the Model Output due to Percent Change in Parameter Values

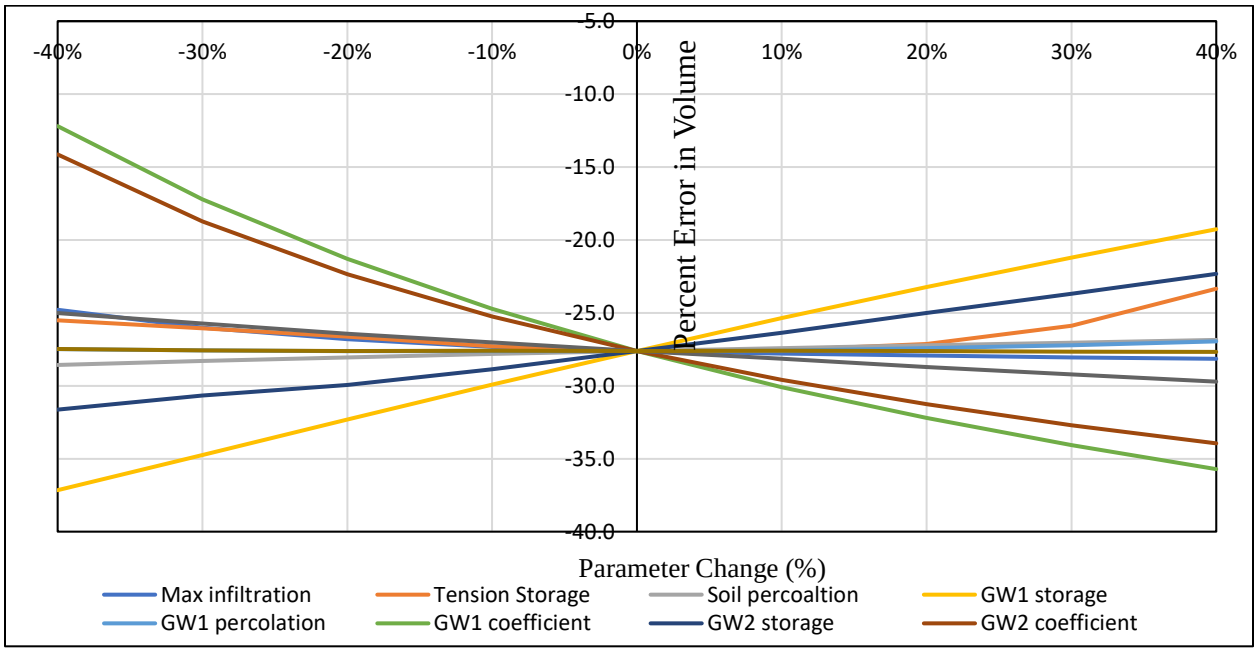

Figure 4.10 Percent Error in Volume of the Model Output due to Percent Change in Parameter Values

For the purpose of ranking the parameters in terms of their relative sensitivity to the objective functions (NSE or PEV), sensitivity parameter (S) was calculated using Eqn. (4.6).

$$S = \frac{(\frac{O_2 - O_1}{O_{12}})}{(\frac{I_2 - I_1}{I_{12}})} \quad (4.6)$$

Where,

I_1 = least value of input parameter

I_2 = highest value of input parameter

I_{12} = average value of I_1 and I_2

O_1 = output value of I_1

O_2 = output value of I_2

O_{12} = average value of O_1 and O_2

Using Eqn. (4.6), two sensitivity parameters (for both NSE and PEV) were calculated for ten parameters within the range of ± 40% of initial estimates and based on the value of S, they were ranked from one to ten. One being the most sensitive (highest S value) and vice versa. Rankings of parameters for NSE and PEV were then added together, and a new ranking was done again based on this sum to obtain the order of sensitivity of parameters for both NSE and PEV (Table 4.7).

Table 4.7 Parameter Ranking Based on the Value of Sensitivity Parameter for NSE and PEV

Parameter	Sensitivity (S) for NSE	Ranking for NSE	Sensitivity (S) for PEV	Ranking for PEV	Ranking for NSE and PEV
GW1 coefficient	0.257	3	1.125	1	1
Tension Storage	0.963	1	0.203	6	2
GW1 storage	0.238	4	0.694	3	3
GW2 coefficient	0.111	6	0.946	2	4
Maximum infiltration	0.533	2	0.214	7	5
GW2 storage	0.064	7	0.203	4	6
Canopy storage	0.019	9	0.155	5	7
Surface Storage	0.159	5	0.065	10	8
Soil percoaltion	0.022	8	0.031	8	9
GW1 percolation	0.01	10	0.009	9	10

4.6 CALIBRATION AND VALIDATION FOR DONOR CATCHMENT

Model calibration is the process of tuning model parameters until model output matches reasonably well with the observed data. This match is quantified using objective functions such as NSE, PBIAS, Peak-weighted root mean square error, etc. The calibration in HEC-HMS can be done manually, and there exist options for automated calibration**.** It was found that using automated calibration alone results in an error which is consistent with the findings of Cunderlik and Simonovic (2004). For HEC-HMS's automated calibration options, the univariate gradient method produces local maxima or minima and the Nelder-Mead method was found to be highly biased with the selection of initial parameter value. Due to these reasons, the manual calibration was first applied to obtain selected or quasi-optimal model parameter values and then the results were refined using automated calibration.

The large number of parameters within SMA model makes calibration procedure complicated and time-consuming. Reducing a number of parameters for calibration simplifies the process of manual calibration. Therefore, the six most sensitive parameters obtained from the sensitivity analysis (Table 4.7) viz. GW1 coefficient, tension storage, GW1 storage, GW2 coefficient, maximum infiltration, and GW2 storage together with GW2 percolation (calibration parameter) was used for manual calibration.

For the manual calibration, observed and modeled peak flow was matched first by changing the tension storage as done by Fleming (2002). Once the observed and modeled peak flows for the period of calibration was reasonably matched, and then other relatively smaller peak events were matched by tuning the maximum infiltration rate. GW1 coefficient was adjusted by matching the slope of falling limb of model output hydrograph with observed hydrograph. GW2 storage and coefficient were adjusted by matching model hydrograph and observed hydrograph during dry seasons. GW1 storage and GW2 percolation rates were finally adjusted to minimize the volumetric error. A flowchart of the manual calibration is shown in Figure 4.11.

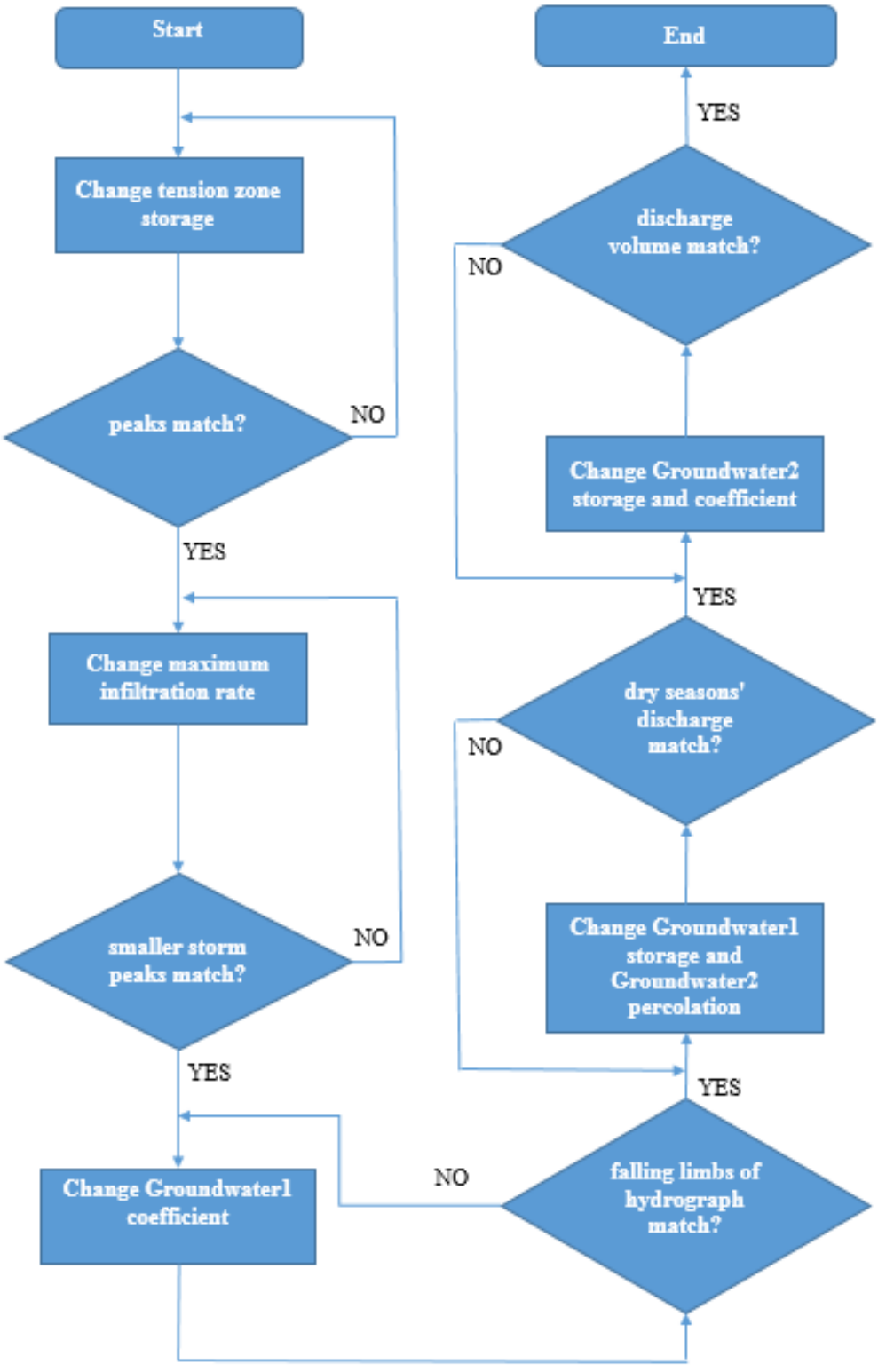

Figure 4.11 Flowchart of the Manual Calibration

After the parameters were tuned using manual calibration, automated calibration using the Nelder-Mead method was used for further refining the results. For calibration and validation of the HEC-HMS SMA model for the donor catchment, a split sample test approach was adopted as indicated by Refsgaard and Knudsen (1996) including 3-5 years of calibration period and a similar length of time for validation. A calibration period of three years from October 2009 to September 2012 was selected. Calibrated model was then used for validation process using a new set of rainfall data for the period of three years from October 2012 to September 2015.

4.6.1 SEMI-ANNUAL PARAMETERIZATION

Throughout the year, a catchment responds differently to the same rainfall event depending on the time of the year such as dry and wet season. This nonlinearity in rainfall-runoff response is not considered in the linear structure of the SMA model. However, this error can be minimized by adopting semi-annual parameterization approach where different parameter sets are developed for the dry and wet season. In this study, a semi-annual approach dividing each calibration years into dry (May-October) and wet period (November-January) was applied and tested. The percent moisture in each storage zone was stored at the end of each dry or wet period using the basin state function in HEC-HMS and then applied as the initial moisture for the next wet or dry period.

4.7 PARAMETER TRANSFER TO RECEIVER CATCHMENT

After calibration and validation process of the donor catchment, ten SMA model parameters were transferred to the receiver catchment. Due to the ease of calculation and lower

sensitivities of canopy storage and surface depression storage parameters, those parameters were not transferred but calculated using soil and landcover data for the receiver catchment.

Due to the semi-distributed approach applied to the donor catchment during model development, calibrated soil parameter had fifteen different values obtained from fifteen subcatchments (Table 5.1). Whereas, since the groundwater parameters are obtained from streamflow analysis at the catchment outlet, the value of groundwater both uncalibrated and calibrated was same for all subcatchments. The receiver catchment being developed as lumped model requires only a single value for each of the parameter. Due to this reason, single parameter value was obtained as the areal average of the individual subcatchments' parameter values.

CHAPTER 5: RESULTS AND DISCUSSIONS

5.1 CALIBRATION OF DONOR CATCHMENT

5.1.1 ANNUAL PARAMETERIZATION APPROACH

After manual and automated calibration for seven parameters of the SMA model, positive change from the uncalibrated parameter values was found for two parameters viz. tension storage and GW1 storage whereas negative change in the values was found for five parameters viz. GW2 storage, GW2 percolation, GW2 coefficient, GW1 coefficient and maximum infiltration rate. Among two parameters with positive change, the highest change was observed for tension storage (+56%) followed by GW1 storage (+49%). Whereas, for parameters with negative changes, the highest change was observed for GW2 coefficient (-33%) followed by GW1 coefficient (-14.9%), GW2 percolation (-15%), maximum soil infiltration (-5%) and GW2 storage (-1%), respectively. Table 5.1 lists the final calibrated parameter values for the SMA model of the donor catchment.

Table 5.1 Final calibrated Parameter Values for SMA Model of Donor Catchment

Subbasin	Maximum Infiltration (in/hr)	Soil Storage (in)	Tension Storage (in)	Soil Percolation (in/hr)	GW1 storage (in)	GW1 percolation (in/hr)	GW1 coefficient (hr)	GW2 storage (in)	GW2 percolation (in/hr)	GW2 coefficient (hr)
W300	1.87	29.24	23.18	1.13	0.15	1.13	40	0.33	0.0085	200
W290	1.75	28.94	21.92	1.19	0.15	1.19	40	0.33	0.0085	200
W280	1.52	21.25	17.76	1.10	0.15	1.10	40	0.33	0.0085	200
W270	2.08	29.96	22.50	1.13	0.15	1.13	40	0.33	0.0085	200
W260	1.75	28.64	23.83	0.85	0.15	0.85	40	0.33	0.0085	200
W250	1.86	25.34	20.84	0.99	0.15	0.99	40	0.33	0.0085	200
W240	1.79	22.99	18.82	1.19	0.15	1.19	40	0.33	0.0085	200
W230	1.73	28.43	23.26	0.90	0.15	0.90	40	0.33	0.0085	200
W220	1.78	22.89	19.44	1.08	0.15	1.08	40	0.33	0.0085	200
W210	1.73	28.50	22.87	0.97	0.15	0.97	40	0.33	0.0085	200
W200	1.89	19.01	16.08	1.38	0.15	1.38	40	0.33	0.0085	200
W190	1.71	18.69	16.34	1.14	0.15	1.14	40	0.33	0.0085	200
W180	1.72	21.14	17.99	1.01	0.15	1.01	40	0.33	0.0085	200
W170	1.58	20.63	17.80	1.04	0.15	1.04	40	0.33	0.0085	200
W160	1.67	19.13	16.90	1.17	0.15	1.17	40	0.33	0.0085	200

Simulated discharges match reasonably well with observed discharges for the donor catchment during the calibration period of 3 years from October 2009 to September 2012 (Figure 5.1). The model seems to overpredict peak discharges for most time of the years except for some storm events in February 2010, March 2011 and August 2012. Statistical analysis for the donor catchment shows that Nash-Sutcliffe efficiency is 0.73, which is rated as good performance for the continuous hydrological model as recommended by Moriasi et al. (2007).

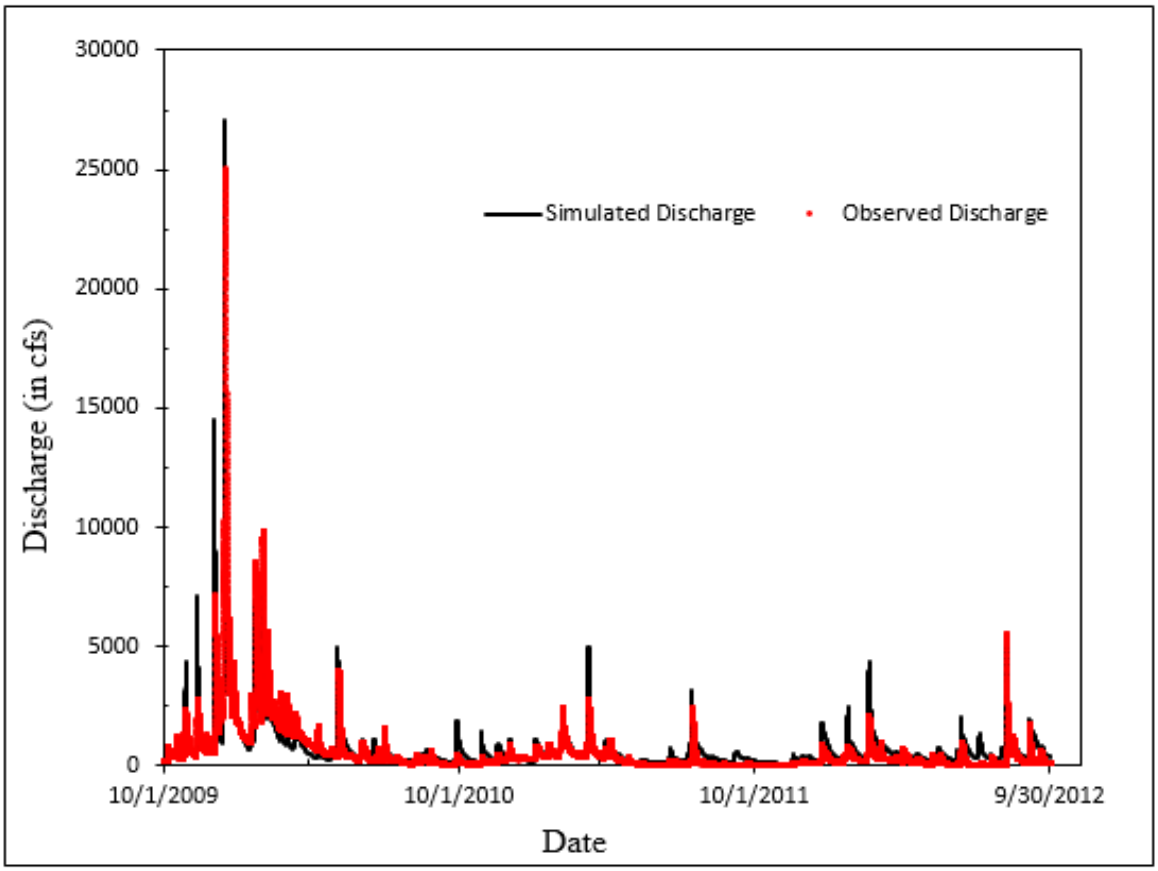

Figure 5.1 Hourly Simulated versus Observed Discharge for Donor Catchment (Oct 2009–Sep2012)

A scatterplot of simulated vs observed discharges during the calibration period is shown in Figure 5.2. It shows that simulated discharges are underestimated during the rising and falling limb

of hydrograph for the storm event on 15th December 2009. However, for the same event, peak discharge is overestimated by the model. For lower flows and smaller storm events, simulated discharges fit reasonably well with the observed discharges as seen from a cluster of points closer to 1:1 line.

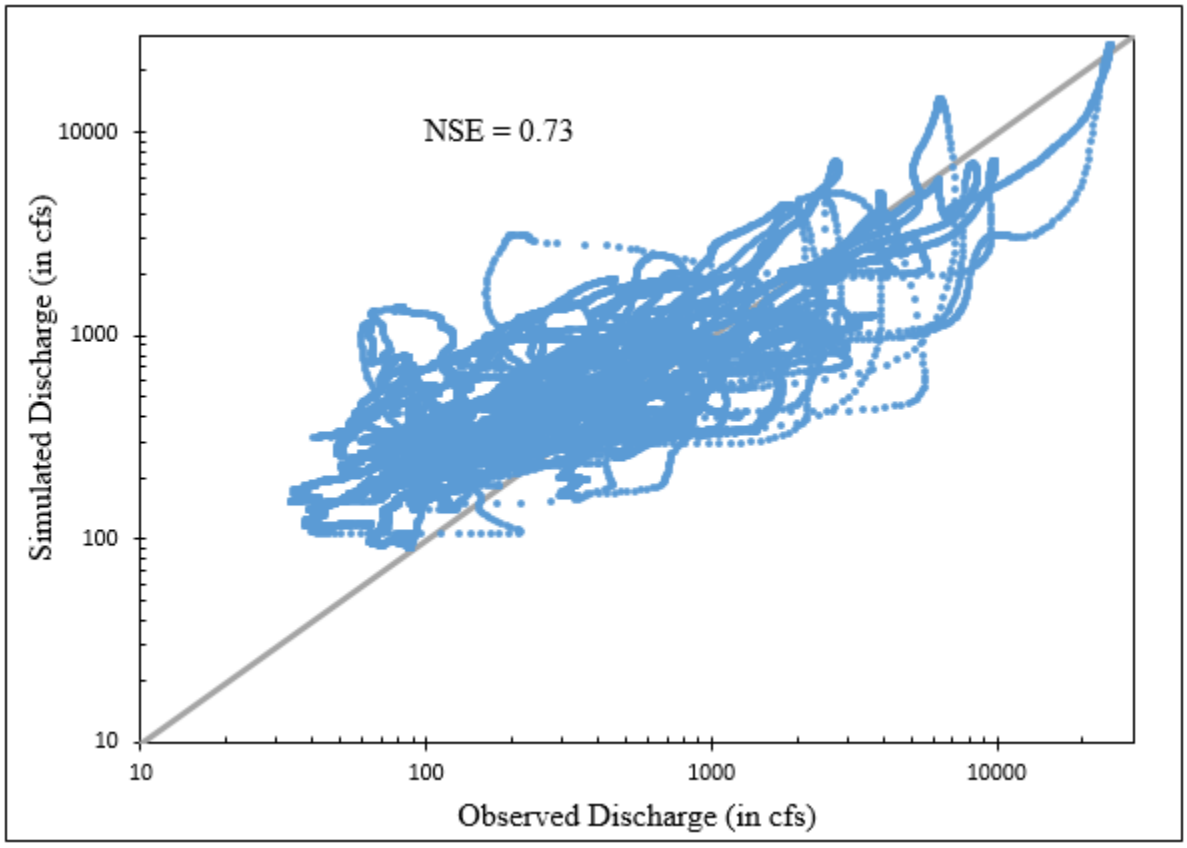

Figure 5.2 Scatterplot of Simulated versus Observed Discharge during Calibration period (Oct 2009–Sep 2012)

As seen from Figure 5.3, cumulative simulated discharge volume matches almost perfectly with observed discharge volume for the first quarter of the calibration period. However, after that quarter, the model continues to underestimate the discharge volume for almost a year increasing the discrepancy in cumulative discharge volume. From late 2010, the model starts producing more discharge volume then observed one and reduces the difference between cumulative discharge

volumes. This difference changes the sign in 2012 and by the end of the calibration period, cumulative simulated discharge volume exceeds cumulative observed discharge volume. The percent bias is -10.4%, which is rated as good performance for the continuous hydrological model.

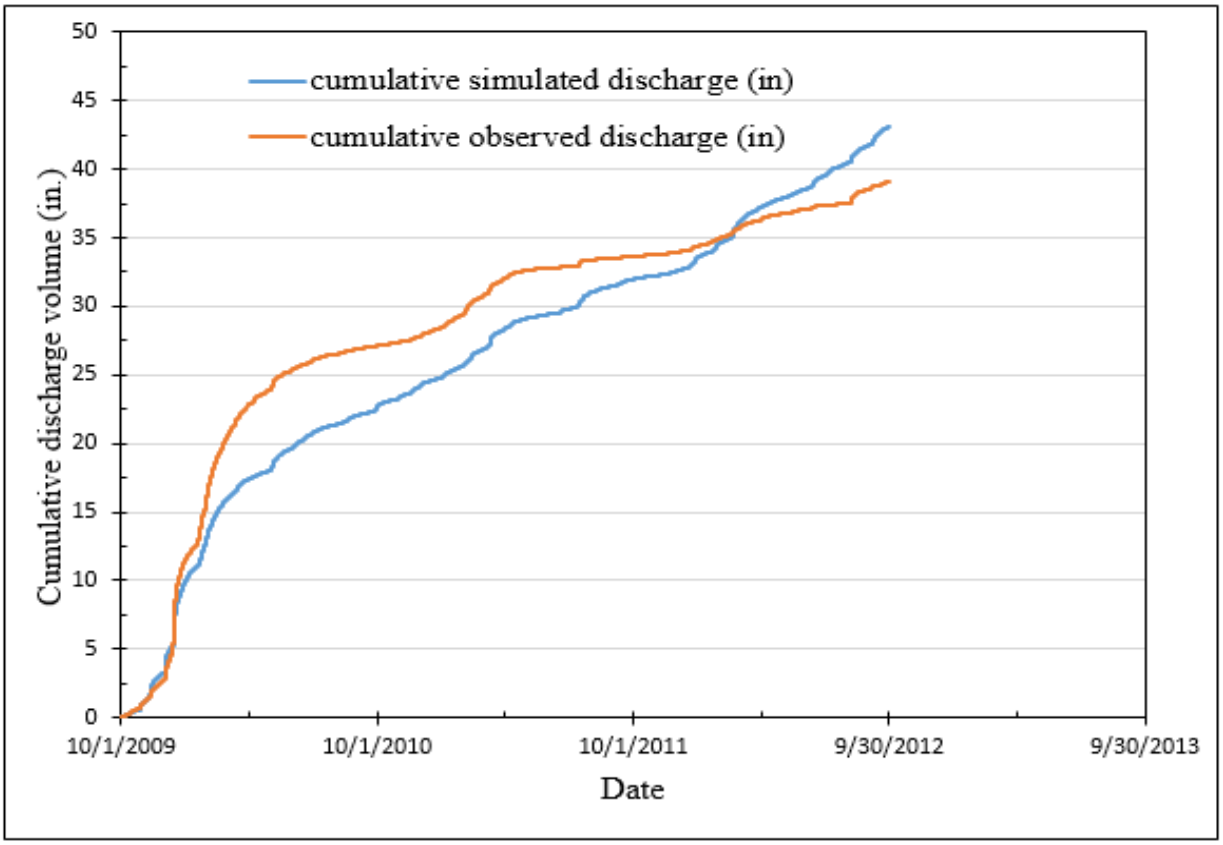

Figure 5.3 Cumulative Simulated versus Observed Discharge Volume during Calibration Period for Donor Catchment (Oct 2009–Sep 2012)

5.1.2 SEMI-ANNUAL PARAMETERIZATION APPROACH

In contrary to the annual parameterized model, semi-annual parameterization approach develops a model with two sets of model parameters for dry and wet seasons. **Error! Reference source not found.** suggests that groundwater parameters differ much depending on the time of the year. Due to the high variability of groundwater parameters during a year and higher sensitivity of tension zone storage, five parameters were varied from an annual model parameter set during semi-annual approach. Manual and automated calibration suggests that variation in GW1 storage, GW2 percolation, and tension storage during dry and wet periods produced best results. Table 5.2 lists the value of these three parameters of each subcatchment for dry and wet seasons. In comparison to wet period, a higher proportion of the precipitation is lost to the soil system and only a small fraction appears as direct runoff. Due to this reason, tension storage and GW1 storage of dry season are lower than the tension storage and GW1 storage of wet season. Furthermore, in the dry season, the amount of water in the soil reaches the aquifer more rapidly and thus more water is lost through the modeled hydrologic system. This is the reason for higher GW2 percolation rate in the dry season compared to the wet season.

Table 5.2 Semi-annual Parameter Values for Dry Seasons and Wet Seasons

Subbasin	Wet Period (Nov-April)			Dry period (May-Oct)		
	Tension Storage (in)	GW1 storage (in)	GW2 percolation (in/hr)	Tension Storage (in)	GW1 storage (in)	GW2 percolation (in/hr)
W300	23.18	0.2	0.0085	22.72	0.15	0.01
W290	21.92	0.2	0.0085	21.48	0.15	0.01
W280	17.76	0.2	0.0085	17.41	0.15	0.01
W270	22.50	0.2	0.0085	22.05	0.15	0.01
W260	23.83	0.2	0.0085	23.35	0.15	0.01
W250	20.84	0.2	0.0085	20.43	0.15	0.01
W240	18.82	0.2	0.0085	18.45	0.15	0.01
W230	23.26	0.2	0.0085	22.79	0.15	0.01
W220	19.44	0.2	0.0085	19.05	0.15	0.01
W210	22.87	0.2	0.0085	22.41	0.15	0.01
W200	16.08	0.2	0.0085	15.76	0.15	0.01
W190	16.34	0.2	0.0085	16.01	0.15	0.01
W180	17.99	0.2	0.0085	17.63	0.15	0.01
W170	17.80	0.2	0.0085	17.44	0.15	0.01
W160	16.90	0.2	0.0085	16.56	0.15	0.01

Figure 5.4 shows the comparison of hourly simulated discharges with the hourly observed discharges. The semi-annual approach during the calibration period (Figure 5.5) didn't improve the model result by a noticeable difference. The NSE value improved from 0.73 to 0.74 and the percent bias improved from -10.4% to -9.5%. The inability of the semi-annual parameterization approach to improve the model by a significant amount can be attributed to the high variation in runoff amount during different years. The year 2009–2010 was one of the wettest years produced very high flows in the donor and receiver catchments compared to drier years 2011 and 2012. Although the semi-annual parameterization approach improved the model result for some of the dry and wet periods (Figure 5.5), the overall model results were not improved, due to the tendency

of NSE to be biased towards higher flows which occurred mostly during the first wet period (October 2009–April 2010).

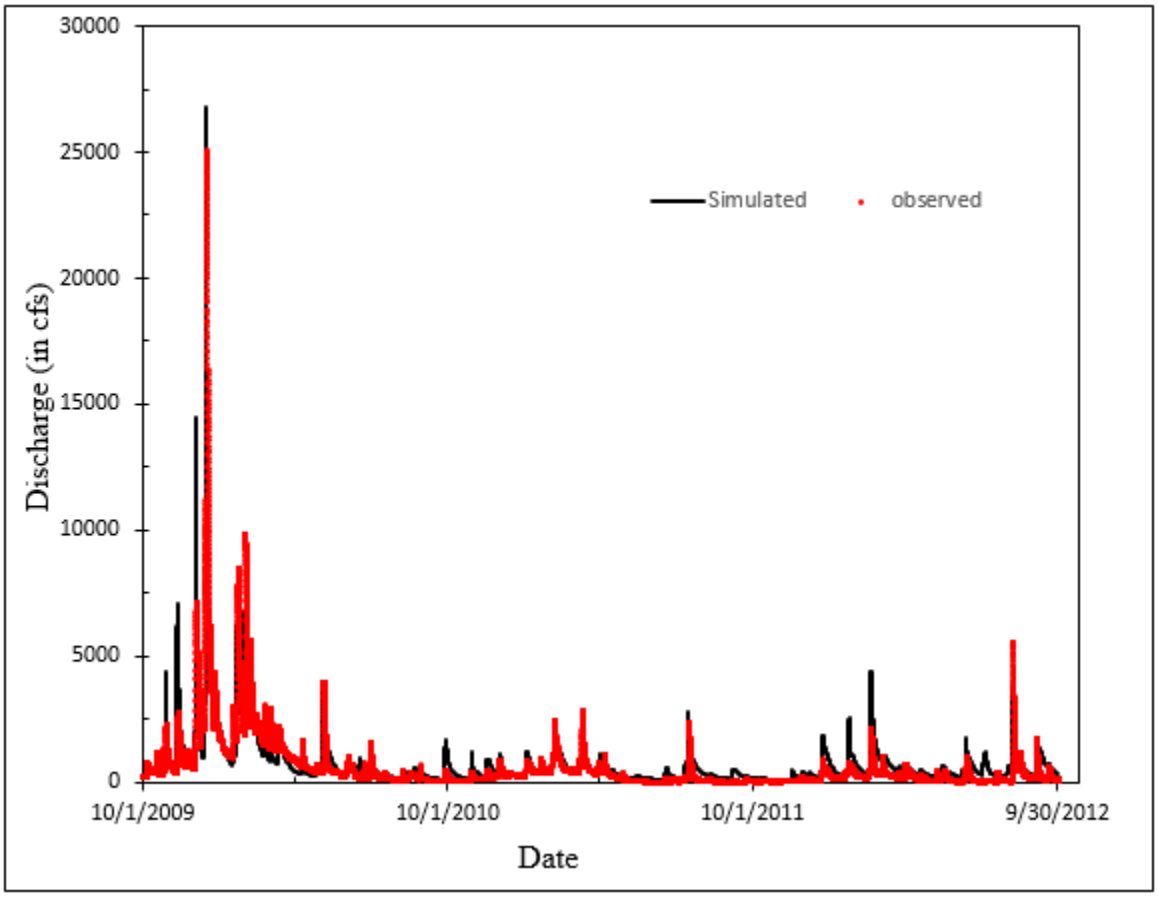

Figure 5.4 Hourly Simulated versus Observed Discharge for Donor Catchment during Calibration Period (Oct 2012–Sep2015) using Semi-annual Approach

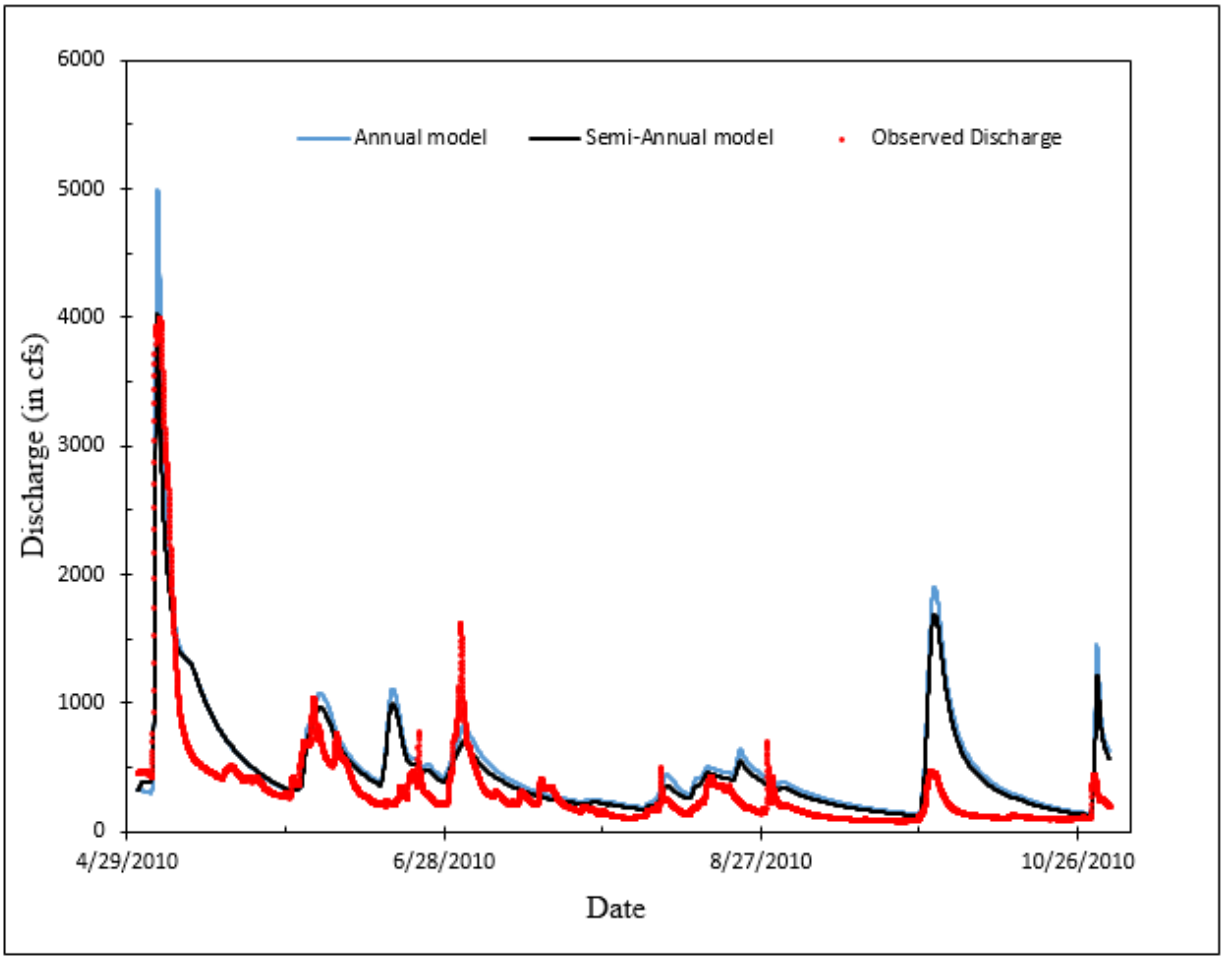

Figure 5.5 Semi-annual Model Comparison with Annual Parameter model for Donor Catchment (May 2010–October 2010)

Due to the inability of the semi-annual parameterization approach to improve the model by a significant amount, and a degree of complexity involved in it, only the annual model was used for validation and subsequent transfer process.

5.2 VALIDATION OF DONOR CATCHMENT

As seen from Figure 5.6, simulated hourly discharges match well with the observed discharges for the donor catchment during the validation period. The model seems to overpredict during most of the storm events, however, underestimates discharge during major storm events in April 2014. Statistical analysis for the donor catchment during the validation period provides an NSE value of 0.63, which is rated as satisfactory performance for the continuous hydrological model.

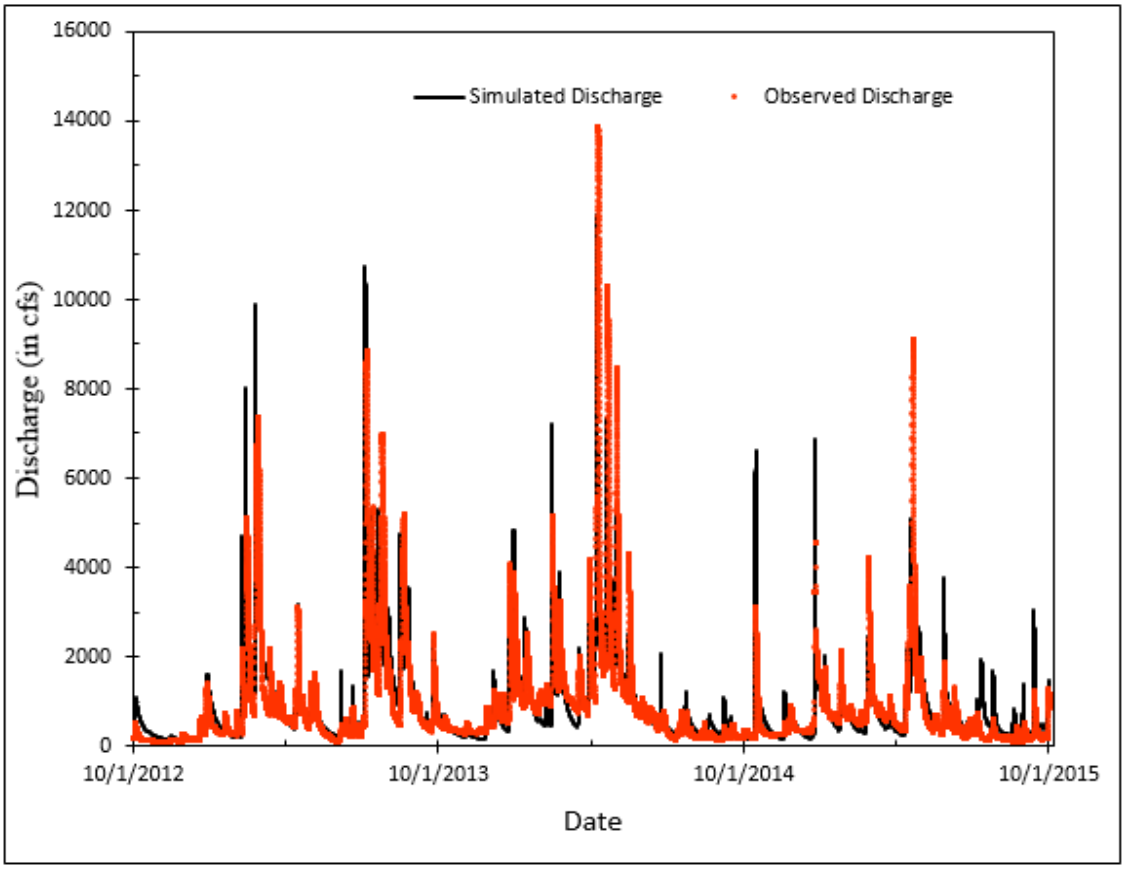

Figure 5.6 Hourly Simulated versus Observed Discharge for Donor Catchment during Validation Period (Oct 2012–Sep2015)

A scatterplot of simulated vs observed discharges during the validation period is shown in Figure 5.7. It shows that the most peak storm event in April 2014 was underestimated by model and peak discharge occur at different times. Like results for the calibration events, lower flows and smaller peak events are matched reasonably well, as a denser cloud near 1:1 line can be seen at lower values.

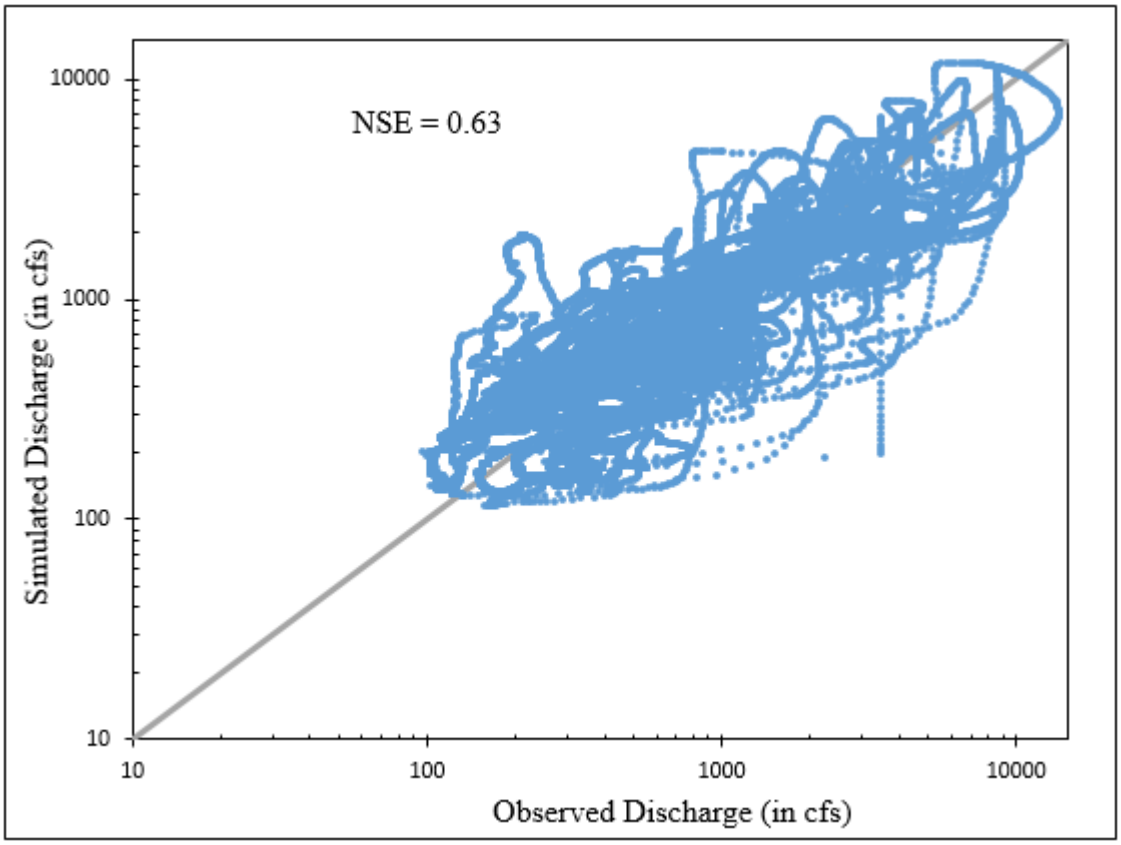

Figure 5.7 Scatterplot of Simulated Versus Observed Discharge during Validation period (Oct 2012–Sep 2015)

As seen from Figure 5.8, cumulative simulated discharge volume matches quite well with cumulative observed discharge volume for the donor catchment during the validation period. From the start of the validation period, the discrepancy in cumulative volumes remains very less until April 2014, from which the discharge volume is underpredicted by the model. This resulted in a

slightly higher difference between cumulative volumes. The PBIAS for the donor catchment during the validation period is 3.8%, which is rated as very good performance for the continuous hydrological model.

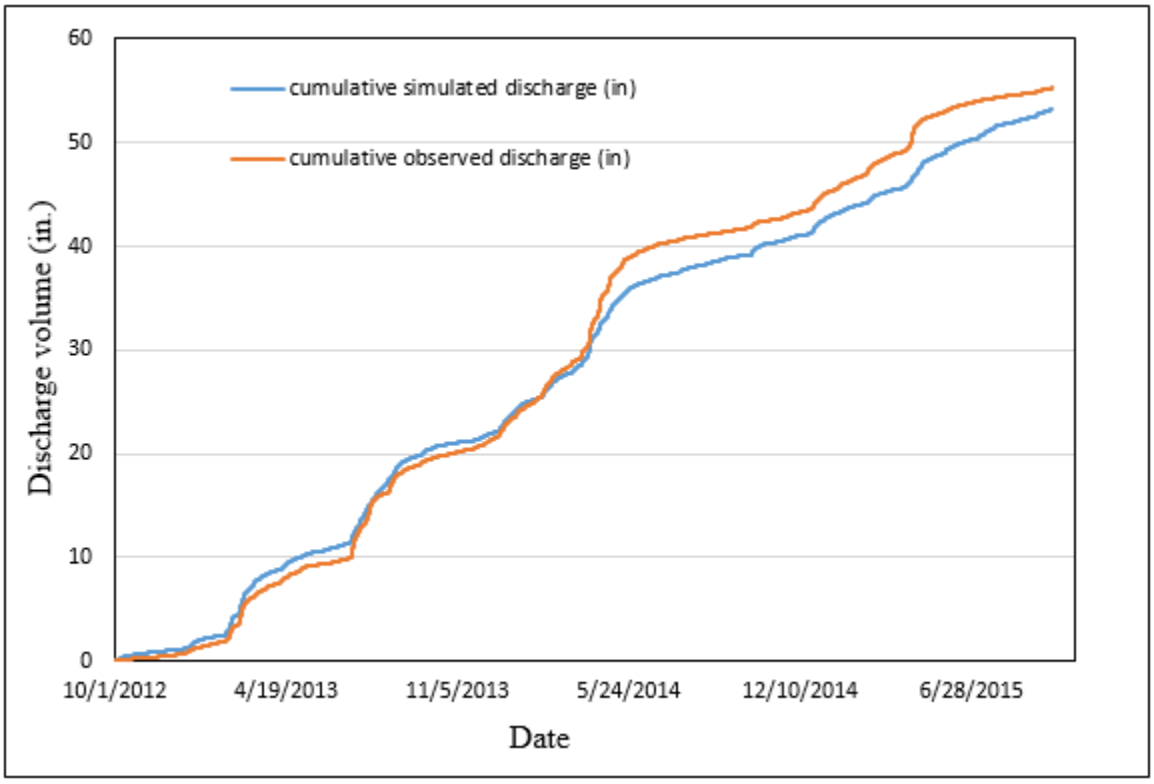

Figure 5.8 Cumulative Simulated versus Observed discharge volume during Validation period for Donor Catchment (Oct 2012–Sep 2015)

5.3 TRANSFER OF PARAMETER AND VALIDATION

All parameters of the SMA model except canopy storage and surface depression storage were transferred to the receiver catchment. Single values of each parameter were calculated as the areal average of the fifteen subcatchments' parameter values. Ten SMA parameters and their respective areal average value are provided in Table 5.3. Surface depression storage and canopy

storage were calculated directly for the receiver catchment using land cover data and soil data due to their lower sensitivities and ease in the calculation.

Table 5.3 Areal Average Value of SMA Parameter from Donor Catchment

Parameters	Areal average value
Maximum Infiltration (in/hr)	1.74
Soil Storage (in)	23.08
Tension Storage (in)	19.21
Soil Percolation (in/hr)	1.06
GW1 storage (in)	0.15
GW1 percolation (in/hr)	1.06
GW1 coefficient (hr)	40
GW2 storage (in)	0.332
GW2 percolation (in/hr)	0.0085
GW2 coefficient (hr)	200

Simulated hourly discharges match well with the observed discharges for the receiver catchment during the transfer validation period (October 2009—September 2012, Figure 5.9). The model seems to perfectly capture the value of peak discharge during a storm event of December 2009 with a small lag in the occurrence of the peak. Due to the coarseness of the precipitation data, the model couldn't correctly simulate some of the storm events in the late transfer validation period. Statistical analysis of the receiver catchment during transfer validation period provides an NSE value of 0.64, which is rated as satisfactory performance for the continuous hydrological model.

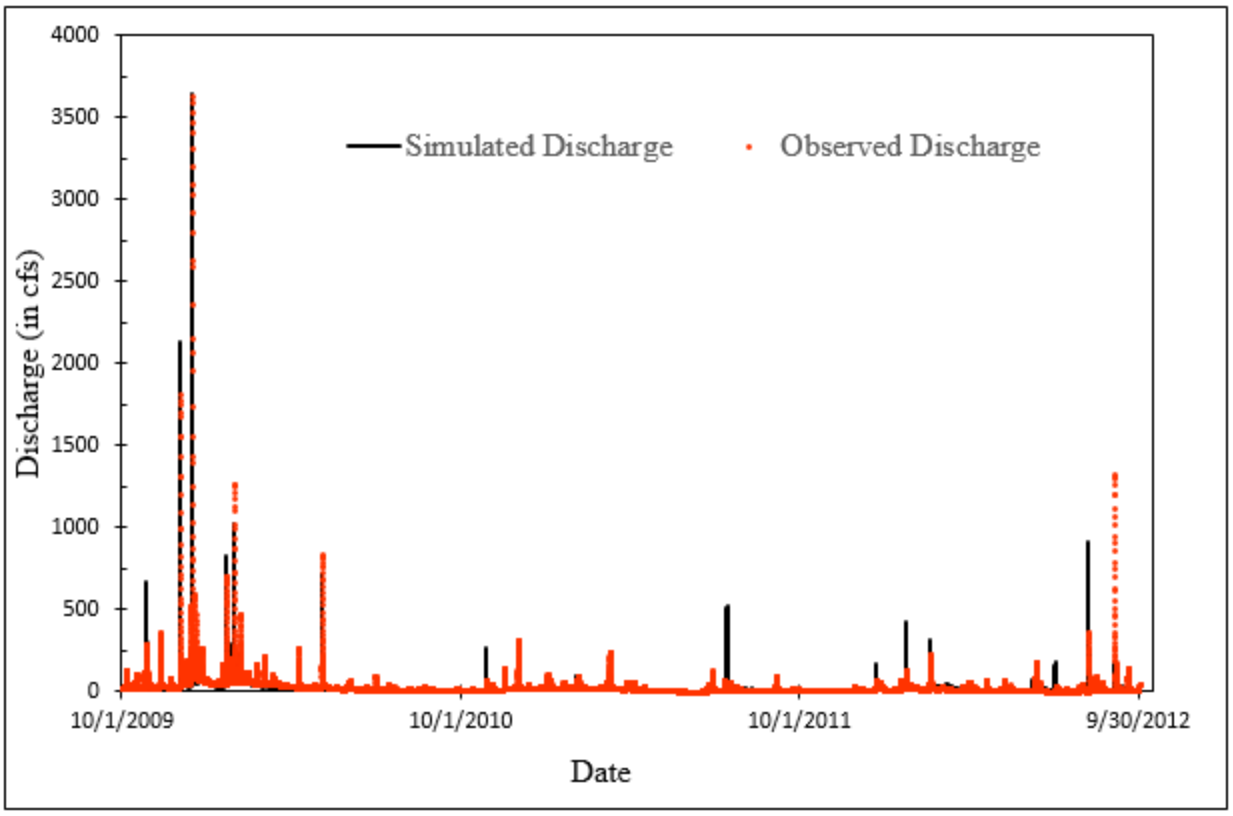

Figure 5.9 Hourly Simulated Versus Observed Discharge for Receiver Catchment during the Transfer Validation period (Oct 2009–Sep2012)

Figure 5.10 shows the scatterplot of simulated vs observed discharges for the receiver catchment during transfer validation period. It shows that the peak storm event was underestimated by the model only by a smaller value. Both storm events and lower flows matched reasonably well, as a denser cloud near 1:1 line can be seen.

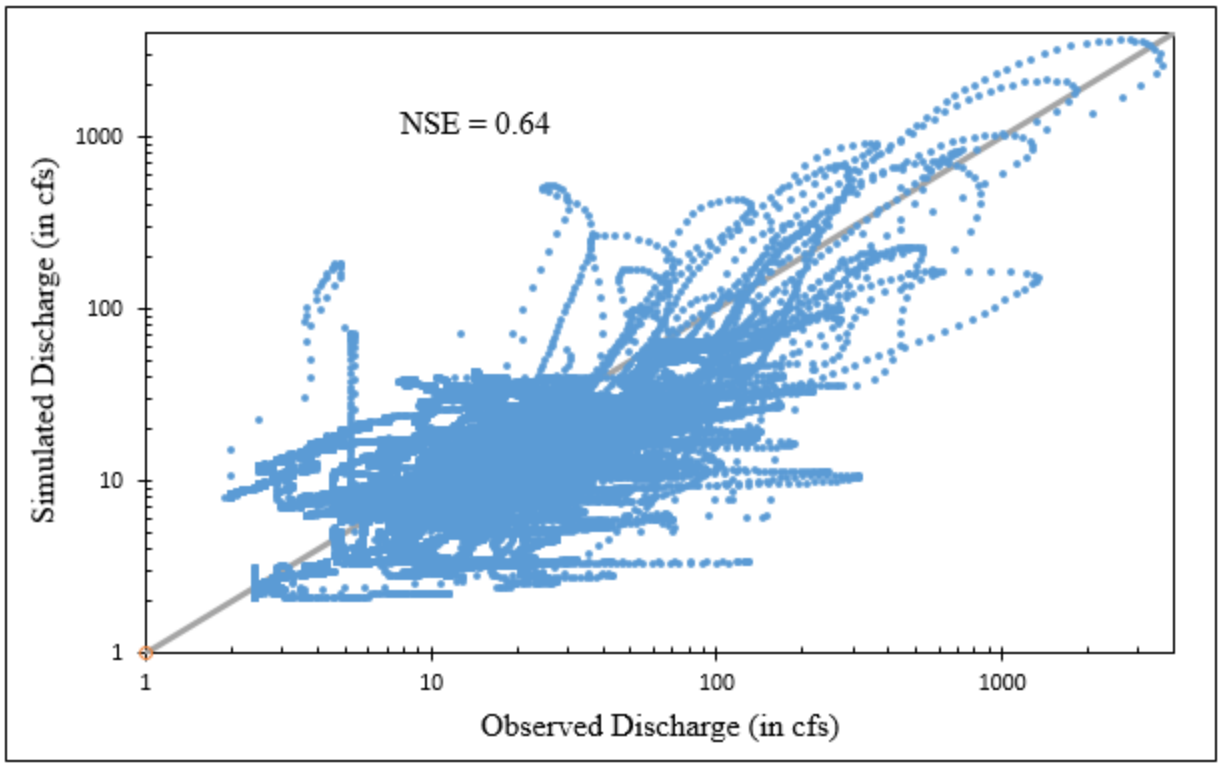

Figure 5.10 Scatterplot of Simulated Versus Observed Discharge during the Transfer Validation Period (Oct 2009–Sep 2012) for Receiver Catchment

Cumulative simulated discharge volume matches reasonably with cumulative observed discharge volume of the receiver catchment for start of the transfer validation period (Figure 5.11). However, after the first quarter year, the discrepancy in cumulative volumes keeps increasing as the model continues underprediction of the discharge volume. The PBIAS for the receiver catchment during the transfer validation period is 24.2% (< 25%), which is still rated as satisfactory performance for the continuous hydrological model.

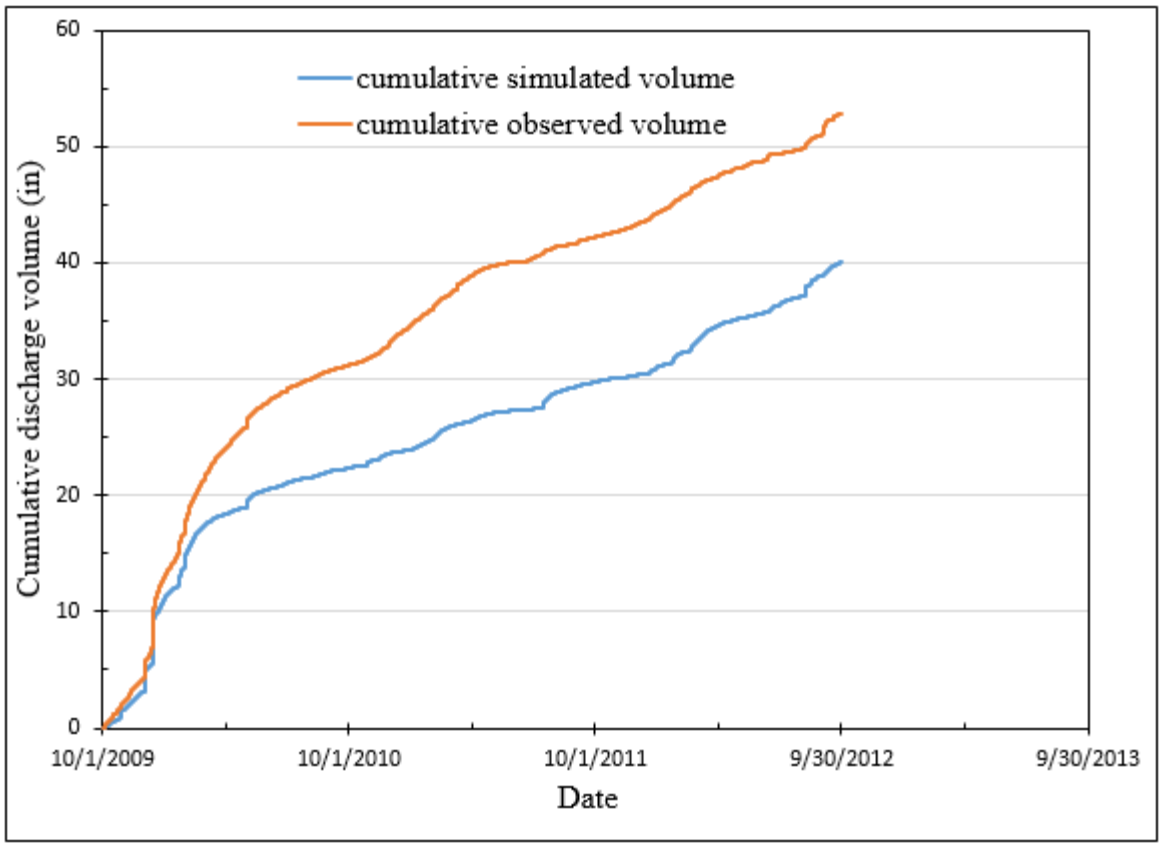

Figure 5.11 Cumulative Simulated versus Observed Discharge Volume during Transfer Validation Period for Receiver Catchment (Oct 2009–Sep 2012)

Alabama experienced severe to extreme drought condition in 2010. During this year, cumulative annual rainfall in Alabama varied from 20 in. to 70 in. The rainfall station used for the receiver catchment is Dothan regional airport, which is at a distance of 35 miles from the outlet. It can be seen from Figure 5.12 that Dothan regional airport experienced rainfall of about 35–40 in. whereas the receiver catchment experienced rainfall of 40–50 in. The discrepancy introduced by coarser spatial resolution of precipitation data resulted in higher PBIAS for 2010 and thus for the transfer validation period.

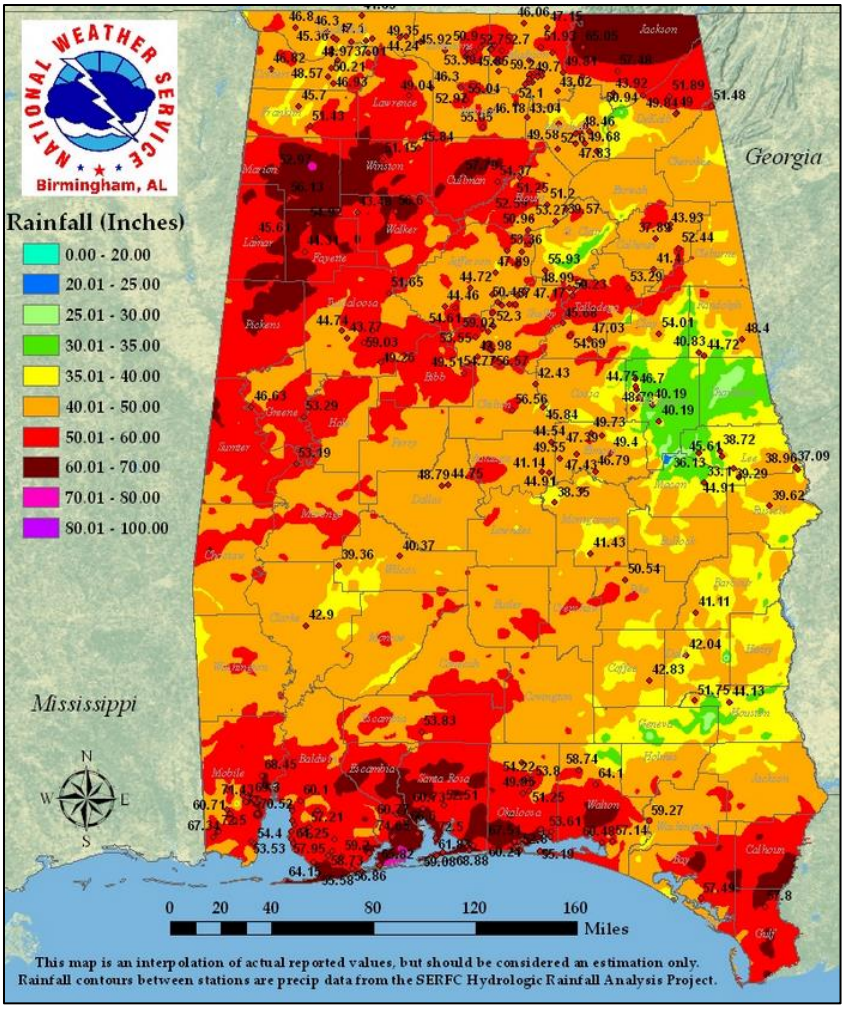

Figure 5.12 Annual Precipitation for Alabama in 2010 (Source: National Weather Service)

CHAPTER 6: APPLICATION TO SOAPSTONE BRANCH

6.1 STUDY AREA

Soapstone branch catchment covers an area of 2.74 sq. miles and is spread in Dale County of Alabama. The catchment outlet is 9.5 miles northwest of Dothan and 6 miles southeast of Newton, Alabama. It is also about 5 miles southeast from the outlet of the donor catchment (draining to Little Choctawhatchee River) and 25 miles west from the outlet of the receiver catchment (Figure 6.1). Soapstone branch catchment is a lowland agricultural catchment primarily comprised of four land cover classes viz. forest, rangeland, agricultural land, and water bodies. Their respective composition is shown in Table 6.1. The elevation of catchment ranges from 200 ft. to 395 ft. with average basin elevation of 320 ft. above mean sea level. The average basin slope is 5.3% and the average annual basin precipitation is 55.91 inches. Soils of different textures viz. fine sandy loam, loamy sand, sandy clay loam, etc. are present within the catchment with the highest composition of fine sandy loam (Service 1995).

Table 6.1 Land Cover Classes and their Respective Composition for Soapstone Branch Catchment

Land cover	Composition
Agricultural land	56.3%
Forest	34.4%
Rangeland	8.7%
Water	0.6%

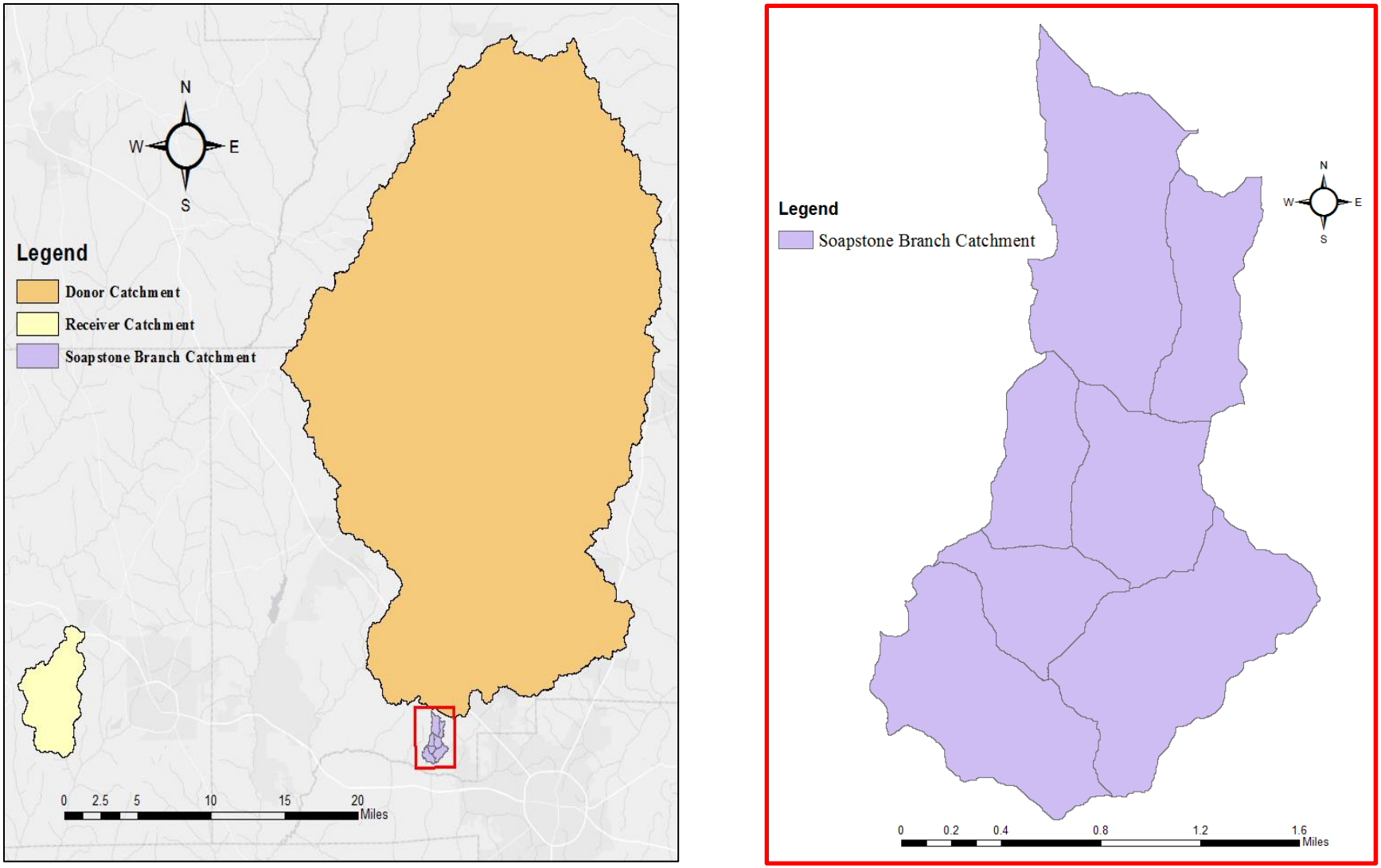

Figure 6.1 Location of Soapstone Branch Catchment Relative to Donor and Receiver Catchment

6.2 INPUT DATA

The input data viz. digital elevation model (DEM), precipitation data, land cover, and evapotranspiration data were required for creating HEC-HMS model of the Soapstone branch catchment. The temporal resolution of the precipitation data and evapotranspiration data were same as that of the previously modeled donor and the receiver catchments, i.e., hourly and daily respectively. Due to the objective of the study to quantify the amount of increase in sediment yield from 2011–2015, NLCD 2011 land cover data which was used in the donor and the receiver catchments was unfit for use. Furthermore, due to the smaller catchment size of Soapstone branch, higher spatial resolution for both DEM and land cover was desired.

6.2.1 DIGITAL ELEVATION MODEL

The 10 m DEM obtained from AlabamaView is very coarse to be used for the Soapstone branch catchment. In the case of large to medium size catchments like the donor catchment, a coarser resolution DEM can be utilized without producing errors of higher degrees. However, due to the smaller size of Soapstone branch, a finer resolution DEM is required. Contour shapefile with 2 feet interval of Choctawhatchee river catchment were obtained from Dale County. This contour shapefile was then converted to 1 m resolution DEM (Figure 6.2) using ArcGIS.

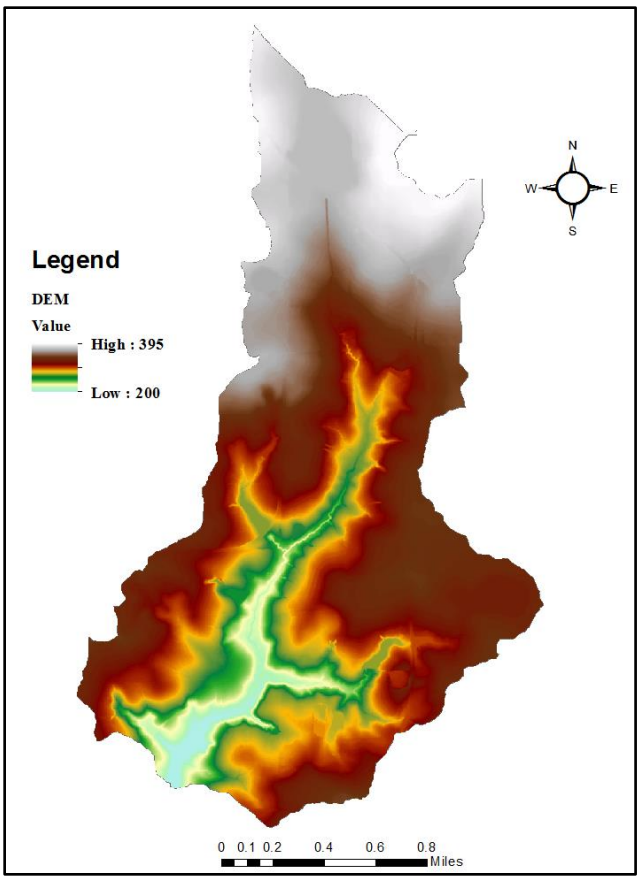

Figure 6.2 Digital Elevation Model of Soapstone Branch Catchment

6.2.2 MULTISPECTRAL AERIAL IMAGERY

The National Land Cover Dataset (NLCD) provides 30 m spatial resolution land cover maps of the entire United States in a period of every 5 years. The most recent land cover data provided by NLCD is for 2011. This dataset is coarser in both spatial and temporal scale. As seen from Figure 1.4, using NLCD land cover dataset of 2011 fails to consider the land cover changes occurring in the catchment from 2011–2015. Furthermore, due to smaller catchment size, a finer spatial resolution is required.

Land cover maps can be generated using satellite data from Landsat platforms or using the National Agriculture Imagery Program (NAIP) dataset. The NAIP dataset has a spatial resolution of 1 m and temporal resolution of 2 years which is suitable for our study. NAIP is controlled by US Department of Agriculture's (USDA) Farm Service Agency (FSA) through Aerial Photography office in Salt Lake City. Initially, NAIP provided aerial images with natural color spectral resolution (red, green, and blue) but starting in 2007, four bands spectral resolution was available viz. red (band 1), green (band 2), blue (band 3), and near-infrared (band 4). Four band NAIP imagery was collected for the catchment for 2011 and 2015.

A satellite image collected over several bands of the electromagnetic spectrum can be displayed as false color composite images. A false color composite image is a type of color rendering methods, where arbitrary colors are selected to display the reflectance from non-visible part of electromagnetic spectrum. For example, the near-infrared reflectance is not visible to human eyes, however, this reflectance is recorded by satellite sensors. So, if a multispectral aerial imagery is displayed with a red color resembling the near-infrared reflectance, then it is a false color composite. False color composite schemes have their applications in proper identification of vegetations in the image and thus helps in image classifications. There are a number of false color composite schemes which can be used for displaying a multispectral image. For NAIP imagery, a 4-1-2 false color composite scheme [Red = Band4 (near-infrared); Green= Band1 (red); Blue= Band2 (Green)] is utilized. A 4-1-2 false color composite map of soapstone branch catchment for 2011 and 2015 is shown in Figure 6.3.

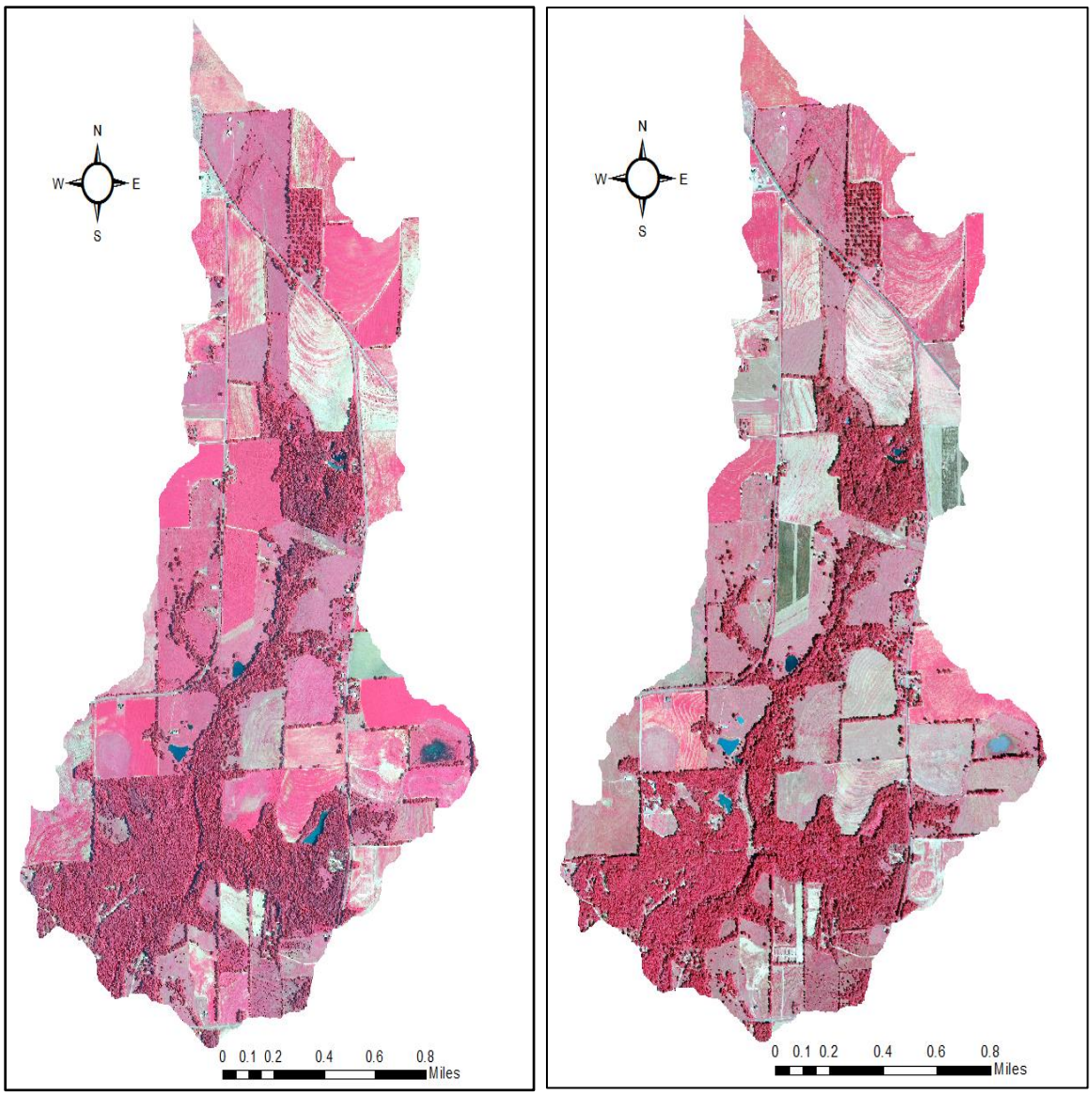

Figure 6.3 False Color Composite (4-1-2 scheme) Image of Soapstone Branch Catchment in 2011(Left) and 2015 (Right)

6.2.3 PRECIPITATION DATA

For accurate hydrologic modeling of the soapstone branch catchment, four precipitation gauges were calibrated and installed in the catchment beginning March 2016. Due to various reasons, all precipitation gauges were not functional throughout the period of March 2016–

September 2016. For streamflow modeling from January 2009–September 2016, precipitation data from Dothan Regional Airport (6.6 miles from Dean Road Bridge) was collected for the period of Jan 2009– February 2016.

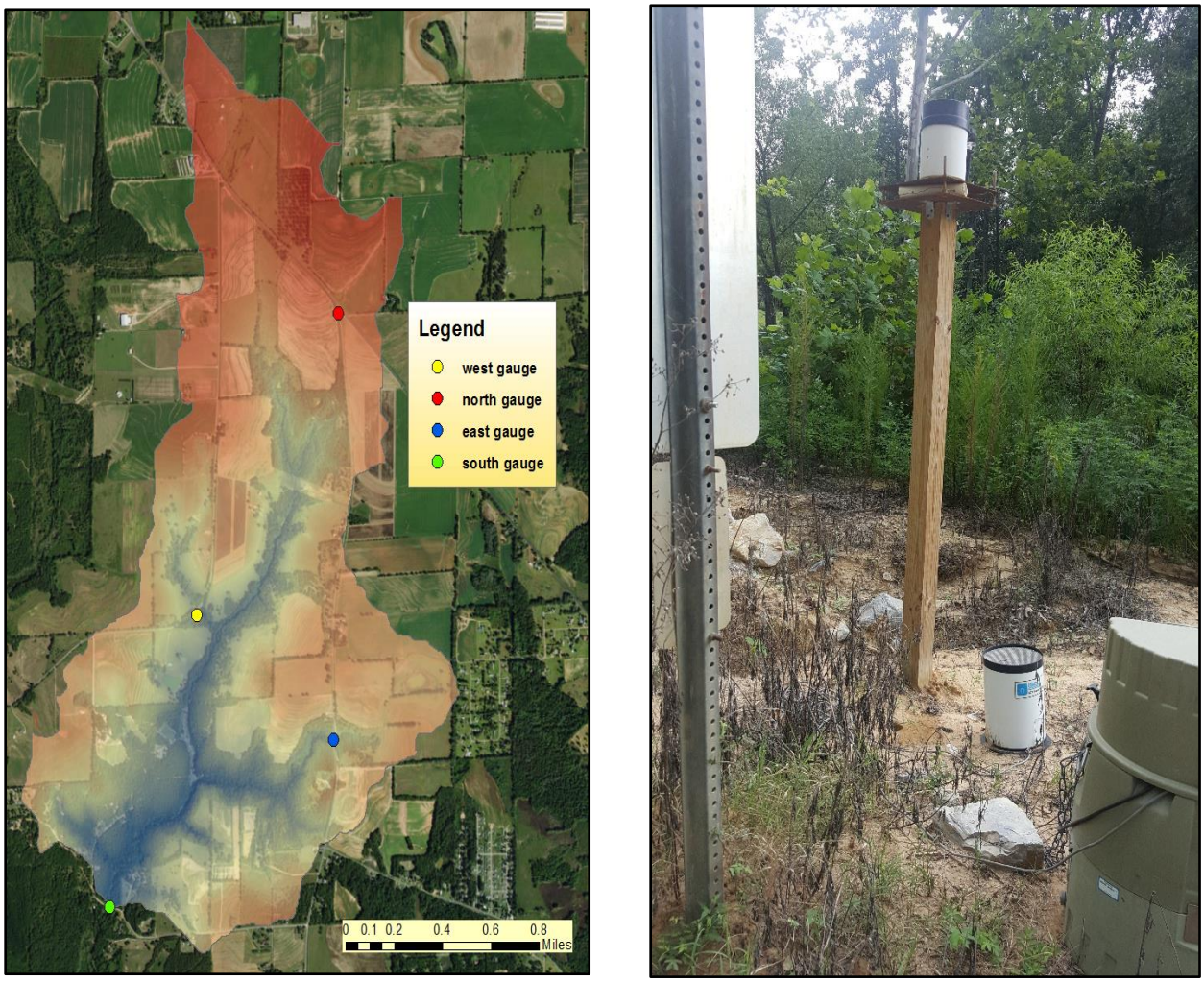

Figure 6.4 Rain Gauge Locations in the Catchment (Left) and Installed Rain Gauge (Right)

6.2.4 EVAPOTRANSPIRATION DATA

Daily pan evapotranspiration data were obtained for stations located in Headland, Alabama for the period of 2009–2013. For years 2014–2016 and days with missing value, monthly average pan evapotranspiration data from Class A pans for the closest station, i.e., Martin Dam provided by NOAA (Farnsworth and Thompson 1983) was used. A correction factor of 0.7 is applied to convert pan evapotranspiration to potential evapotranspiration.

6.3 METHODOLOGY FOR STREAMFLOW SIMULATION

6.3.1 CATCHMENT DELINEATION AND STREAM DEFINITION

HEC-GeoHMS was used for catchment delineation from the DEM created earlier. A stream definition of 0.4 sq. km. was selected using a trial and error method to match the generated streams with the natural streams. This procedure divided the catchment into seven subcatchments (Figure 6.5): W80–W140.

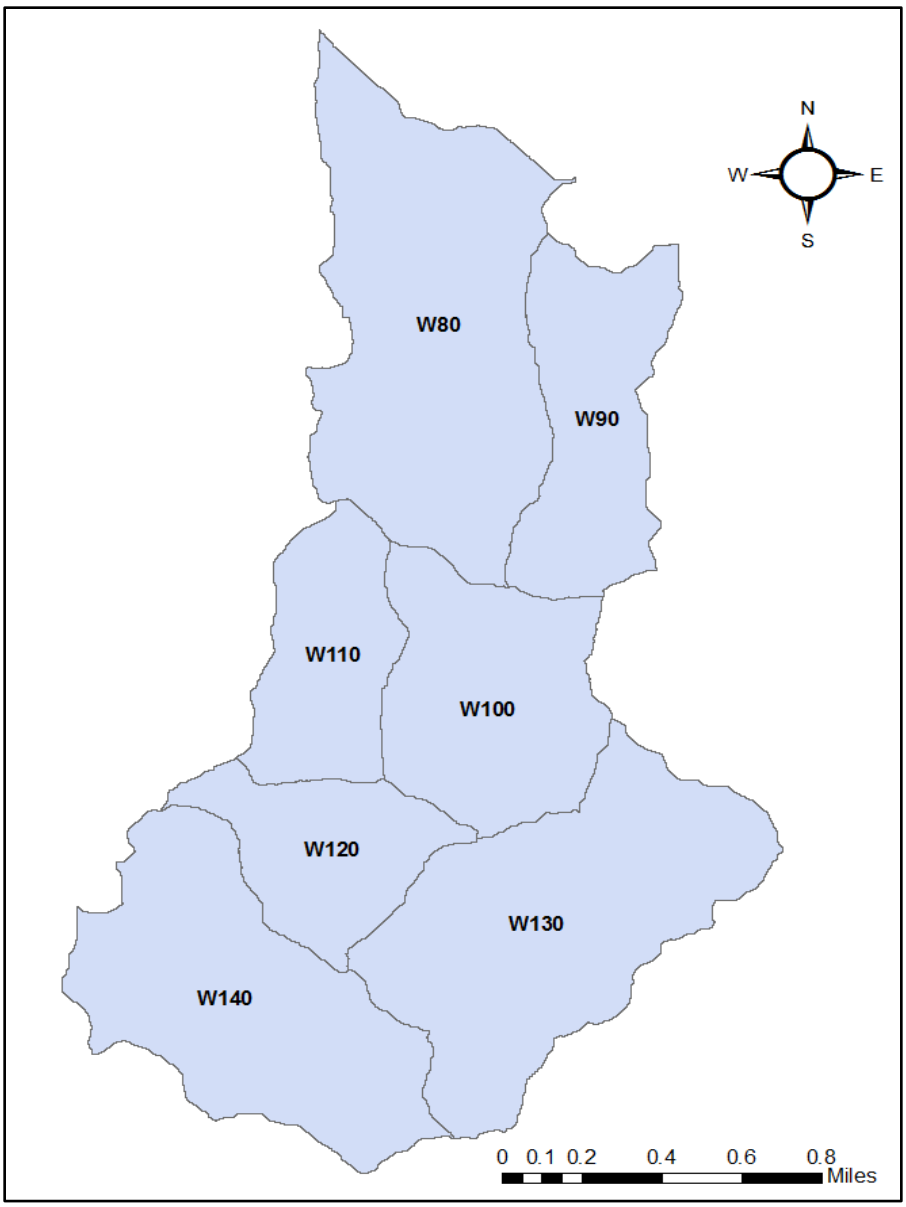

Figure 6.5 Delineated Soapstone Branch Catchment and Partition into Subcatchments

6.3.2 LAND COVER MAP GENERATION

The NAIP imagery can be converted into land cover maps using two types of classification schemes viz. unsupervised and supervised classification scheme. In unsupervised classification, users can enter the desired number of classes to which s/he desires to initially classify the original

image. The software then classifies as per designed algorithm to group pixels into various spectral classes. Unlike this method, in supervised classification, the user selects training sites for each final desired class and, based on the spectral signature of those training sites, software categorizes the original image. The accuracy of unsupervised classification scheme can be further improved by using a cluster busting technique (Bossler et al. 2004). In the cluster busting technique, a subset of the image is selected and unsupervised classification scheme is applied to the respective subset image. The overlay of the subset and the originally classified image results into an image with higher accuracy.

Two different NAIP datasets collected in 2011 and 2015 were used. Unsupervised classification using the Iterative Self-Organizing Data Analysis Technique (ISODATA) with 40 classes was applied using ERDAS IMAGINE 2016 software. Using multispectral NAIP imagery, these 40 classes were categorized into 4 different land use types viz. forest, agricultural land, water, and rangeland. Rangelands and agricultural lands have similar spectral reflectance and are often difficult to differentiate with a smaller number of classes in unsupervised classification. For improving accuracy, the cluster busting technique was applied. An area of land surrounding the forest and rangeland was clipped from the original image and then, the unsupervised classification was carried out on the clipped subset (Figure 6.6). Final overlay of the clipped and initially classified image produced the final land cover map (Figure 6.7).

Land cover maps were prepared using classification and cluster busting techniques for 2011 and 2015. Accuracy assessment for both land cover classification was performed in ERDAS Imagine software. In accuracy assessment, a number of test points is selected by the user and then ERDAS Imagine places those points over the area being classified either by random procedure or stratified random procedure (user's choice). Those distributed points are then provided a land cover

class based on their spectral signature. Newly entered land cover class for those points is compared with the originally classified land cover class. The software then calculates overall accuracy and Kappa statistics based on this comparison. Overall accuracy is the simple accuracy assessment which calculates the percentage of the match during the comparison. However, Kappa statistic reflects the difference between agreement achieved and the agreement expected by chance. A Kappa value of 0.7 indicates that there is 70% better agreement than by chance alone. For 2011, overall classification accuracy was 95% and overall Kappa statistics was 0.9149 whereas, for 2015, overall classification accuracy was 100% and overall Kappa statistics was 1.0.

Rangeland area increased whereas forest area decreased from 2011 to 2015 (Figure 6.7). Statistical analysis of land cover data from 2011 to 2015 shows that forest area reduced from 34.4% to 28.7%, agricultural land increased from 56.3% to 58.1% and rangeland increased from 8.7% to 12.6%.

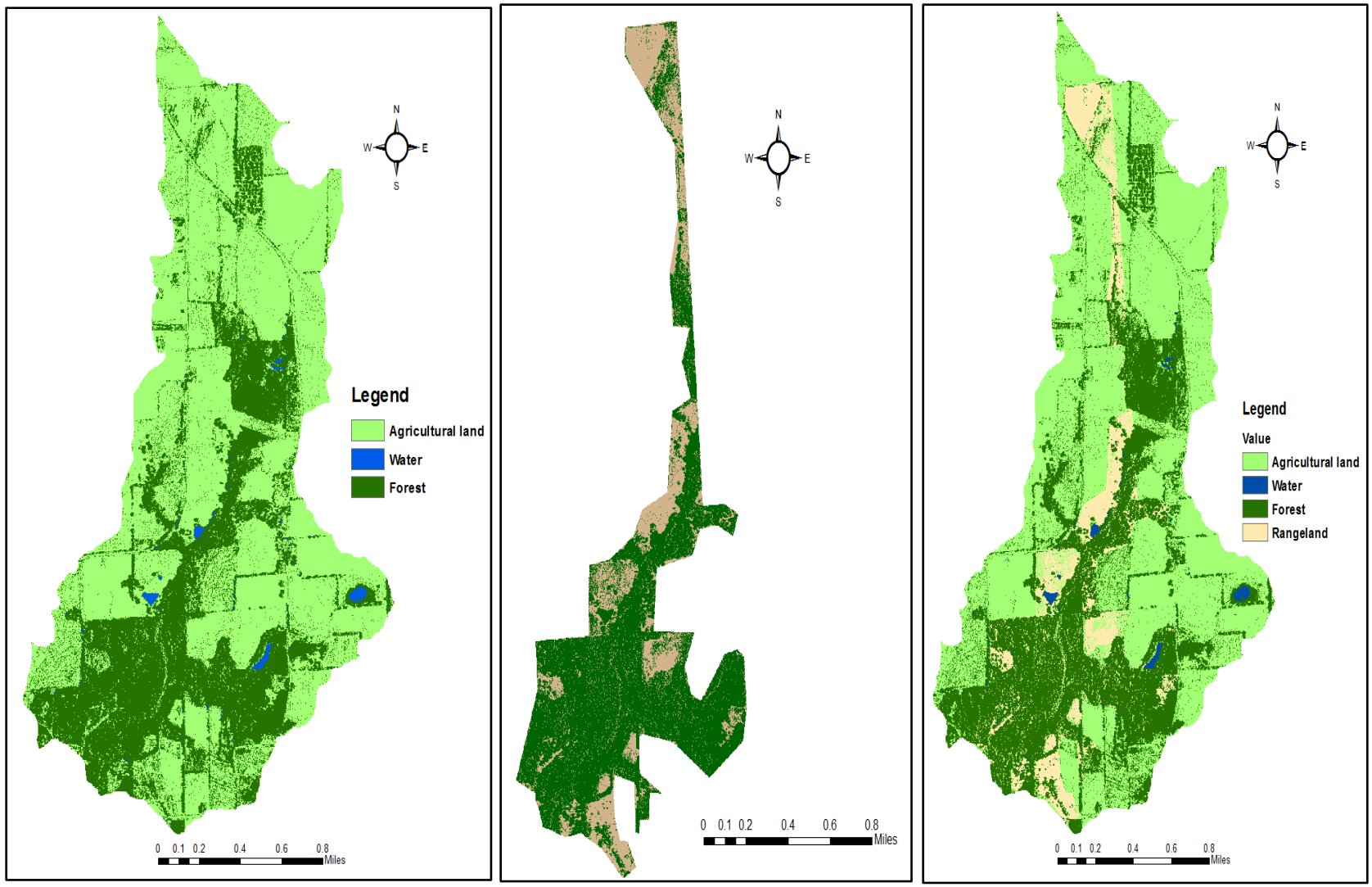

Figure 6.6 Cluster Busting Technique Applied to Area Surrounding Forest: Before (Left), Cluster busting (Middle) and After (Right)

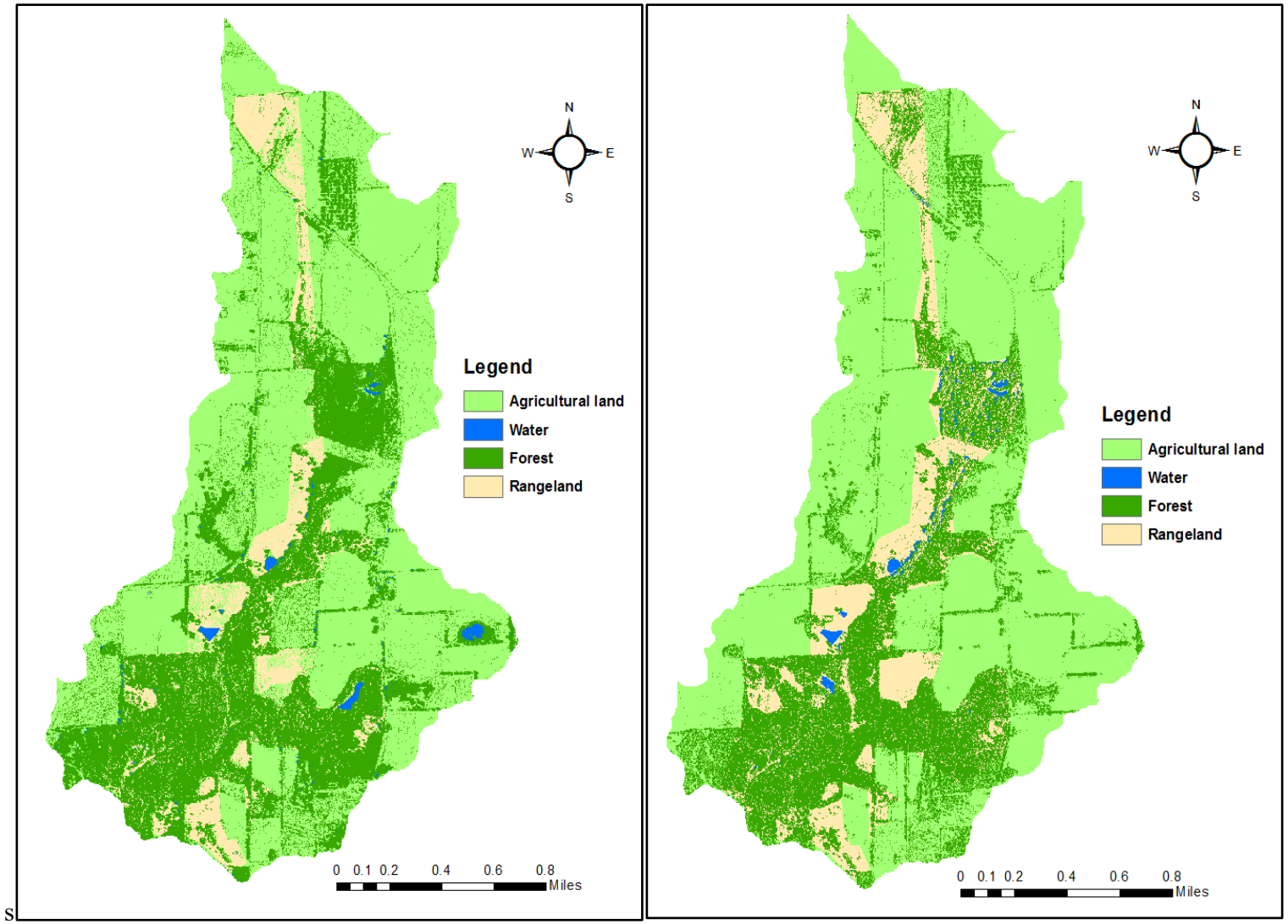

Figure 6.7 Land Cover Map of Soapstone Branch Catchment Developed from NAIP Imagery for 2011 (Left) and 2015 (Right)

6.3.3 CURVE NUMBER AND BASIN LAG

The soil data of Dale County was used for producing the HSG map for the catchment (Figure 6.8). The combination of HSG map and land cover map produced the CN grids of the catchment for 2011 and 2015 (Figure 6.9). The procedure of creating CN grid in the Soapstone branch catchment using the land cover map and HSG is similar to the procedure used in the donor and receiver catchment and is provided in detail in section 4.3.

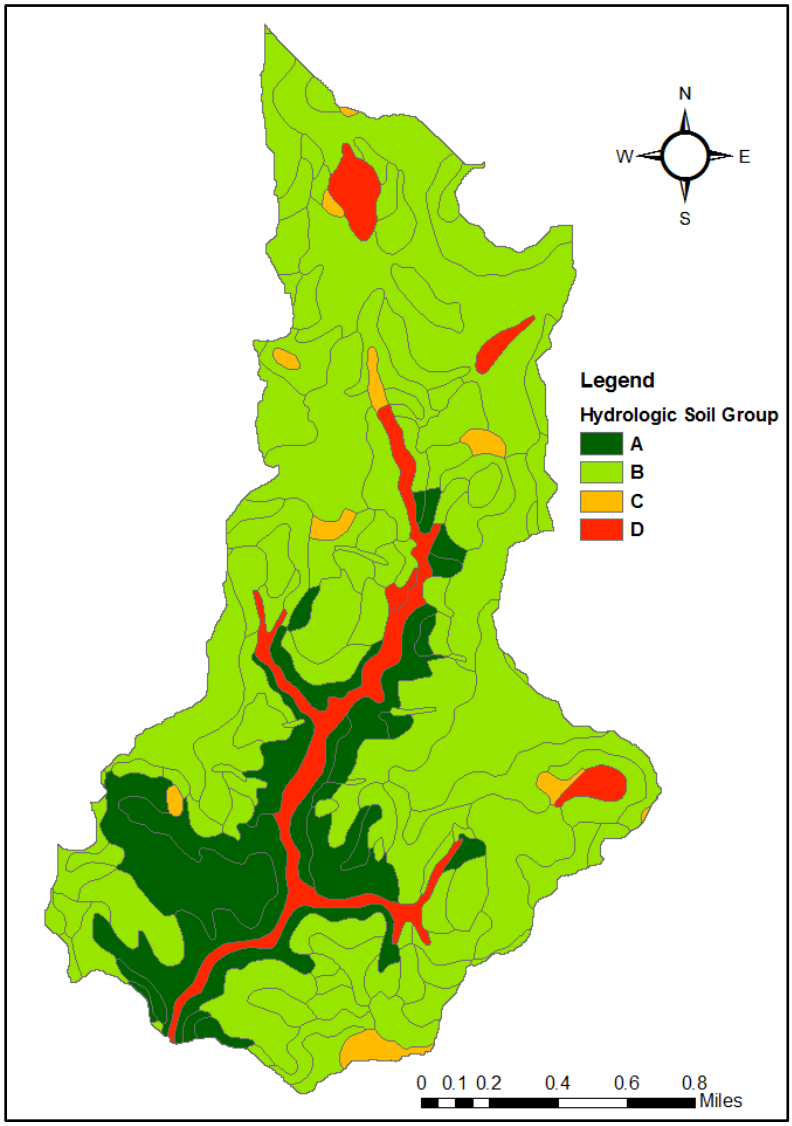

Figure 6.8 Hydrologic Soil Group Map of Soapstone Branch Catchment

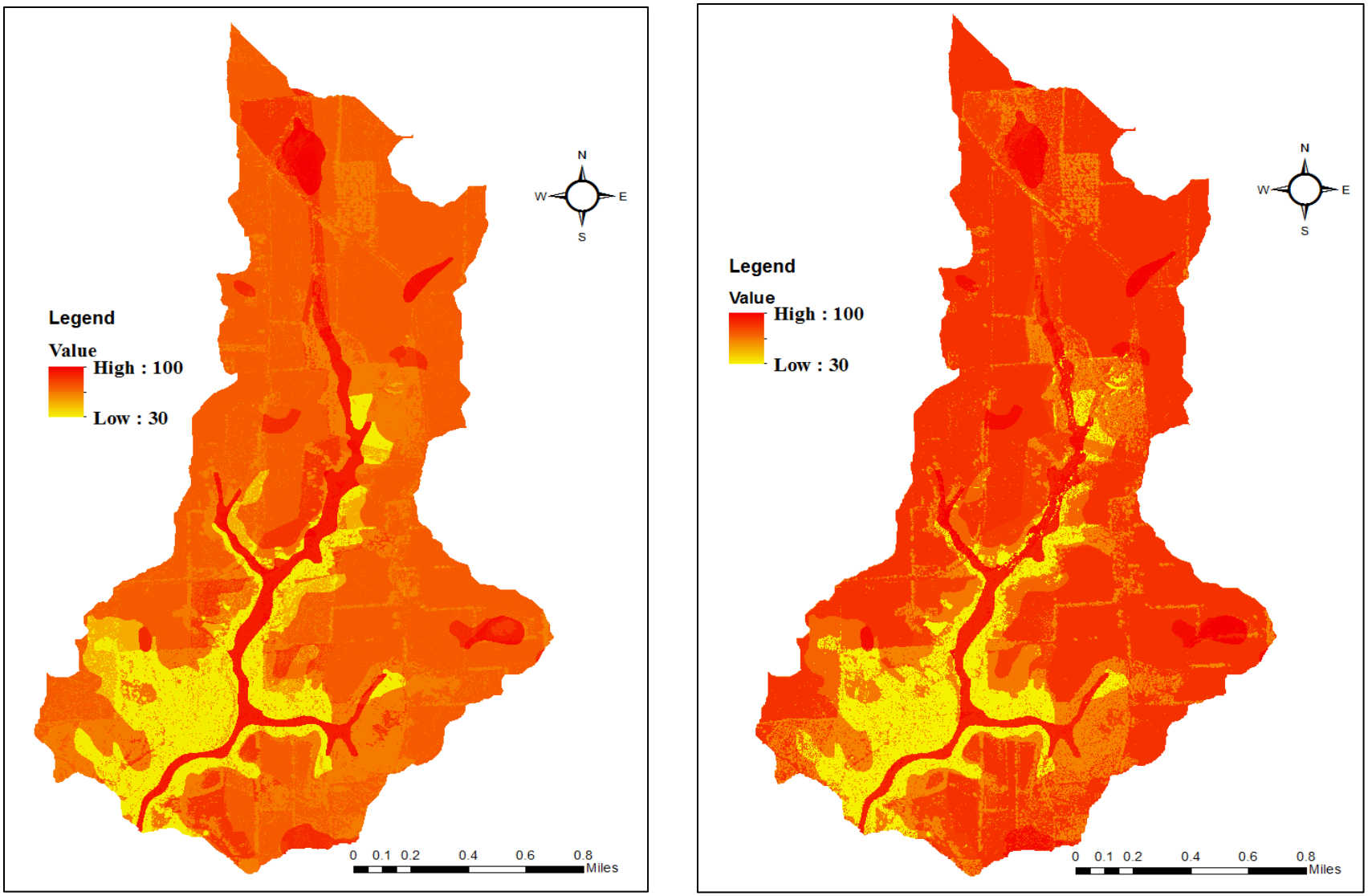

Figure 6.9 Curve Number Grid of Soapstone Branch Catchment for 2011 (Left) and 2015 (Right)

Table 6.2 shows that curve number of each subcatchments increased by a small amount from 2011 to 2015, thus, reducing the basin lag. However, for subcatchments W140, W130 and W110, increase in curve number was higher than the increase in other subcatchments as expected since deforestation and land cover changes in this subcatchments were of significant amount than any other catchment.

Table 6.2 Curve Number and Basin Lag Computation at Subcatchment Scale for 2011 and 2015

Subcatchment	Curve Number (2011)	Curve Number (2015)	Basin lag 2011 (in minutes)	Basin lag 2015 (in minutes)
W140	65	66	46	44
W130	73	75	52	50
W120	67	67	37	37
W110	77	78	33	31
W100	75	75	32	32
W90	77	78	54	53
W80	78	79	64	63

6.3.4 PARAMETER TRANSFER

Similar to the receiver catchment, HEC-HMS model parameters were transferred from the donor catchment to the Soapstone branch catchment. However, unlike lumped receiver catchment, Soapstone branch catchment is a semi-distributed catchment with seven subcatchments. Therefore, the areal average of the parameters (Table 5.3) obtained from the donor catchment was applied to each individual subcatchments.

6.4 PARAMETER ESTIMATION FOR MUSLE

6.4.1 SOIL ERODIBILITY FACTOR

Soil erodibility factor (K factor) is defined as the rate of soil loss per rainfall erosion index unit measured on a unit plot of 72.6 ft. length and 9% slope. The unit plot is in clean-tilled fallow condition with tillage upslope and downslope. K factor can be obtained from soil data available at SSURGO database. USDA soil data viewer provides an easy way of mapping K factor of the soil data provided county. K factor obtained from USDA for Dale County was then clipped for the Soapstone branch catchment (Figure 6.10). An areal average K factor value of 0.19 was obtained for the Soapstone branch catchment.

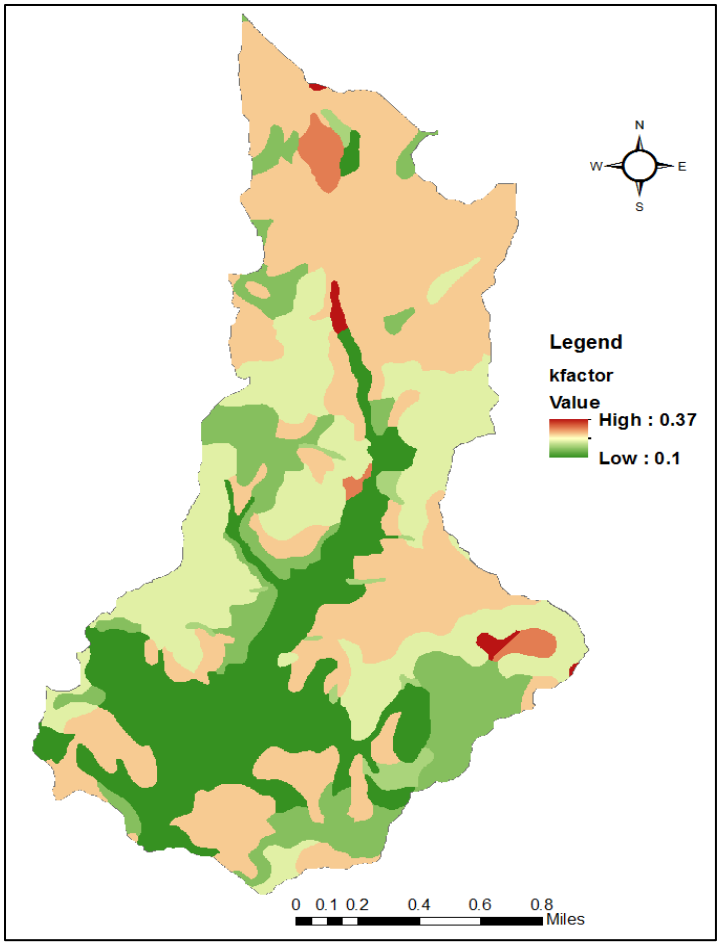

Figure 6.10 Spatial Distribution of K factor in the Soapstone Branch Catchment

6.4.2 TOPOGRAPHIC FACTOR

Topographic factor (LS factor) accounts for the effect of slope length and slope steepness on the quantity of soil erosion. It is the ratio of soil loss per unit area from a field slope to the amount of soil loss from a plot of 72.6 ft. length with 9% uniform slope. LS factor can be computed by using Equation (6.1).

$$LS = \left(\frac{X}{72.6}\right)^{m} * (0.065 + 0.045 * S + 0.0065 * S^2) \quad (6.1)$$

Where,

X = slope length (ft.)

S = Slope gradient (%)

m = exponent depending on S and can be obtained from Table 6.3.

Table 6.3 Exponent m-value in LS factor for different slope

Slope (in %)	m-value
>5	0.5
3-5	0.4
1-3	0.3
<1	0.2

Slope length (X) can be calculated for each raster grid using Equation (6.6).

$$X = flow\ accumulation * cell\ size \quad (6.2)$$

From available DEM, a slope grid and flow accumulation grid were created. Then, LS factor grid (Figure 6.11) was prepared using Equation (6.5) and (6.6). An areal average LS factor value of 0.98 was computed for the Soapstone branch catchment.

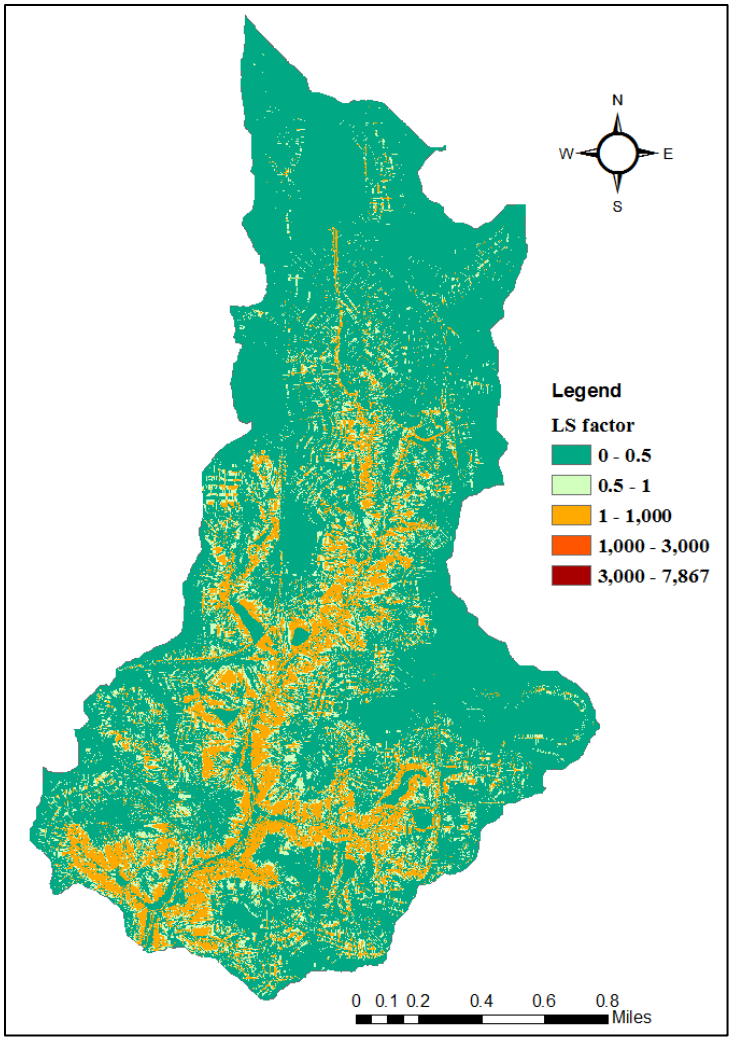

Figure 6.11 Spatial Distribution of LS factor in the Soapstone Branch Catchment

6.4.3 COVER MANAGEMENT FACTOR

The cover management factor (*C* factor) is the ratio of soil loss from a land covered by a specific crop to the soil loss under continuous bare fallow land condition. The *C* factor depends on a variety of factors such as the type of vegetation, their stage of growth, and their respective cover percentage. The *C* factor for any area can be developed using normalized difference vegetation index (NDVI). NDVI is a numerical indicator which describes the greenness, i.e., relative health and density of vegetation. The value of NDVI ranges from -1 to +1 and can be calculated using

data from the visible red band and near infrared band of satellite imagery. The mathematical expression for NDVI is given in Equation (6.3). NDVI value so produced can be used to develop cover factor using Equation (6.4) (Gitas et al. 2009).

$$NDVI = \frac{NIR - VR}{NIR + VR} \tag{6.3}$$

Where,

NIR = near infra-red

VR= visible red

$$C = \exp(-a\frac{NDVI}{b - NDVI}) \tag{6.4}$$

Where,

a, *b* = empirical constant

Gitas et al. (2009) have suggested a value of 2 and 1 for *a* and *b*, respectively. Using the near infra-red band (band 4) and visible red band (band 1) of aerial images (from NAIP) for the catchment, NDVI value raster grid was created for both 2011 and 2015.

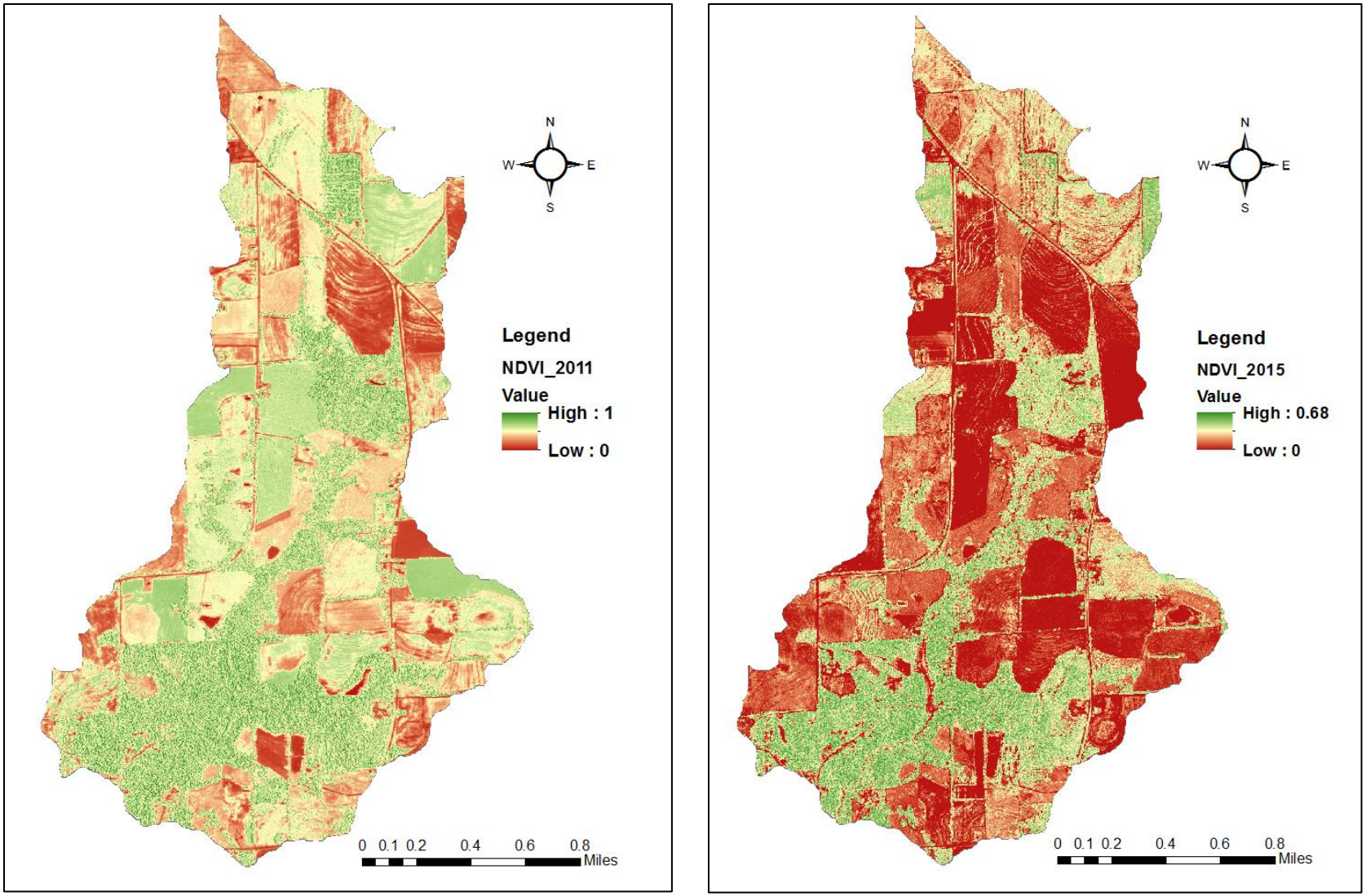

Figure 6.12 Spatial Variation of NDVI Values of the Soapstone Branch Catchment in 2011 (Left) and 2015 (Right)

Raster calculation on NDVI raster grid for 2011 and 2015 (Figure 6.12) using Eqn. (6.4) produced *C* factor grid of catchment for 2011 and 2015, respectively. However, it can be noted from Figure 6.12, that, compared to 2011, 2015 has less crop in the agricultural land indicated by dark red zones with lower NDVIs. During data collection of aerial imageries of the catchment for these two years, an attempt was made to obtain data for the same month. However, due to data limitation, aerial imageries were obtained for different months, i.e., August 2011 and September 2015. Due to the probable crop rotation going on in the agricultural land and different crop growth season, agricultural land has different NDVIs and *C* factor for 2011 and 2015. Since the objective of this study is to quantify the difference in sediment yield due to land cover changes and not the crop type or growth season, an additional computational step was applied.

For 2011, land cover class corresponding to agricultural land was clipped out and the average value of *C* factor for agricultural land was calculated. This average value was then applied to all raster grid of *C* factor for 2015 which correspond to agricultural land (Figure 6.14). This additional computation avoids the effect of agricultural crop growth and their seasonality on the sediment yield.

Furthermore, an attempt was made to quantify the amount of change in C factor by neglecting the effects of deforestation near stream. For this task, the forest area where major deforestation activities were experienced from 2011–2015, as observed from aerial imageries (Figure 1.4), was clipped out from the 2011 imagery and overlaid on 2015 aerial imagery. A new hypothetical C factor grid was then obtained using the procedure explained earlier (Figure 6.15).

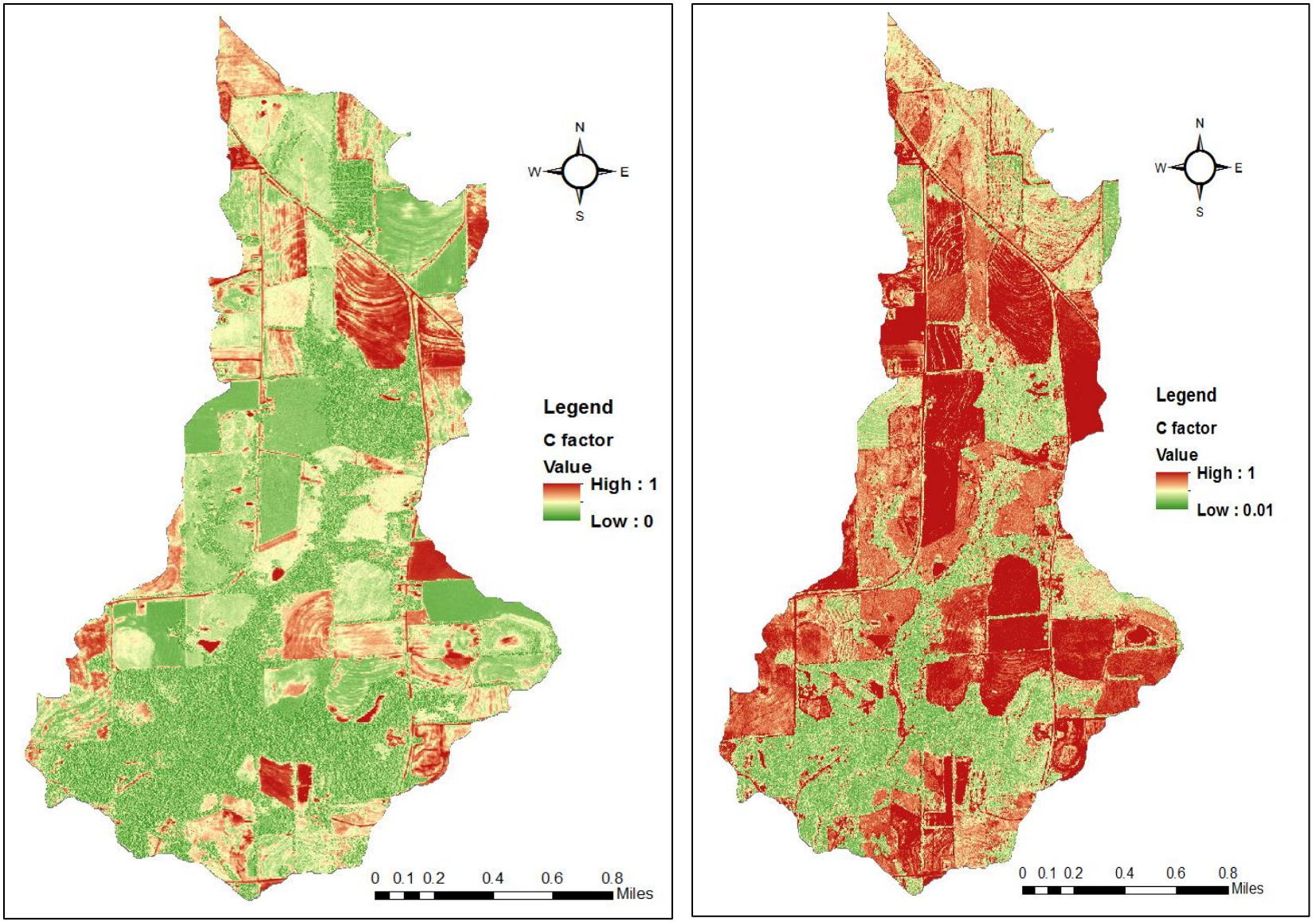

Figure 6.13 Spatial distribution of *C* factor raster grid of Soapstone Branch Catchment in 2011 (Left) and 2015 (Right)

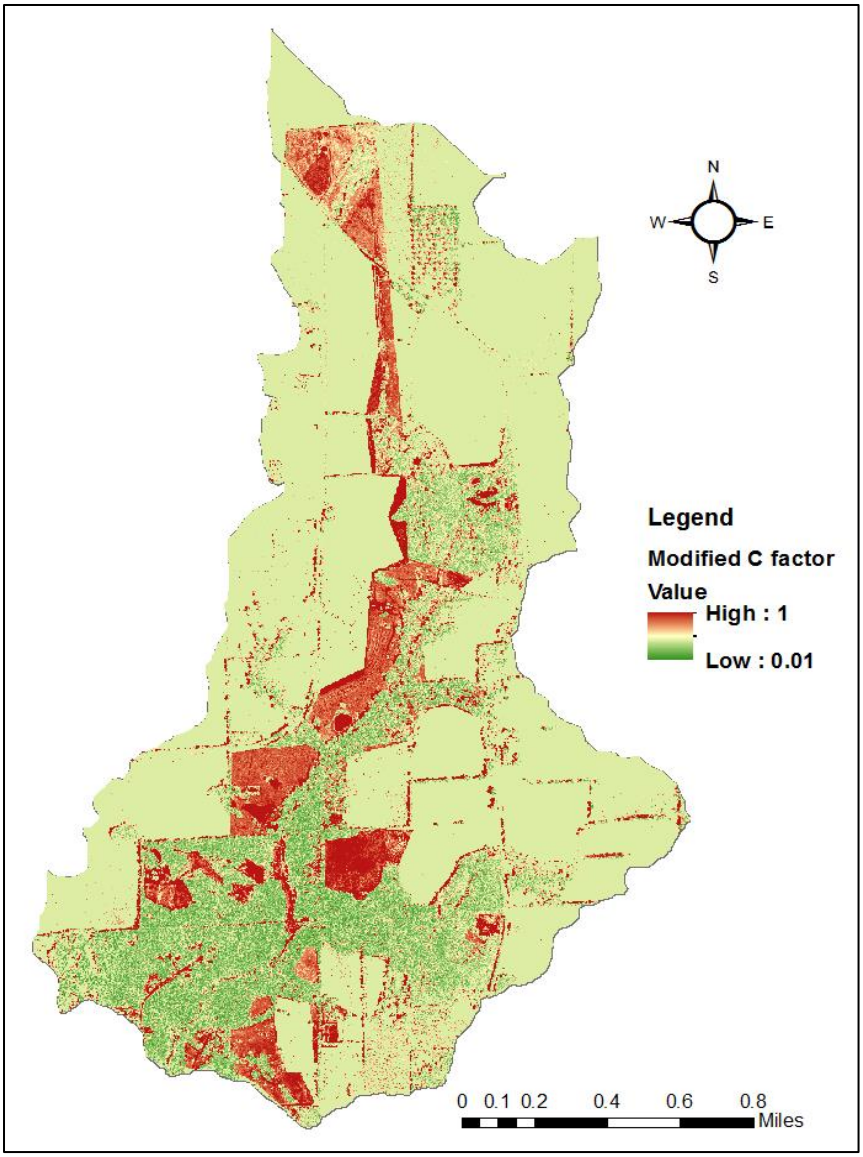

Figure 6.14 Modified *C* factor raster grid of the Soapstone Branch Catchment in 2015

An areal average value of *C* factor grid was computed for the entire catchment both in 2011 and 2015. Average *C* factor value of the Soapstone branch catchment in 2011 was 0.347 which increased to 0.678 in 2015. However, the modification of *C* factor grid to neglect the influence of crop rotation and crop growth season produced an areal average value of 0.466 in 2015. Therefore, an overall increase of 34.3% in *C* factor was experienced by the Soapstone branch catchment due to deforestation.

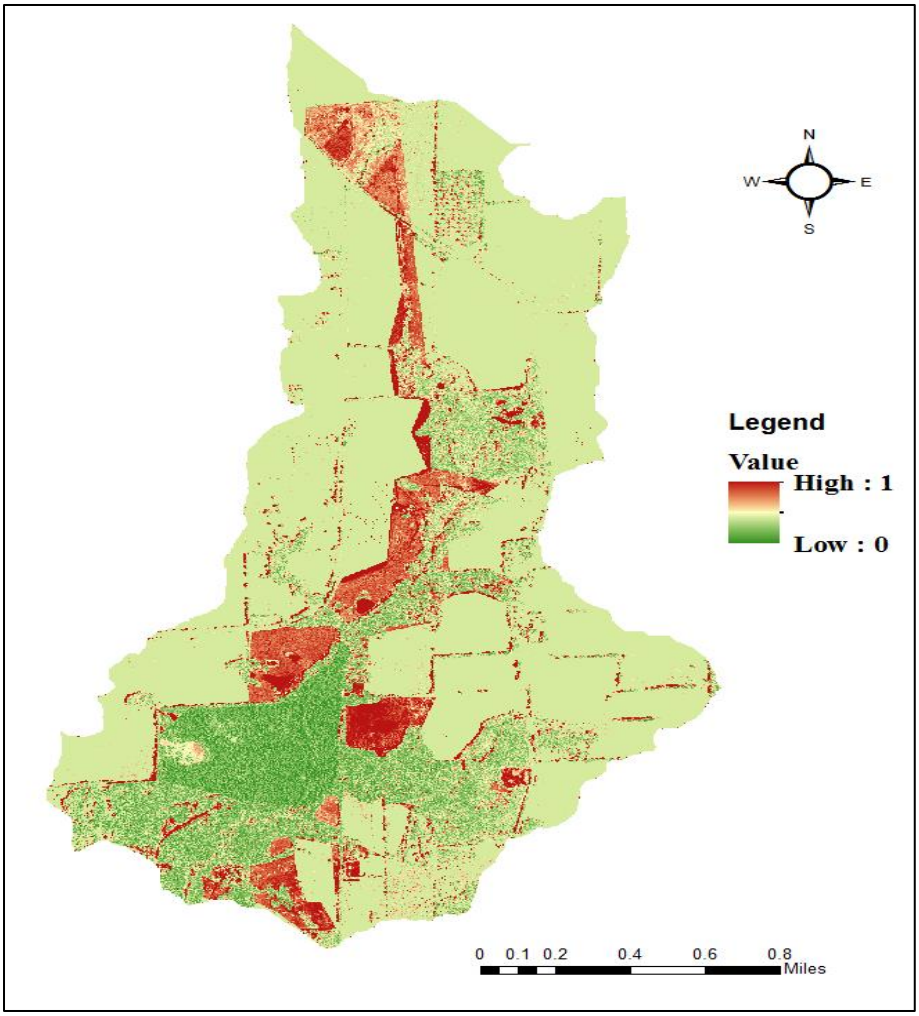

Figure 6.15 C factor grid of Soapstone branch in 2015 obtained by neglecting the effects of deforestation

An areal average C factor value of 0.449 was obtained by neglecting the effects of deforestation from 2011–2015 which corresponds to 29.4% increase since 2011. This indicates that only 4.9% increase in C factor was due to major deforestation activities. Remaining 29.4% increase in C factor may be due to the change in the size of rangeland, grass cover in rangeland, increase in agricultural area, thinning of forest which is not visible in aerial imagery, etc. This hypothetical C factor grid was obtained to quantify the effects of deforestation and other activities

on C factor. Table 6.4 lists the areal average value of C factor and percentage increase in C factor from 2011 for different landcover conditions.

Table 6.4 Areal Average C Factor Value and Percent Change for Different Scenarios

	Areal average C	Percent change (%) from 2011
2011 landcover condition	0.347	N/A
2015 landcover condition due to all possible changes	0.678	95.4
2015 landcover after removing crop rotation	0.466	34.3
2015 landcover after removing major deforestation and crop rotation	0.449	29.4
2015 landcover with deforestation	0.364	4.9

6.4.4 SUPPORT PRACTICE FACTOR

Support practice factor (*P* factor) is defined as the ratio of soil loss with support practice to the amount of soil loss with up and down hill farming. Soil conservation practices such as contouring, contour strip-cropping, and terracing reduce the soil erosion and thus have lower *P* factor values. The value of *P* factor ranges from 0 to 1. Table 6.5 provides the typical values of *P* factor for different practices (Kuok et al. 2013). Due to the absence of any such practices in the Soapstone branch catchment, a P factor of 1 was selected for a conservative sediment yield estimation.

Table 6.5 *P* factor values for different soil conservation practices

Soil conservation	P value
None	1
Contouring	0.6
Contour strip-cropping	0.35
Terracing	0.15

6.5 HEC-HMS MODEL SETUP

HEC-GeoHMS was used for developing the background map file and distributed-basin schematic model file. It also performed the tasks of the automatic naming of three river reaches and seven subcatchments, checks for errors in the catchment and connectivity of streams. HEC-HMS model setup for the donor catchment is shown in Figure 6.16.

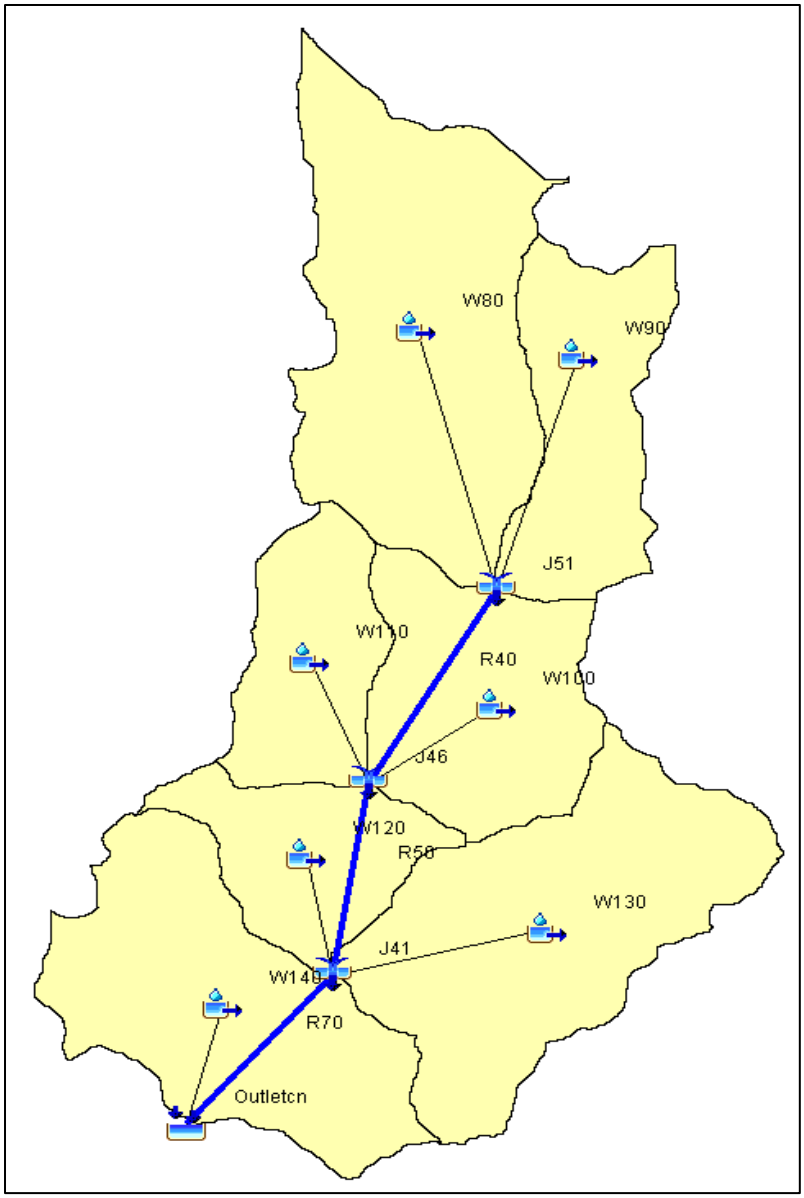

Figure 6.16 HEC-HMS Setup for Soapstone Branch Catchment

6.6 CONTINUOUS STREAMFLOW SIMULATION

Semi-distributed continuous SMA model of the Soapstone branch catchment was run from January 2009–September 2016 using a combination of Dothan rainfall data (January 2009–February 2016) and installed rain gauge data at the site (March 2016–September 2016). Similar to

the donor and the receiver catchment, an initial warmup period of nine months was used. A 10-min simulation time interval was selected for model run due to the smaller response time of sub-catchments. Figure 6.17 shows the simulation result from SMA model of the Soapstone branch catchment for the period of seven years (October 2009–September 2016).

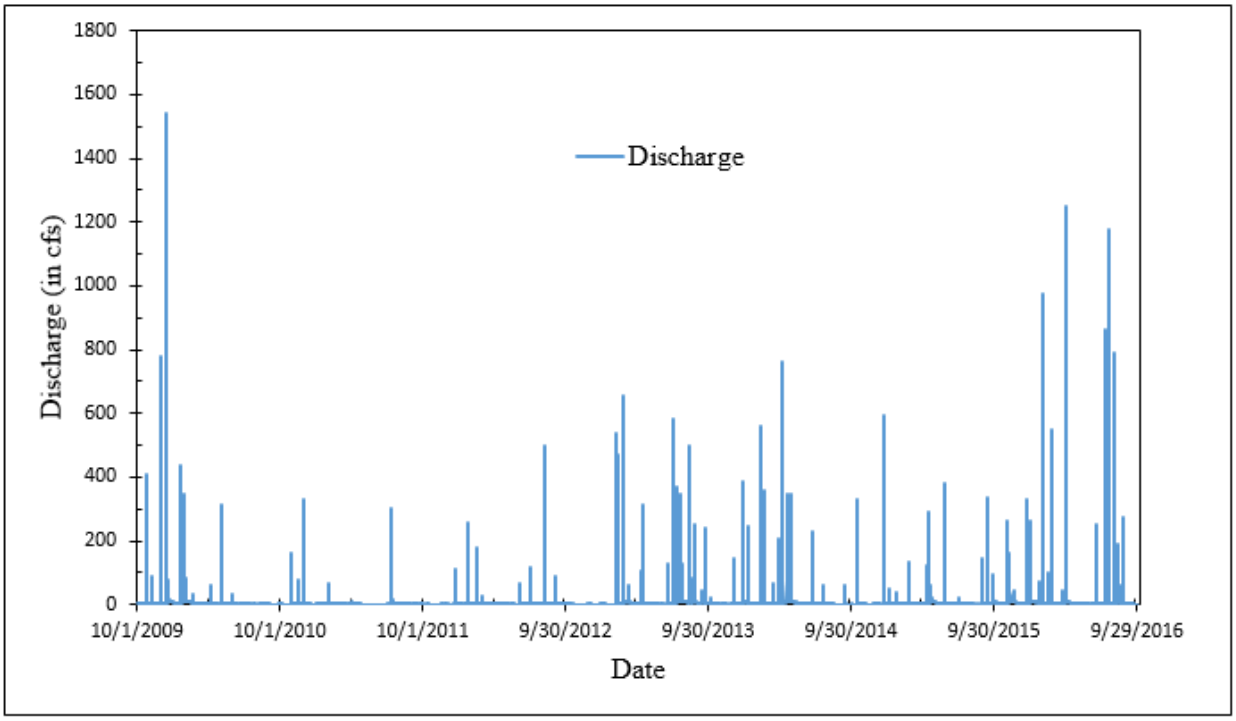

Figure 6.17 SMA Model Result of Soapstone Branch Catchment (October 2009–September 2016)

6.7 EVENT BASED CURVE NUMBER METHOD

6.7.1 MODEL DEVELOPMENT

An event based hydrologic model provides information on how the catchment responds to an individual rainfall event. The CN method discussed in Section 4.3 and Section 6.3.3 can be also used for developing an event based model. CN is a dimensionless empirical parameter which

determines the proportion of rainfall available as direct runoff during each storm event by considering the effects of land cover, soil type, and hydrological conditions.

The event based CN method can be expressed as:

$$Q = \frac{(P - I_a)^2}{(P - I_a) + S} \quad (6.5)$$

Where,

Q = Direct runoff volume in inches

I_a = Initial abstraction in inches

S= Potential maximum retention after runoff begins in inches

$$S = \frac{1000}{CN} - 10 \quad (6.6)$$

CN values obtained by combining HSGs and land cover types are subjected to variability due to rainfall intensity, soil moisture conditions, etc. These reasons causing variability in CN are combined to form Antecedent Runoff Condition (ARC), previously called antecedent moisture condition. ARC is divided into three different classes viz. I for dry conditions, II for average conditions and III for wetter conditions. CN developed so far corresponds to ARC class II. The adjustment of ARC II CN to ARC I CN or ARC III CN is provided in Table 6.6 (McCuen 2005).

Table 6.6 Adjustment of Curve Number for Dry condition (I) and Wet condition (III)

ARC II CN	Corresponding CN for ARC	
	I	III
100	100	100
95	87	99
90	78	98
85	70	97
80	63	94
75	57	91
70	51	87
65	45	83
60	40	79
55	35	75
50	31	70
45	27	65
40	23	60
35	19	55
30	15	50
25	12	45
20	9	39
15	7	33
10	4	26
5	2	17
0	0	0

Classification of catchment state into ARC classes is based on past rainfall conditions. Total 5-day antecedent rainfall which defines these three ARC of a catchment is listed in Table 6.7 (McCuen 2005).

Table 6.7 Rainfall Limits Defining the Antecedent Runoff Condition

ARC	Total 5-day Antecedent Rainfall (in.)	
	Dormant Season	Growing Season
I	< 0.5	<1.4
II	0.5-1.1	1.4-2.1
III	>1.1	>2.1

Apart from 5-day antecedent rainfall, catchment state into ARC classes depends on the season (Table 6.7). Since the Soapstone branch catchment is an agricultural catchment, the season of the crop growth defines the ARC classes together with antecedent rainfall. Two major crops grown in the Soapstone branch catchment are corn and cotton. The growing season for corn is from March–August whereas for cotton is April–September (NASS 1997). Therefore, the period from March–September was considered as the growing season and October–February was considered as the dormant season for crops in Soapstone branch catchment. Table 6.8 and Table 6.9 lists the adjustment of CN for ARC class I and class III for both 2011 and 2015. For the event based model of the Soapstone branch catchment, the 5-day antecedent rainfall and the growing/dormant season were checked for each event and then corresponding CNs were applied for individual events.

Table 6.8 2011 Curve number and adjustment for ARC classes

Subbasin	2011 CN	CN (ARC I)	CN (ARC III)
W140	65	45	82
W130	73	54	87
W120	67	47	83
W110	77	59	89
W100	75	56	88
W90	77	59	89
W80	78	62	90

Table 6.9 2015 Curve Number and adjustment for ARC Classes

Subbasin	2015 CN	CN (ARC I)	CN (ARC III)
W140	66	46	82
W130	75	57	88
W120	67	47	83
W110	78	61	90
W100	75	57	88
W90	78	60	90
W80	79	61	91

6.7.2 COMPARISON WITH SMA MODEL

Six storm events from three different ARC classes and, one from before 2011 and another after 2011 were selected for comparison with the SMA model. Details of each individual storm events are provided in Table 6.10.

Table 6.10 Selected Storm Events

Storm Events	Total 5-day antecedent precipitation (in.)	ARC Class	Event Precipitation (in.)	Event duration (hr)
4/8/2010	0.01	I	0.99	3
2/7/2013	0.14	I	2.65	11
12/2/2009	0.8	II	3.95	23
1/23/2012	0.98	II	1.34	4
12/14/2009	3.02	III	5.28	18
2/10/2013	2.78	III	1.23	1

The uncalibrated event-based CN model produced lower discharges than the SMA model did for all storm events as shown in Figure 6.18, Figure 6.19 and Figure 6.20. This underestimation is the highest in ARC class I condition and gradually decreases as the antecedent rainfall condition in the catchment increases. The difference in discharge is the minimum for ARC class III conditions. Also, the discharge produced by calibrated SMA model and uncalibrated CN model matches quite well for intense storm events as shown in Figure 6.19 (A) and Figure 6.20 (A).

For storm events occurring after 2011, the storm events were simulated using CNs and basin lag from both 2011 and 2015. It was found that event-based model prepared using 2015 CN performed better than event model based on 2011 CN.

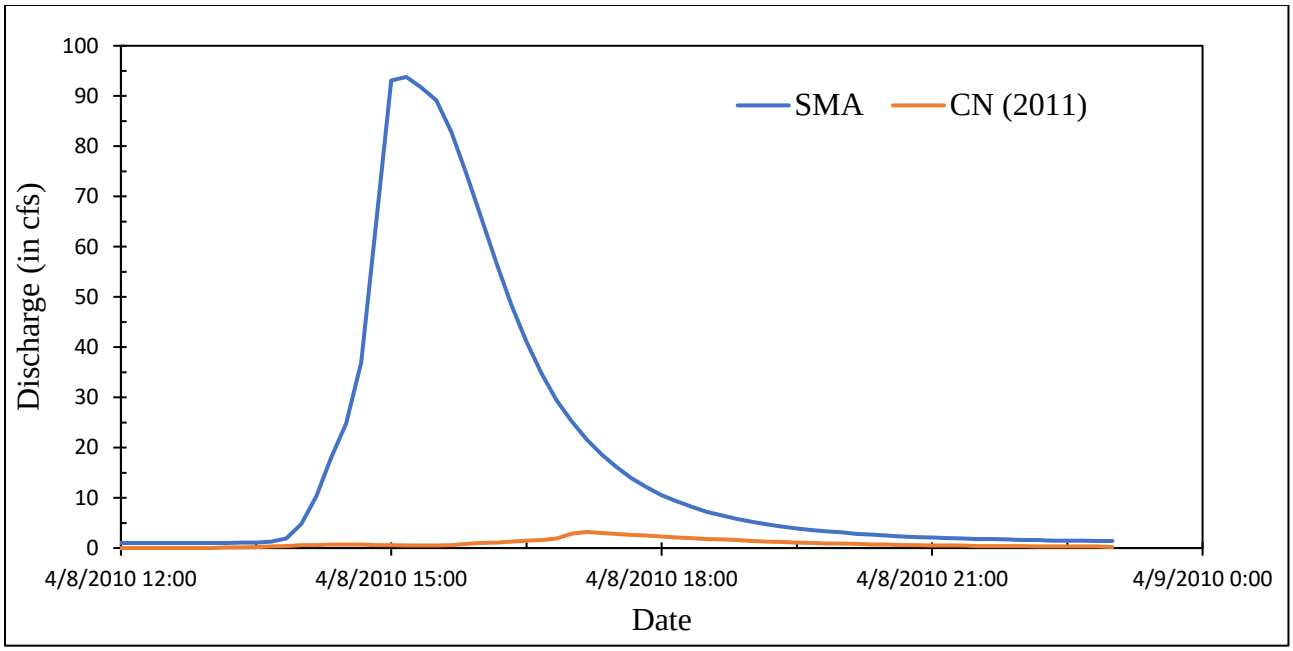

(A)

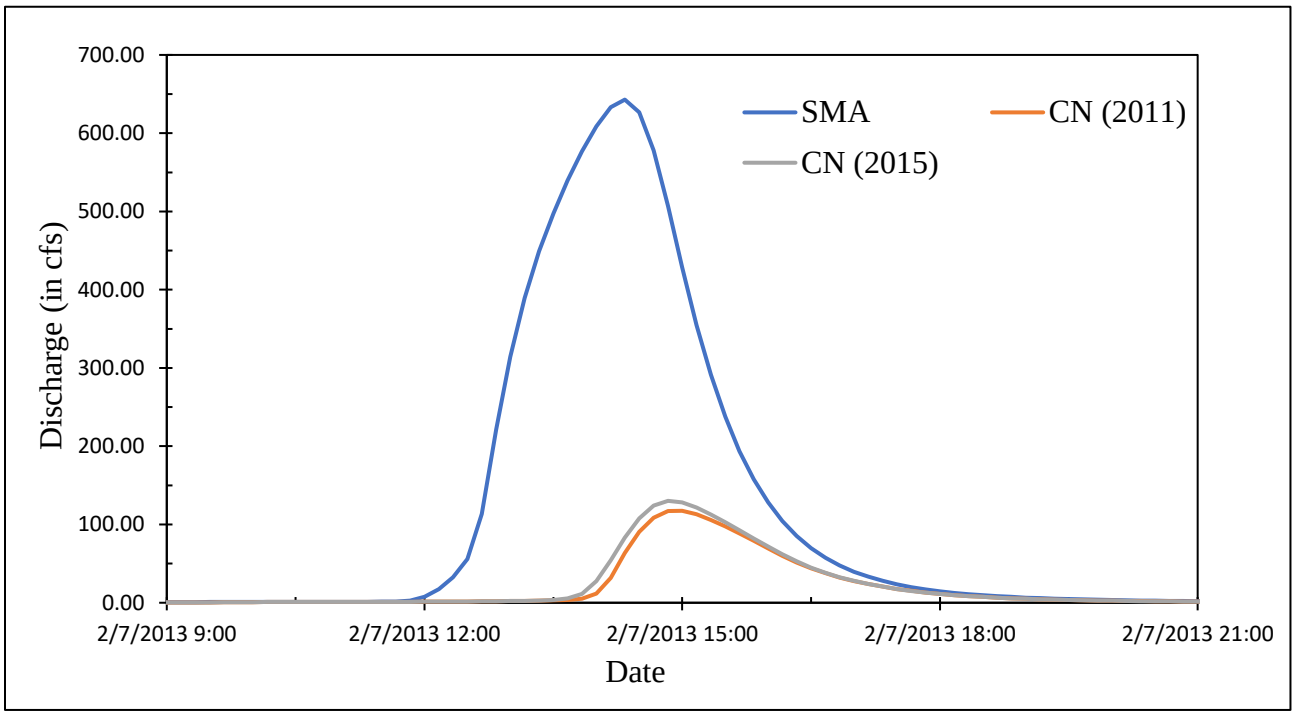

(B)

Figure 6.18 Comparison of SMA Model with Uncalibrated Event-based CN Model for ARC Class I Condition with Storm Events Before 2011 (A) and After 2011 (B)

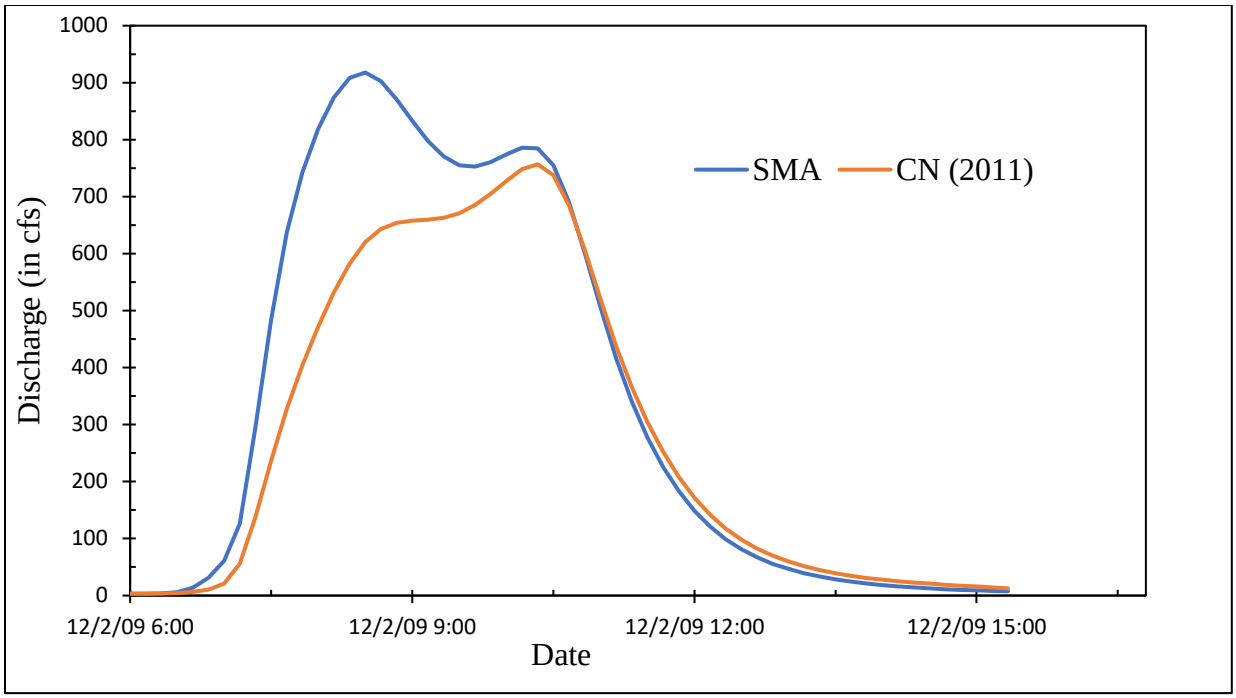

(A)

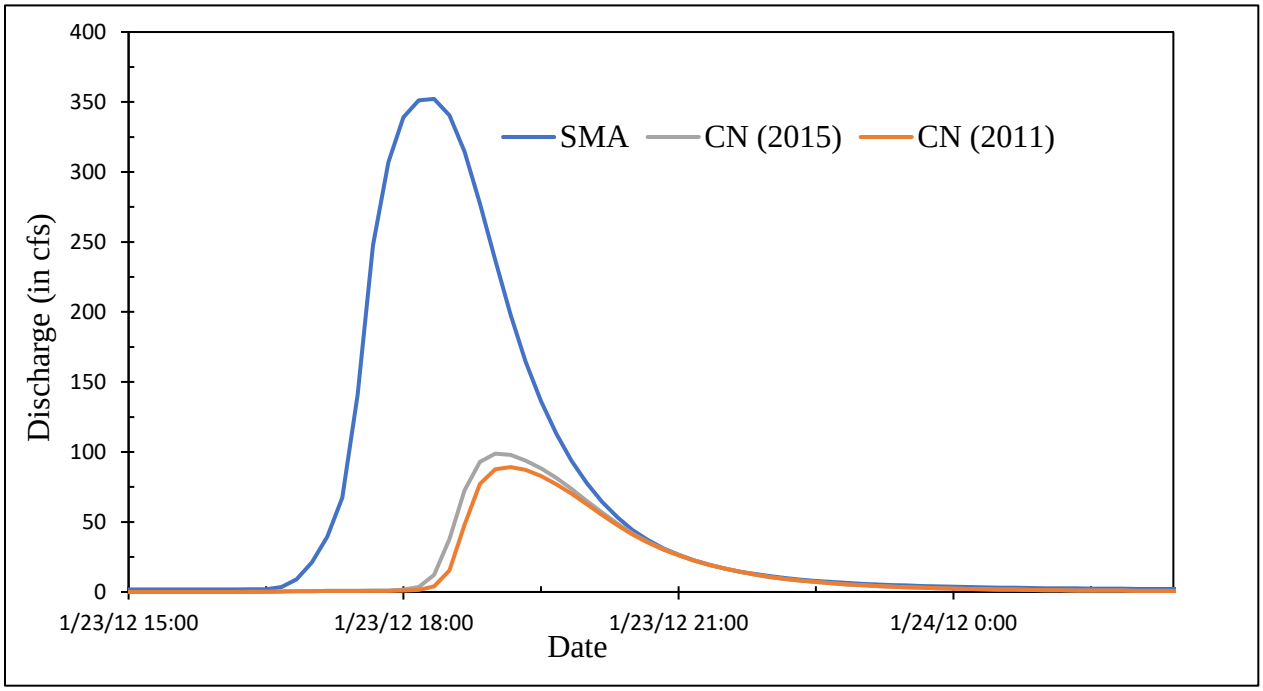

(B)

Figure 6.19 Comparison of SMA model with Uncalibrated Event-based CN model for ARC Class II Condition with Storm Events Before 2011 (A) and After 2011 (B)

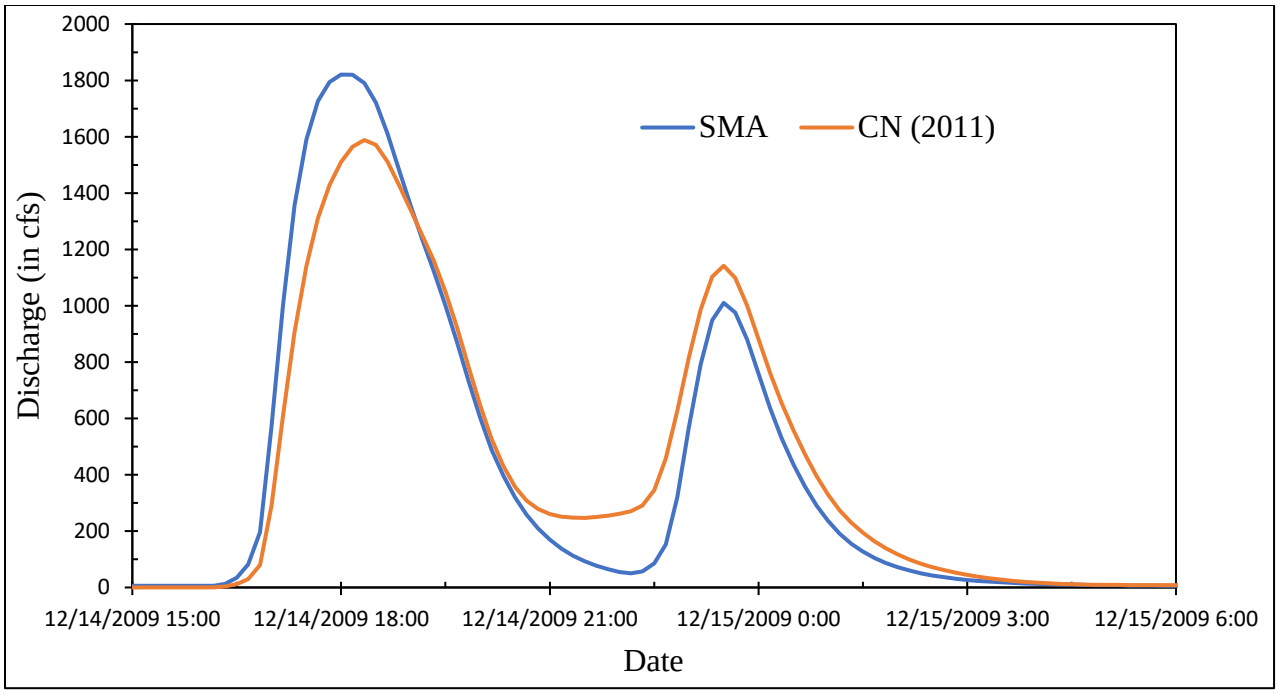

(A)

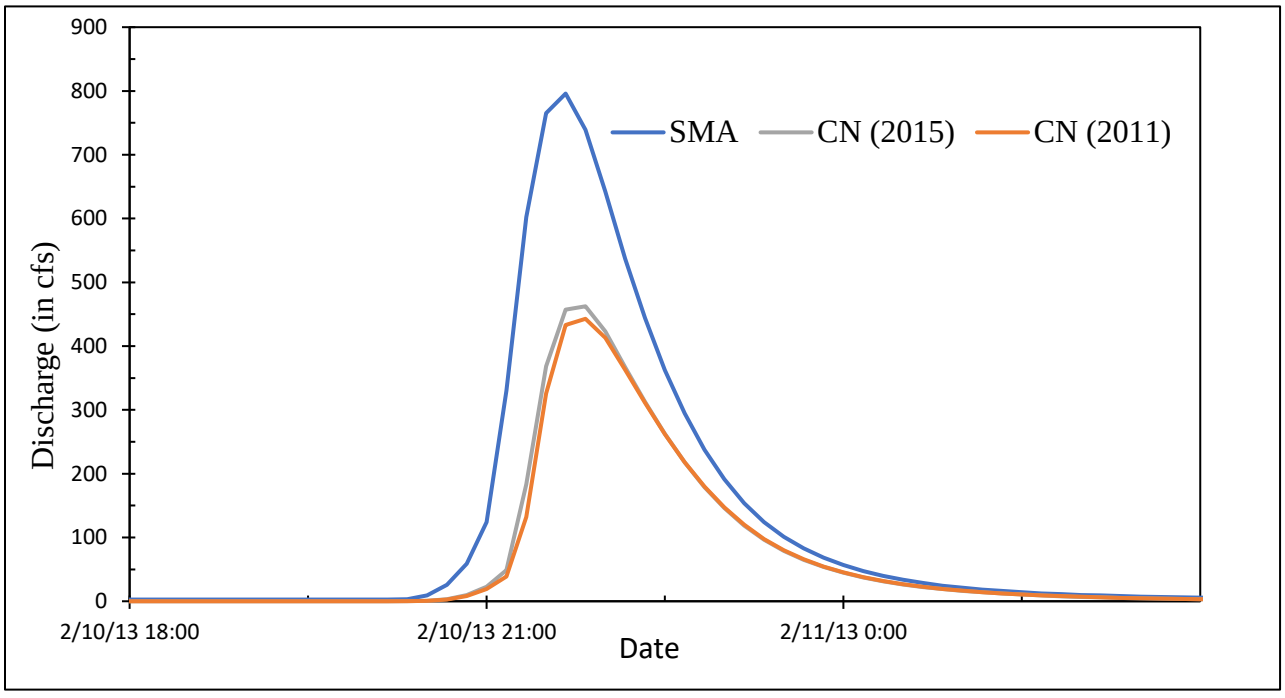

(B)

Figure 6.20 Comparison of SMA model with uncalibrated event-based CN model for ARC class III condition with storm events Before 2011 (A) and After 2011 (B)

6.7.3 CALIBRATION OF EVENT BASED MODEL USING SMA MODEL

An attempt was made for calibrating the event-based model using simulated discharge from SMA model “as observed”. Since CN for ARC class I and ARC class III depend upon CN for ARC class II, so that, the storm event of 23rd January 2015 (

Figure 6.19 (B)) corresponding to ARC class II condition was selected for calibration. CN values for seven subcatchments were varied until CN model discharges matched with SMA model discharges.

This calibrated CN for ARC class II was then, adjusted for dry and wet catchment condition to determine ARC class I and ARC class III CN using Table 6.6 and is listed in Table 6.11. It was found that a 15% increment in ARC class II CN produces the best match between SMA model and CN model discharges. The same increment of 15 % was applied to 2011 ARC class II CN at first and then adjusted for dry and wet catchment condition (Table 6.12).

Table 6.11 Calibrated 2015 CN values for ARC class I, II, and III

Subbasin	2015 CN	calibrated ARC II CN	calibrated ARC I CN	calibrated ARC III CN
W140	66	76	59	89
W130	75	86	72	94
W120	67	77	59	89
W110	78	90	78	96
W100	75	86	72	94
W90	78	89	77	96
W80	79	90	79	96

Table 6.12 Calibrated 2011 CN values for ARC class I, II, and III

Subbasin	2011 CN	calibrated ARC II CN	calibrated ARC I CN	calibrated ARC III CN
W140	65	75	56	88
W130	73	84	69	93
W120	67	77	59	89
W110	77	88	75	95
W100	75	86	71	94
W90	77	89	76	96
W80	78	90	78	96

From Figure 6.21, Figure 6.22, and Figure 6.23, it can be seen that the calibrated CN model's output discharge match quite well with the SMA model's discharge for ARC class II and III condition. However, even if, the calibrated CN model produces better match than the uncalibrated event model for ARC class I condition, the calibrated CN model underpredicts the discharge. Furthermore, this underprediction increases as the total 5-day antecedent rainfall decreases (Figure 6.21).

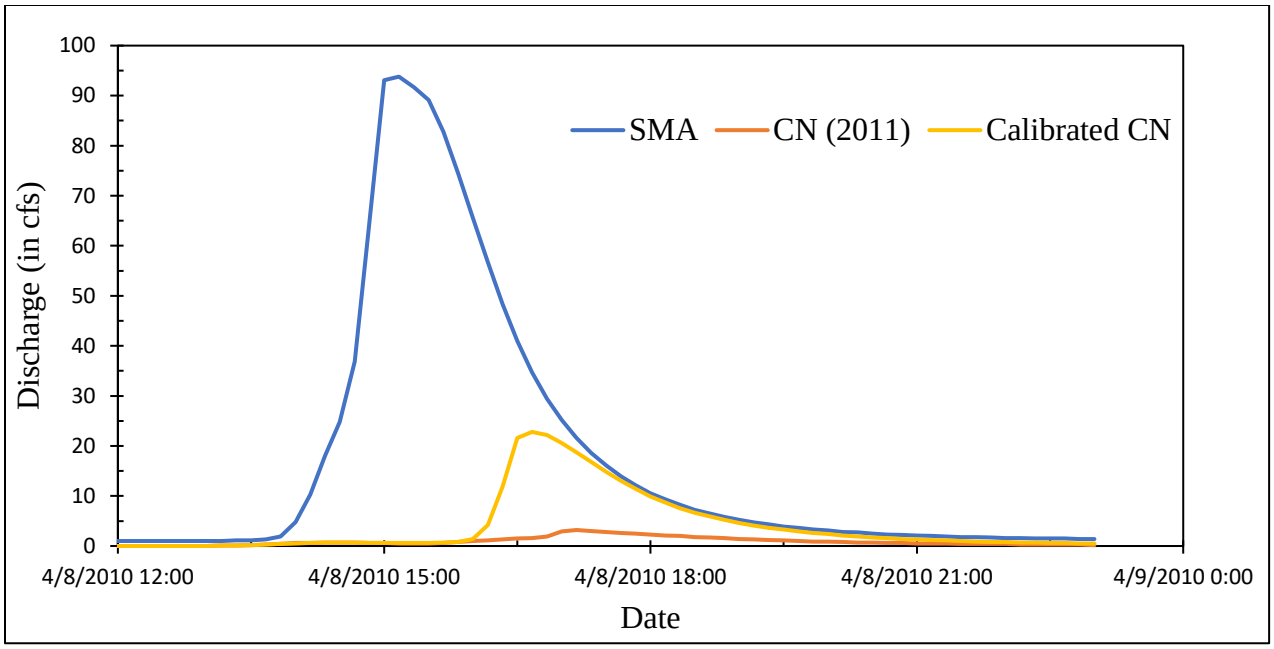

(A)

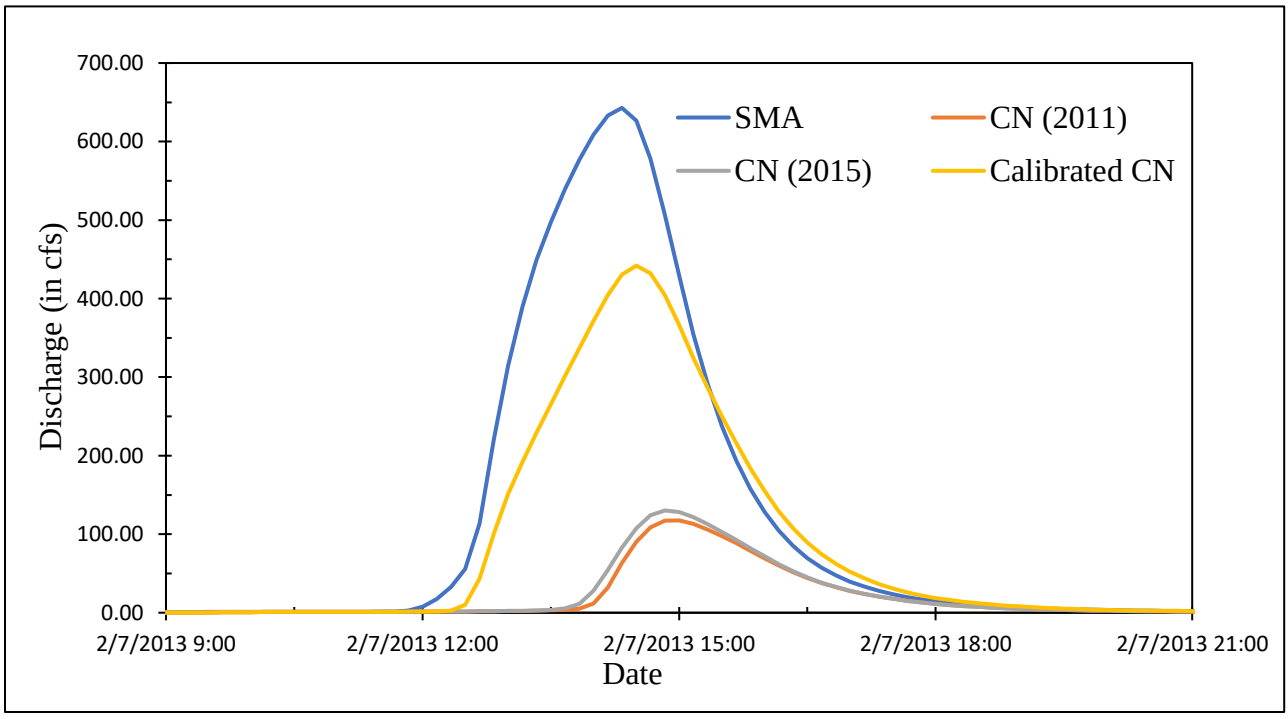

(B)

Figure 6.21 Comparison of SMA Model with Calibrated Cn Model for ARC class I Condition with Storm Events Before 2011 (A) and After 2011 (B)

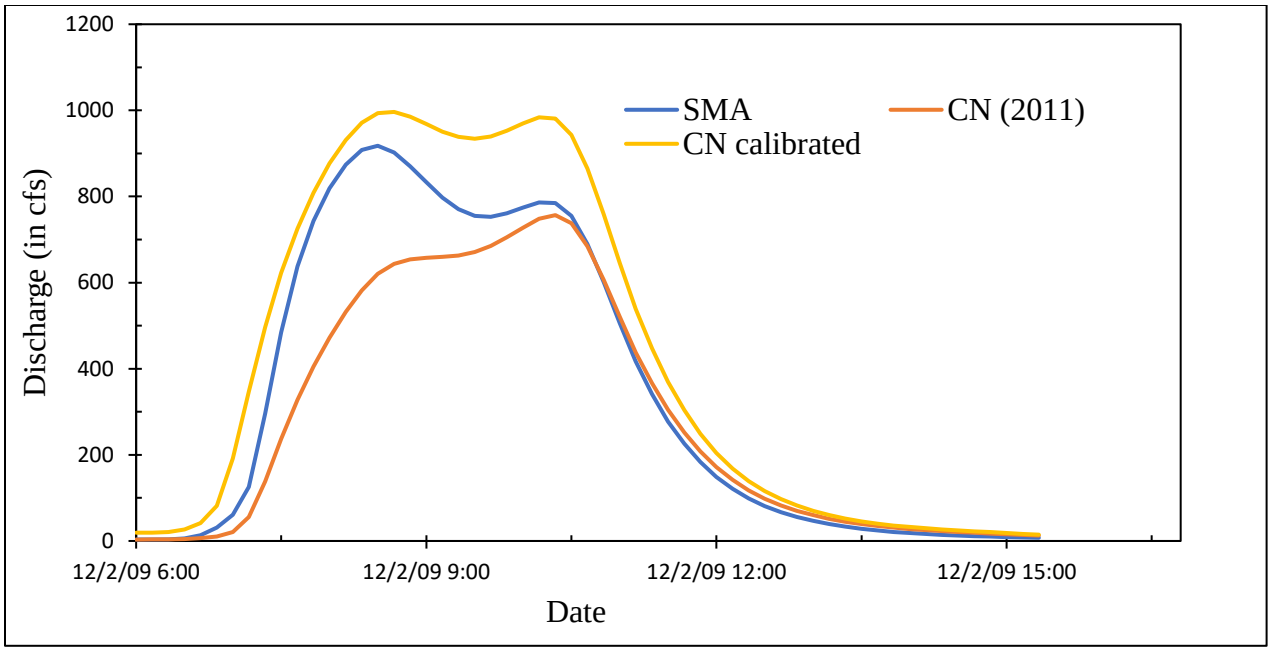

(A)

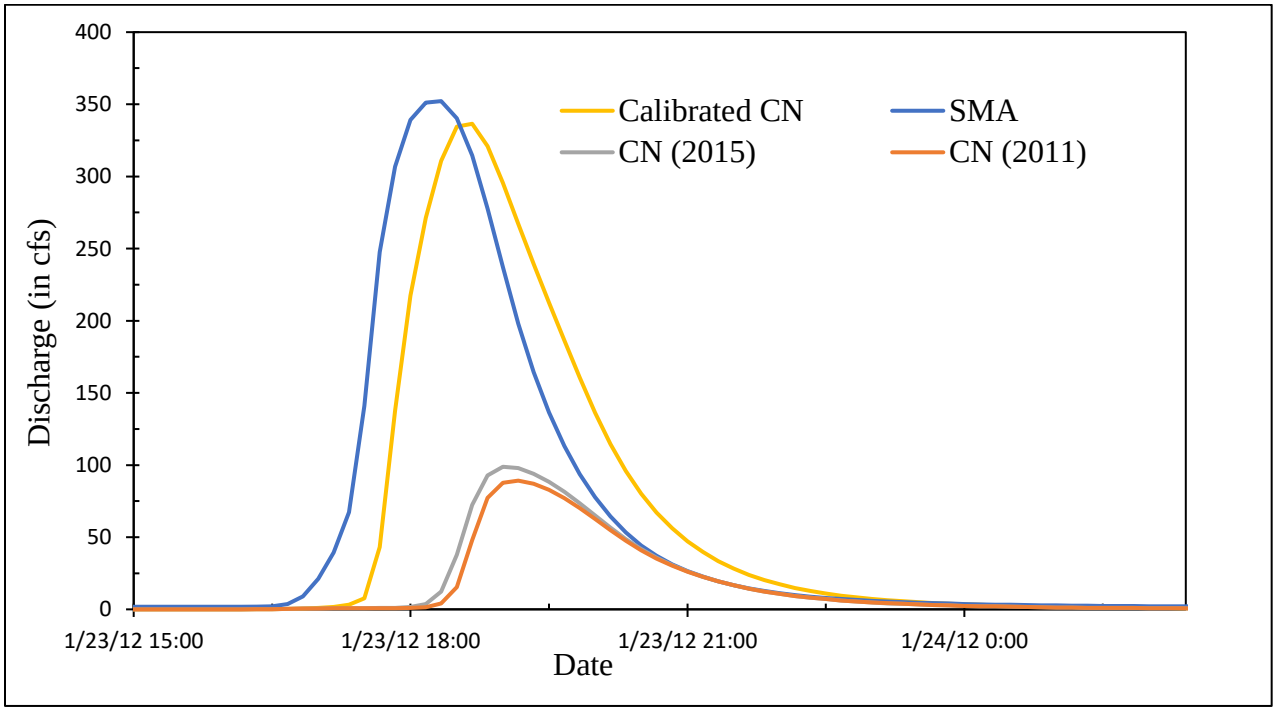

(B)

Figure 6.22 Comparison of SMA Model with Calibrated CN model for ARC class II condition with Storm Events Before 2011 (A) and After 2011 (B)

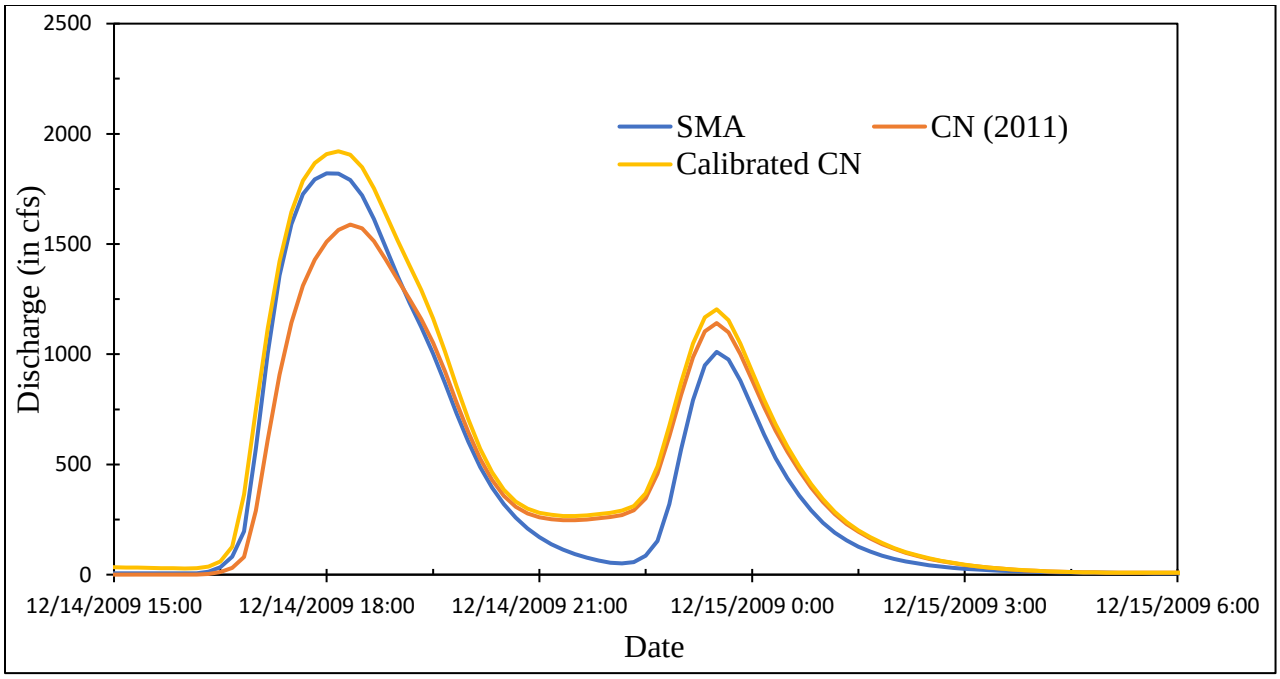

(A)

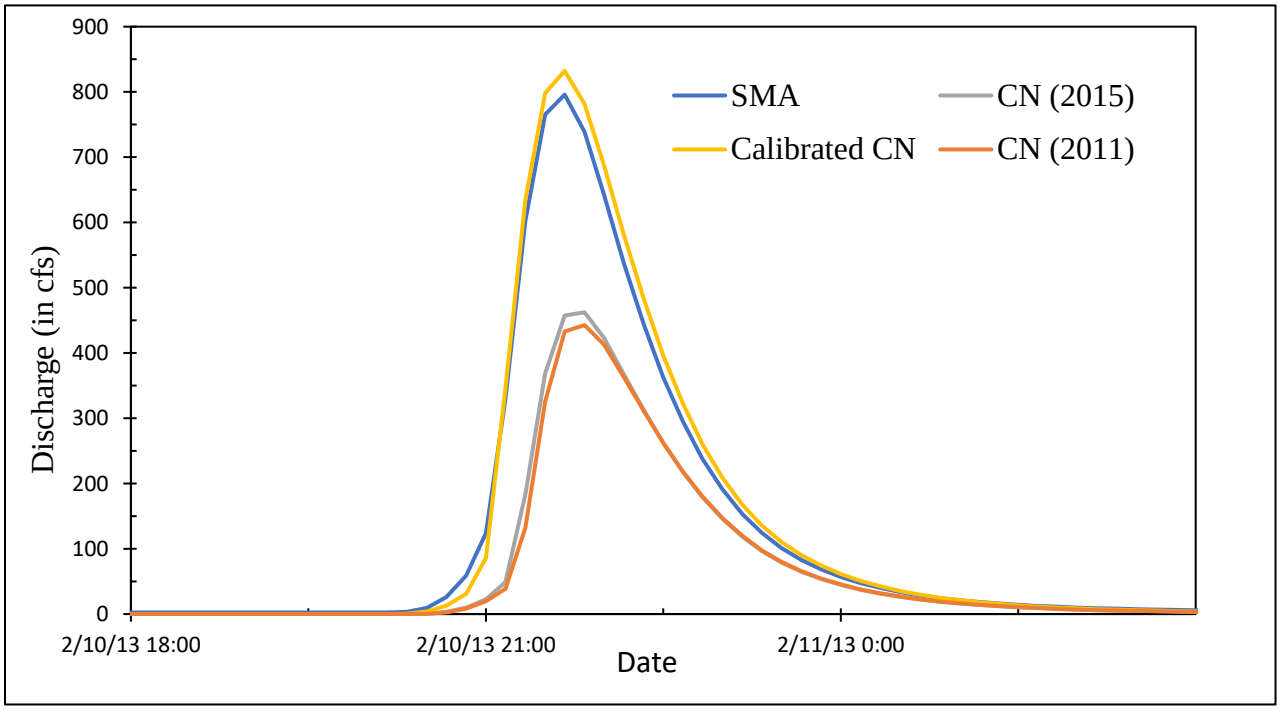

(B)

Figure 6.23 Comparison of SMA model with Calibrated CN Model for ARC class III Condition with Storm Events Before 2011 (A) and After 2011 (B)

6.8 SEDIMENT YIELD AT DEAN ROAD BRIDGE

Using the calibrated CN model, sediment yield at the outlet of the Soapstone branch catchment, i.e., Dean road bridge was calculated for three different events, i.e., 7th February 2013 (ARC Class I), 23rd January 2012 (ARC Class II), and 10th February 2013 (ARC Class III). For each event, calibrated CN value and the cover factor of 2011 and 2015 were used to determine the difference in sediment yield due to increasing deforestation and agricultural land expansion in the catchment. Calculation of sediment yield for each event requires the volume of runoff and peak runoff for those events. The value of peak runoff and volume of runoff for each selected event with 2011 and 2015 scenarios is presented in Table 6.13.

Table 6.13 Peak runoff and volume of runoff for three storm events with 2011 and 2015 scenarios

Event	ARC Class	Rainfall depth (in.)	Rainfall duration (hrs)	2011		2015	
				Peak runoff (cfs)	Volume of runoff (acre-ft)	Peak runoff (cfs)	Volume of runoff (acre-ft)
2/7/2013	I	2.65	11	402.9	83.8	442	92.9
1/23/2012	II	1.34	4	310.7	54.4	336.5	59.2
2/11/2013	III	1.23	1	787.9	98.2	832.2	102.8

Based on the areal average values of K, LS, C, and P factor of the Soapstone branch catchment, sediment yield was calculated for each of the three events listed in Table 6.13 . For both 2011 and 2015 catchment condition and the results are shown in Figure 6.24. The sediment yield was estimated to be higher in 2015 due to change of land cover. The increase (%) of sediment yield from 2011 to 2015 was, therefore, calculated and plotted from each event (Figure 6.24). The percentage increase was the highest for the ARC I event, but the sediment yield (in tons) was the highest for the ARC III event.

Furthermore, the sediment yield was also calculated by neglecting the deforestation in the vicinity of stream channel (Figure 6.25). The sediment yield was the highest for ARC III storm whereas the percentage increase was maximum for ARC I storm condition. Also, it shows that the percentage increase in sediment yield due to other factors is more than 35% from 2011–2015. These increases are due to the fact that other factors such as increase in rangeland area, agricultural area, thinning of forests, etc. had more pronounced effect on producing sediment than the deforestation near stream alone.

The difference between Figure 6.25 and Figure 6.24 gives sediment yield due to the deforestation near stream alone. The major deforestation area estimated from aerial images was 8.4 acres (365973 sq. ft.), which is 1.4 % of the total forest area in the Soapstone Branch watershed and 0.5% of the total watershed area. Estimated stream length in the watershed is about 6.9 km. If we assume the sediment deposition is average 6 ft. in the streams, it has 75010 cubic yards of sediment deposited. During the field visit, it was found that the sediment deposit started much upstream of the river reach nearby the major deforestation and was about 6–7 ft. deep. The field visit along the stream stopped roughly 3 km upstream from the Dean Road Bridge, and no attempt was made to walk further upstream and to determine where the starting point of sediment deposit in the stream was. This indicates the sediment deposit most likely was not due to deforestation alone, which indirectly supports the above finding. Table 6.14 shows the percent change of sediment yield from 2011 to 2015 due to change in different factors viz. runoff energy factor, C factor, etc.

Table 6.14 Percent changes of sediment yield from 2011 to 2015 due to different factors

Factor	ARC Class I	ARC Class II	ARC Class III
Change of runoff energy factor	11.6	9.6	5.8
Change of C due to all possible changes	95.4	95.4	95.4
Change of C neglecting crop rotation	34.3	34.3	34.3
Change of C neglecting crop rotation and deforestation	29.4	29.4	29.4
Change of C including only deforestation	4.9	4.9	4.9

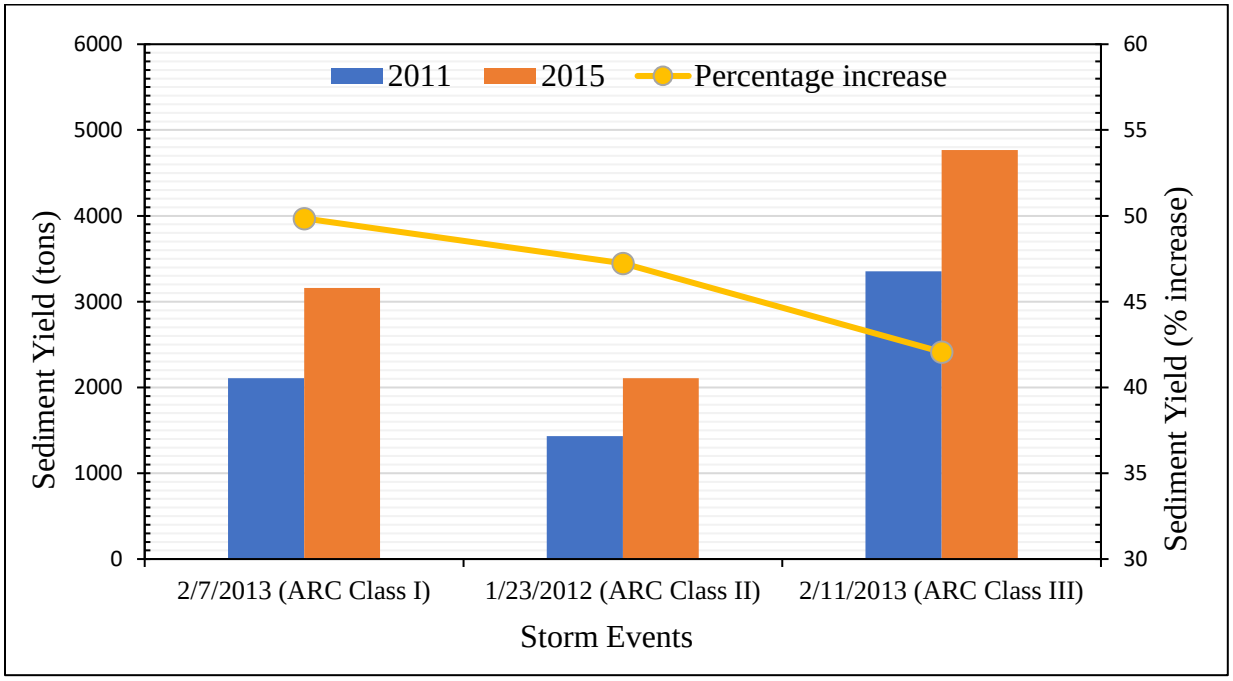

Figure 6.24 Sediment Yield and Percentage Increase for each ARC Class Condition Storms from the Soapstone Branch Catchment in 2011 and 2015 Scenarios

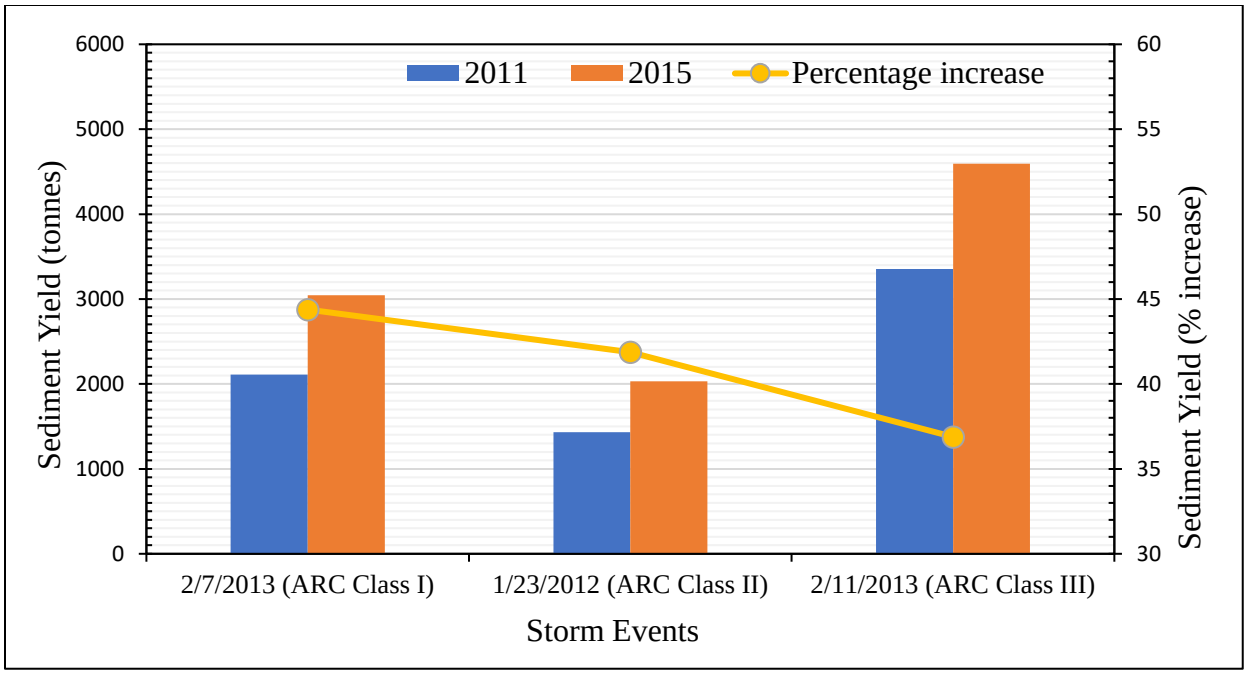

Figure 6.25 Sediment Yield and Percentage Increase for each ARC Class Condition Storms from the Soapstone Branch Catchment in 2011 and 2015 Scenarios by Neglecting Deforestation

CHAPTER 7: SUMMARY AND CONCLUSIONS

7.1 SUMMARY

This study was motivated by a serious aggradation problem occurring on the Soapstone branch catchment, a tributary of Little Choctawhatchee River in Dale County, Alabama. Historical aerial imageries of the catchment revealed increasing deforestation occurring in a short period of time 2011–2015. The application of HEC-HMS model together with MUSLE for quantifying the change in discharge and sediment yield due to human activities was explored in this study.

Apart from topographic and physiographic factors required for computing sediment yield, discharge data at catchment outlet is required. Soapstone branch catchment being an ungauged catchment lacked discharge time series information. Initial attempts of installing AV sensor in the catchment for obtaining discharge data failed due to severe aggradation occurring after each event and sensor getting buried. As an alternative to obtain discharge data, parameter transfer approach from nearby gauged donor catchment draining to Choctawhatchee River was undertaken. However, parameters in curve number method are highly sensitive and predominant land use types in the donor catchment and the soapstone branch catchment is variable. Due to this reason, a less-sensitive SMA model which depends mostly on soil data was used for parameter transfer.

A continuous SMA model was developed for the donor catchment (Choctawhatchee River catchment draining near Newton, Alabama) using land cover and soil data. Due to the limitation of precipitation data, the model was run from January 2009–September 2015, where the period of study was partitioned into nine months of warmup and three years of both calibration and validation each. For identification of sensitive parameters for ease in calibrating the model, a

sensitivity analysis was performed. Based on this sensitivity analysis, six most sensitive parameters were selected for manual and automated calibration. The NSE value of 0.73 and PBIAS of -10.4% during the calibration period and a NSE value of 0.63 and PBIAS of 3.8% during the validation period were obtained. This suggested that the model is capable of simulating streamflow quite well. However, before the parameters were transferred to the Soapstone branch catchment, the transfer process was tested on another gauged receiver catchment.

A receiver catchment draining into Little Double Bridges Creek and located near to both the donor and Soapstone branch catchments was selected. For testing the efficiency of parameter transfer process, this gauged catchment was treated as ungauged and all calibrated parameters were transferred. Transferred parameters and locally developed parameters were then used to develop the model. The model was run from January 2009–September 2012 with the warmup period of nine months and three years of transfer validation period. An NSE value of 0.64 and PBIAS of 24.2% were obtained during the transfer validation period. This validated the parameter transfer using SMA model.

After the parameter transfer process was validated for the SMA model, parameters were finally transferred to the Soapstone branch catchment. Precipitation data from the nearby Dothan regional airport prior to 2016 was used together with the installed rain gauge data since 2016. The model was run from January 2009–December 2016 with nine months of warmup period. Due to lower sensitivity of SMA model to changes in land cover and MUSLE being an event based sediment yield model, an event based method was required.

Two event based curve number models were initially developed, based on land cover information from 2011 and 2015. Apart from land cover and soil data, CN model is highly affected by antecedent runoff condition (ARC). Therefore, those two event based models were then,

expanded into six different CN models considering three ARC classes for each one of them. Six corresponding storm events were selected and simulated. These six simulated events were compared against SMA model results. The uncalibrated CN model results didn't match well with the calibrated SMA model results. Since, CN model for ARC class I and ARC Class III are dependent on CN model for ARC class II, CN model for ARC class II was calibrated using SMA model results. The calibrated CN ARC class II model was then adjusted for CN ARC class I and class III model. All calibrated CN models except ARC class I model in 2011 scenario matched quite well with the SMA model results.

Three storm events corresponding to each ARC class types after 2011 were simulated using 2011 and 2015 land cover scenario. An increase in peak runoff and volume of runoff due to land cover change from 2011–2015 was found for each of these events. A final application of MUSLE together with CN model revealed an increase of more than 40% in sediment yield due to land cover changes in the catchment. Furthermore, a hypothetical scenario with assumption of no major deforestation in the vicinity of stream reveals an increase of sediment yield of more than 35 % from 2011 to 2015. This suggests increase in rangeland area, agricultural land, thinning of forests, etc. have more pronounced effects on sediment yield than streamside deforestation.

7.2 CONCLUSIONS

It can be concluded that SMA model is well capable for parameter transfer process to simulate streamflow in the ungauged catchment. Furthermore, in absence of discharge data, an event based method calibrated using a calibrated continuous model can be used for estimating sediment yield. An overall goal of the study to quantify the change in discharge and sediment yield due to land cover change in an ungauged catchment is achieved.

7.3 FUTURE STUDIES

Sediment yield during each storm event calculated using MUSLE can be utilized to develop a sediment time-series in HEC-HMS. The development of sediment time-series from the total sediment yield for each storm events require multiple parameters which can be obtained from a local flow and the sediment-load relationship, but the measurement of the sediment load in streams is still a challenging task. Some water samples were collected at the Dean Road Bridge using an ISCO sampler. The total suspended solids (TSS) concentrations and turbidity of water samples are being analyzed in the laboratory. A TSS-turbidity curve developed after water sampling from storm events can then be used to calibrate the sediment time-series. Furthermore, it has been found that the watershed scale, i.e., the size of subcatchments selected affects the value of key calibrated parameter (Zhang et al. 2013) and therefore may affect the efficiency of parameter transfer. This theory can be tested in parameter transfer using SMA to find the optimized number of subcatchments which leads to the highest efficiency in parameter transfer.

For the delineation of the donor catchment, it had a very large subcatchment (drainage area of 615 sq. km) when the limit for the stream definition was 75 sq. km. When the limit for the stream definition was 45 sq. km, the donor catchment will have 6 more subcatchments. The drainage areas of subcatchment range from 26 to 209 sq. km. (mean 84 sq. km with a standard deviation of 47 sq. km), therefore, the drainage size of subcatchments becomes more uniform. Additional study could be done using updated watershed delineation to verify how the size of subcatchment affect the parameter transfer.

REFERENCES

ASCE (1993). "Criteria for Evaluation of Watershed Models." *Journal of Irrigation and Drainage Engineering*, 119(3), 429-442.

Arekhi, S. (2012). "Runoff modeling by HEC-HMS model (Case study: Kan watershed, Iran)." *International Journal of Agriculture and Crop Sciences*, 4(23), 1807-1811.

Arguez, A., Durre, I., Applequist, S., Vose, R. S., Squires, M. F., Yin, X., Heim Jr, R. R., and Owen, T. W. (2012). "NOAA's 1981–2010 US Climate normals: an overview." *Bulletin of the American Meteorological Society*, 93(11), 1687-1697.

Bennett, T. H. (1998). "Development and application of a continuous soil moisture accounting algorithm for the Hydrologic Engineering Center Hydrologic Modeling System (HEC-HMS)." University of California, Davis.

Blöschl, G. (2005). *Rainfall-runoff modeling of ungauged catchments*, Wiley Online Library.

Bossler, J. D., Jensen, J. R., McMaster, R. B., and Rizos, C. (2004). *Manual of geospatial science and technology*, CRC Press.

Colman, E. (1947). "A Laboratory Procdure For Determining The Field Capacity Of Soils." *Soil Sci.*, 63(4), 277-284.

Cosby, B., Hornberger, G., Clapp, R., and Ginn, T. (1984). "A statistical exploration of the relationships of soil moisture characteristics to the physical properties of soils." *Water resources research*, 20(6), 682-690.

Cunderlik, J., and Simonovic, S. P. (2004). *Calibration, verification and sensitivity analysis of the HEC-HMS hydrologic model*, Department of Civil and Environmental Engineering, The University of Western Ontario.

Diamond, H. J., Karl, T. R., Palecki, M. A., Baker, C. B., Bell, J. E., Leeper, R. D., Easterling, D. R., Lawrimore, J. H., Meyers, T. P., and Helfert, M. R. (2013). "US Climate Reference Network after one decade of operations: Status and assessment." *Bulletin of the American Meteorological Society*, 94(4), 485-498.

Farnsworth, R. K., and Thompson, E. S. (1983). *Mean monthly, seasonal, and annual pan evaporation for the United States*, US Department of Commerce, National Oceanic and Atmospheric Administration, National Weather Service.

Feldman, A. D. (2000). *Hydrologic modeling system HEC-HMS: technical reference manual*, US Army Corps of Engineers, Hydrologic Engineering Center.

Fleming, M. (2002). "Continuous hydrologic modeling with HMS: parameter estimation and model calibration and validation." Msc Thesis, Tennessee Technological University.

Gitas, I. Z., Douros, K., Minakou, C., Silleos, G. N., and Karydas, C. G. (2009). "Multi-temporal soil erosion risk assessment in N. Chalkidiki using a modified usle raster model." *EARSeL eProceedings*, 8(1), 40-52.

Gupta, H. V., Sorooshian, S., and Yapo, P. O. (1999). "Status of automatic calibration for hydrologic models: Comparison with multilevel expert calibration." *Journal of Hydrologic Engineering*, 4(2), 135-143.

Halwatura, D., and Najim, M. (2013). "Application of the HEC-HMS model for runoff simulation in a tropical catchment." *Environmental modelling & software*, 46, 155-162.

Hamon, W. R. (1960). "Estimating potential evapotranspiration." Massachusetts Institute of Technology.

Holberg, J. A. (2015). "Downward model development of the soil moisture accounting loss method in HEC-HMS: Revelations concerning the soil profile." Purdue University.

Homer, C., Dewitz, J., Yang, L., Jin, S., Danielson, P., Xian, G., Coulston, J., Herold, N., Wickham, J., and Megown, K. (2015). "Completion of the 2011 National Land Cover Database for the conterminous United States–representing a decade of land cover change information." *Photogrammetric Engineering & Remote Sensing*, 81(5), 345-354.

Johnson, M. S., Coon, W. F., Mehta, V. K., Steenhuis, T. S., Brooks, E. S., and Boll, J. (2003). "Application of two hydrologic models with different runoff mechanisms to a hillslope dominated watershed in the northeastern US: a comparison of HSPF and SMR." *Journal of Hydrology*, 284(1), 57-76.

Johnston, P., and Pilgrim, D. (1976). "Parameter optimization for watershed models." *Water Resources Research*, 12(3), 477-486.

Kinnell, P. (2005). "Why the universal soil loss equation and the revised version of it do not predict event erosion well." *Hydrological Processes*, 19(3), 851-854.

Knebl, M., Yang, Z.-L., Hutchison, K., and Maidment, D. (2005). "Regional scale flood modeling using NEXRAD rainfall, GIS, and HEC-HMS/RAS: a case study for the San Antonio River Basin Summer 2002 storm event." *J. Environ. Manag.*, 75(4), 325-336.

Kuok, K. K., Mah, D. Y., and Chiu, P. (2013). "Evaluation of C and P factors in universal soil loss equation on trapping sediment: case study of Santubong River." *Journal of Water Resource and Protection*, 5(12), 1149.

McCuen, R. H. (2005). *Hydrologic analysis and design*, Prentice-Hall, Englewood Cliffs, N.J.

McCuen, R. H., Knight, Z., and Cutter, A. G. (2006). "Evaluation of the Nash–Sutcliffe efficiency index." *Journal of Hydrologic Engineering*, 11(6), 597-602.

Morgan, R. P. C. (2009). *Soil erosion and conservation*, John Wiley & Sons.

Moriasi, D. N., Arnold, J. G., Van Liew, M. W., Bingner, R. L., Harmel, R. D., and Veith, T. L. (2007). "Model evaluation guidelines for systematic quantification of accuracy in watershed simulations." *Transactions of the ASABE*, 50(3), 885-900.

Nash, J., and Sutcliffe, J. V. (1970). "River flow forecasting through conceptual models part I—A discussion of principles." *Journal of hydrology*, 10(3), 282-290.

NASS, U.-. (1997). "Usual Planting and Harvesting Dates for US Field Crops." *Agricultural Handbook*, 628.

Oudin, L., Andréassian, V., Perrin, C., Michel, C., and Le Moine, N. (2008). "Spatial proximity, physical similarity, regression and ungaged catchments: A comparison of regionalization approaches based on 913 French catchments." *Water Resources Research*, 44(3).

Pak, J. H., Fleming, M., Scharffenberg, W., Gibson, S., and Brauer, T. (2015). "Modeling Surface Soil Erosion and Sediment Transport Processes in the Upper North Bosque River Watershed, Texas." *Journal of Hydrologic Engineering*.

Pannell, D. J. (1997). "Sensitivity analysis: strategies, methods, concepts, examples." *Agric Econ*, 16, 139-152.

Rawls, W. J., Brakensiek, D., and Saxtonn, K. (1982). "Estimation of soil water properties." *Transactions of the ASAE*, 25(5), 1316-1320.

Refsgaard, J. C., and Knudsen, J. (1996). "Operational validation and intercomparison of different types of hydrological models." *Water Resources Research*, 32(7), 2189-2202.

Reybold, W. U., and TeSelle, G. W. (1989). "Soil geographic data bases." *Journal of Soil and Water Conservation*, 44(1), 28-29.

Samuel, J., Coulibaly, P., and Metcalfe, R. A. (2011). "Estimation of continuous streamflow in Ontario ungauged basins: Comparison of regionalization methods." *Journal of Hydrologic Engineering*, 16(5), 447-459.

Santhi, C., Arnold, J. G., Williams, J. R., Dugas, W. A., Srinivasan, R., and Hauck, L. M. (2001). "Validation of the swat model on a large rwer basin with point and nonpoint sources." *JAWRA Journal of the American Water Resources Association*, 37(5), 1169-1188.

Service, U. S. N. R. C. (1995). *Soil Survey Geographic (SSURGO) Data Base: Data Use Information*, National Cartography and GIS Center.

Singh, J., Knapp, H. V., Arnold, J., and Demissie, M. (2005). "Hydrological modeling of the Iroquois River watershed using HSPF and SWAT." *JAWRA Journal of the American Water Resources Association*, 41(2), 343-360.

Sivapalan, M. (2003). "Prediction in ungauged basins: a grand challenge for theoretical hydrology." *Hydrological Processes*, 17(15), 3163-3170.

Smith, D. D. (1941). "Interpretation of soil conservation data for field use." *Agric. Engg.*, 22, 173-175.

Song, X.-m., Kong, F.-z., and Zhu, Z.-x. (2011). "Application of Muskingum routing method with variable parameters in ungauged basin." *Water Science and Engineering*, 4(1), 1-12.

Speth, J. G. "Towards an effective and operational international convention on desertification." [Unpublished] 1994. Presented at the Third INC-D Session of the Intergovernmental Negotiating Committee on the International Convention on Desertification United Nations New York 17 January 1994.

Srinivasan, R., Zhang, X., and Arnold, J. (2010). "SWAT ungauged: hydrological budget and crop yield predictions in the Upper Mississippi River Basin." *Transactions of the ASABE*, 53(5), 1533-1546.

USDA, N. (1972). "National Engineering Handbook." *Hydrology Section*, 4, 4-10.

Viessman, W., and Lewis, G. L. (2003). *Introduction to hydrology*, Pearson Education, Upper Saddle River, N.J.

Williams, J. R. (1975). "Sediment-yield prediction with universal equation using runoff energy factor."

Zhang, Y., and Chiew, F. H. (2009). "Relative merits of different methods for runoff predictions in ungauged catchments." *Water Resources Research*, 45(7).

Zingg, A. W. (1940). "Degree and length of land slope as it affects soil loss in run-off." *Agric. Engng.*, 21, 59-64.